Surfactant adsorption to soil components and soils

Munehide Ishiguro[1]* and Luuk K. Koopal[2#]

[1]*Research Faculty of Agriculture, Hokkaido University, Sapporo, Japan.*

[2]*Physical Chemistry and Soft Matter, Wageningen University and Research, Wageningen, The Netherlands.*

Corresponding author. Tel.: +81 11 706 2565; fax.: +81 11 706 2494.

E-mail address: ishi-m@env.agr.hokudai.ac.jp

[#] Visiting professor, Research Faculty of Agriculture, Hokkaido University, Sapporo, Japan, May-July 2015.

ABSTRACT

Soils are complex and widely varying mixtures of organic matter and inorganic materials; adsorption of surfactants to soils is therefore related to the soil composition. We first discuss the properties of surfactants, including the critical micelle concentration (CMC) and surfactant adsorption on water/air interfaces, the latter gives an impression of surfactant adsorption to a hydrophobic surface and illustrates the importance of the CMC for the adsorption process. Then attention is paid to the most important types of soil particles: humic and fulvic acids, silica, metal oxides and layered aluminosilicates. Information is provided on their structure, surface properties and primary (proton) charge characteristics, which are all important for surfactant binding. Subsequently, the adsorption of different types of surfactants on these individual soil components is discussed in detail, based on mainly experimental results and considering the specific (chemical) and electrostatic interactions, with hydrophobic attraction as an important component of the specific interactions. Adsorption models that can describe the features semi-quantitatively are briefly discussed. In the last part of the paper some trends of surfactant adsorption on soils are briefly discussed together with some complications that may occur and finally the consequences of surfactant adsorption for soil colloidal stability and permeability are considered. When we seek to understand the fate of surfactants in soil and aqueous environments, the hydrophobicity and charge density of the soil or soil particles, must be considered together with the structure, hydrophobicity and charge of the surfactants, because these factors affect the adsorption. The pH and ionic strength are important parameters with respect to the charge density of the particles. As surfactant adsorption influences soil structure and permeability, insight in surfactant adsorption to soil particles is useful for good soil management.

Keywords: humic substances, silica, metal (hydr)oxides, kaolinite, montmorillonite, soil components

Contents

1. Introduction

Surfactants have an amphiphilic character, which means that they are composed of a polar (hydrophilic) and an apolar (hydrophobic) part. A fundamental property of surfactants in solution is their ability to form micelles (colloidal-sized surfactant aggregates) at a characteristic surfactant concentration, the *critical micelle concentration* or *CMC*. At the CMC the surfactant monomers aggregate into micelles with the hydrophobic tail groups located in the core of the micelle and the hydrophilic head groups in the aqueous interface. In this way the unfavourable contacts of water with the apolar tails are minimized. Micellization gives surfactants their excellent detergency and solubilization properties; due to solubilization (partially) hydrophobic organic compounds dissolve in a micellar solution much better than in water alone. Another characteristic feature of surfactants is their tendency to adsorb at interfaces, mostly in an oriented fashion. The name surfactant is derived from this property; it is a contraction of surface-active agent. By surfactant adsorption the particle surface characteristics change; for instance, by adsorbing with their hydrophobic part to a hydrophobic surface the hydrophilic part protrudes in solution and makes the particle surface hydrophilic, which facilitates wetting and dispersion of the particles in aqueous solutions [1]. Due to their specific character surfactants are widely used chemicals. In household applications they are used in detergents, soaps and shampoos. In industrial applications surfactants are used for emulsification, dispersion, flocculation, wettability, flotation, foaming and so on [2]. In agricultural applications, surfactants are used for the formulation of hydrophobic agricultural chemicals to make these chemicals easily dispersible in water and as anticaking agents for chemical fertilizers [3]. In some cases surfactants are used in soil and groundwater remediation [4, 5]. The disadvantage of the application of large amounts of surfactants worldwide (>15 Mton/year) [6], is that their

discharge is a cause of water pollution [7] and from the aqueous environment surfactants can easily bind to soil components. Dissolved surfactants are considered contaminants in aqueous environments and, in principle, they should be removed from wastewater before entering receiving waters. The ‘Handbook of Detergents, Part B, Environmental impact’ [8] considers the environmental aspects of most surfactant types. Recent information on the aquatic toxicity, biodegradability, and bioaccumulation, which are relevant for the assessment of surfactant ecotoxicity, can be found in [9-13]. Rebello et al. [10] conclude in their review: “…regarding surfactants as non-pollutants is a mistake. Visible manifestations of surfactant toxicity are available in the case of microbes, plants and animals”.

Soils are complex materials; they contain both inorganic particles and organic matter, see e.g.[14]. Roughly speaking, inorganic particles can be divided into primary minerals (physically weathered minerals from rocks), silicas, metal (hydr)oxides and layered aluminosilicates (clays) and within these three groups the particle sizes can vary largely. In general the primary minerals and silica particles make-up the sand and silt fraction, metal (hydr)oxides and aluminosilicates contain the smaller particle size fractions with large specific surface areas. All these soil particles contain in the normal pH range a surface charge, depending on the nature of the particles, which is largely or partly variable by changing the pH. This primary charge is due to the adsorption of protons and/or hydroxyl ions to functional groups (sites) present at the surface of the particles. Soil organic matter, which potentially acts as sorbent, originates from living organisms. It consists of structurally randomized macromolecular residues due to partial degradation, rearrangement and recombination of the original organic structures [15]. Mostly a distinction is made between non-humic and humic substances. Non-humic substances are chemically recognizable in biochemistry and are transitory in soil. Humic substances are not easily degradable and carry specific functional groups that can dissociate depending on the

structure of the group. As most groups are acidic the humic substances also carry a charge that is variable with pH.

The nature of the surface sites of the inorganic particles and the functional groups of the organic particles, determine the particle charge and chemistry and charge govern to a large extent the sorption of other components, including surfactants, to the particles. Important for surfactant binding are the precise sites present at the surface as they determine the chemical nature of the surface and the primary particle charge. The chemical nature determines the “specific” or “chemical” interactions with the polar and apolar parts of the surfactant molecules and the charges determine the electrostatic interaction, which can be either attractive or repulsive, depending on the charge signs of surfactant and particles. Together these interactions determine the mode of the surfactant adsorption to the particles (with their hydrophilic or their hydrophobic part directed to the surface). As far as we are aware, there is no comprehensive review on surfactant sorption to soils, most likely this is due to the complicated and diverse nature of the soils and the many different types of surfactants.

In the present paper first the properties of surfactants are considered in some detail, including surfactant adsorption on the air/water interface, which can illustrate the importance of the CMC for the adsorption process and gives an impression of surfactant adsorption to a hydrophobic surface. Surfactant–soil interactions are determined by the soil components; therefore attention is given to the different types of soil particles: humic substances, silica and metal oxides and aluminosilicates. Information is provided on their structure, surface properties and primary charge characteristics, which are all important for surfactant binding. Subsequently, the adsorption of different types of surfactants on these individual soil components is discussed in detail, based on mainly experimental results and considering the various specific (chemical) and electrostatic interactions. Adsorption models that can describe the features semi-quantitatively are explained and discussed. In the last

part of the paper some trends of surfactant adsorption on soils are discussed together with some complications that may occur and finally the consequences of surfactant adsorption for soil colloidal stability and permeability are considered.

2. Surfactants and their characteristics

2.1. Surfactant types

The chemistry of the polar and apolar part of surfactants can be quite different for different surfactants and based on the nature of the polar head group surfactants are classified into anionics, cationics, nonionics, and zwitterionics. The principal surfactant demand is composed of four types of surfactants: linear alkylbenzene sulfonates (LAS), fatty alcohol ethoxylates (AE), fatty alcohol ether sulfates (FES) and fatty alcohol sulfates (FAS). Both Western Europe and the US rely on the alcohol derivatives for 60-70% of the major surfactants but in the rest of the world it is 15-30%, globally LAS is the most used surfactant [16]. Next to synthetic surfactants also natural surfactants and biosurfactants exist. Some examples of synthetic and natural surfactants are depicted in Fig. 1.

Biosurfactants are surfactants that are produced extracellularly or as part of the cell membrane by bacteria, yeasts and fungi. Mulligan [17] and Bustamante et al. [18] give examples of biosurfactants and their structures and review the environmental applications for soil remediation and water treatment. Biosurfactant applications in the environmental industries are promising due to their biodegradability, low toxicity and effectiveness in enhancing biodegradation and solubilization of low solubility compounds.

2.2. Surfactant adsorption at water/air surfaces

The attraction of surfactants for aqueous solution/air surfaces is due to hydrophobic attraction. Hydrophobic attraction is the thermodynamically favorable tendency of the

surfactant hydrocarbon moiety to escape from the aqueous environment to an apolar environment (air). With adsorption the hydrophobic attraction is the difference between the Gibbs energy (energetic and entropic contributions) of the surfactant tails in aqueous solution and that in the adsorbed state. The adsorption of surfactants at liquid interfaces is generally studied by measuring the surface tension, γ, and using the *Gibbs equation* to obtain the adsorption [19, 20].

$$\mathrm{d}\gamma = -s_a^{(1)}\mathrm{d}T - \sum_{i=2} \Gamma_i^{(1)}\mathrm{d}\mu_i$$

where $s_a^{(1)}$ is the relative surface entropy per unit area, T the absolute temperature, $\Gamma_i^{(1)}$ is the relative adsorption of component i and μ_i is the chemical potential of i. The quantities $s_a^{(1)}$ and $\Gamma_i^{(1)}$ are conveniently determined by assuming that the solvent (component 1) adsorption is zero ($\Gamma_1 = 0$). In the case of surfactant adsorption from *ideally dilute* aqueous solutions the Gibbs equation can be approximated as [21-23]:

$$\mathrm{d}\gamma = -pRT\,\Gamma_{surfactant}\,\mathrm{d}\ln c_{surfactant} \qquad (1)$$

where p = 1 for nonionic surfactants (they are only affected by the presence of electrolytes when the electrolyte changes the solvent quality), but for ionic surfactants

$$p = 1 + \frac{c_{surfactant}}{c_{surfactant} + c_{salt}}$$

This notation of the Gibbs equation has used the equality $\mathrm{d}\mu_i = RT\mathrm{d}\ln c_i$ for all components present and the implicit assumptions are made that the ion concentrations from the background electrolyte are constant, that T is constant, that the adsorption, $\Gamma_{surfactant}$, is a simplified notation for $\Gamma_i^{(1)}$ and that for ionic surfactants the surfactant co-ion adsorption can be neglected. The latter assumption holds best for highly charged surfaces, i.e. at sufficient surfactant ion adsorption. Schematically the effect of surfactants on the surface tension of aqueous solutions is shown in Fig. 2.

In Fig. 2a $\gamma(\ln c)$ curve is shown, firstly the surface tension progressively decreases with increasing surfactant concentration (region I). In region II the decrease becomes approximately linear and at the start of region III the *critical micelle concentration* or CMC is reached. Typically, micelles are clusters of 50−200 surfactant molecules. For surfactant concentrations somewhat above the CMC (region III) the monomer concentration stays about constant and so does the chemical potential of the monomeric surfactant. With the Gibbs equation the adsorption, Γ, can be calculated from the derivative of the $\gamma(\ln c)$ curve. A typical result is depicted in Fig. 2b. The adsorption first increases but in region II, where the slope of the $\gamma(\ln c)$ curve becomes constant (within experimental error), the adsorption reaches a plateau value. In general, the maximum adsorption depends on the effective size of the hydrated head group. In region III the monomer concentration remains constant. Application of the Gibbs equation in region III is not possible because the monomer surfactant concentration stays equal to the CMC, but there is general consensus that the adsorption stays at the level reached at the CMC. For ionic surfactants the $\gamma(\ln c)$ curve depends on the ionic strength, see Fig. 3. For the calculation of the adsorption with the Gibbs equation the factor p comes into play, the extreme situations are p=2 in the absence of salt and p=1 when the salt concentration is much larger than the surfactant concentration. For the intermediate situations p has to be calculated and can gradually increase with increasing surfactant concentration. The maximum attainable adsorption, Γ^{∞}, depends on the salt concentration and increases with increasing ionic strength. This is due to a decrease in electrostatic repulsion between the surfactant head groups, which reduces the effective head group size. The order of magnitude of adsorption of a univalent surfactant is 1-4 μmol/m^2 [24], which corresponds to about 0.1-0.4 C/m^2 and indicates that the adsorption occurs (due to hydrophobic attraction) even at a considerable electrostatic repulsion between the surfactant ions.

2.3. Micelles and their shape

The presence of micelles at surfactant concentrations above the CMC is a very important property of surfactants. Micelles are governed by energetic and geometric considerations. A comprehensive review on the models that describe micellization can be found in [25]. In a micelle the hydrophobic attraction between the hydrophobic moieties is just balanced by the repulsion between the hydrated head groups. The hydrophobic attraction is in this case the difference between the Gibbs energy of the surfactant tails in the aqueous solution and that in the core of the micelles. The shape of the micelles depends on the geometric characteristics of the surfactant molecules. In general, the concentration at which the CMC occurs depends on the surfactant structure and solution conditions. With respect to the surfactant structure the variation in the length of the hydrophobic tail of the surfactant is the most important factor and, in general, the CMC decreases as the hydrophobic character of the surfactant increases, see Fig. 2c. For nonionics also the head group size is important; in general the CMC and the surface tension at the CMC increases with the head group size, see Fig. 2d.

The solution conditions affect the CMC of nonionic surfactants when the solvent quality for the head groups is affected. For ionic surfactants the ionic strength and type of surfactant counterion are important. By way of illustration, Fig. 3 shows how the NaCl concentration affects the surface tension of an ionic surfactant: sodium dodecyl pyridinium chloride (C12PC). It is obvious that the salt concentration changes both the CMC and the slope of the curves. The presence of electrolytes in solution reduces the CMC by shielding the electrostatic repulsion between the ionic head groups. In soils, the CMC of ionic surfactants is likely to be reduced due to the salts present in the soil-solution.

The above illustrates that the CMC of surfactants in aqueous solution varies with surfactant structure and presence of electrolyte in the case of ionic surfactants; the presence of various organic compounds and the temperature also affect the CMC. Although the CMC of a surfactant may vary under different conditions, the CMC is a characteristic property of a

surfactant. Tabulated values of many surfactants (for ionic surfactants with specification of the salt concentration or ionic strength) can be found in [24, 26, 27].

The shape of the micelles varies from surfactant to surfactant and for ionic surfactants the salt concentration is also affecting the micelle shape. In general, the micelle shape depends on the area of the apolar tail, V_o/l_o, where V_o is the tail volume in the micelle and l_o the extended tail length, and the equilibrium area, a_e, of the polar/ionic head group at the micelle surface. The parameter V_o varies with the number of hydrophobic groups, chain unsaturation, chain branching and chain penetration by other compatible hydrophobic groups, while a_e is mainly governed by electrostatic interactions and head group hydration. For ionic surfactants a_e depends on the ionic strength and for large tails the tail packing in the micelle is non-uniform and affects also the equilibrium head group area [28, 29]. The ratio tail area over head group area, $V_o/a_e l_o$, is called the "*critical packing parameter*" or *CPP* and the CPP value provides a good indication of the shape of the micelles [30-32]. In aqueous media and $0<CCP<0.3$ the micelles are spherical (single chained surfactants with large head group areas), for $0.3<CCP<0.5$ the micelles are cylindrical (single chained surfactants with small head group areas) and for $0.5<CCP<1$ curved bilayers (lamellar) are formed (double chained surfactant with large head group areas) and for CCP=1 flat bilayers (double chained surfactant with small head group areas). For CCP>1 only inverted micelles can exist. When the surfactant concentration is raised above the CMC, linear growth of micelles is the dominating type of growth. Some knowledge about the shape of the micelles is also important because in the adsorbed state surfactants already tend to form micellar type aggregates before the CMC is reached.

3. Soil components

3.1. Humic substances

The soil organic fraction contains the non-humic substances (e.g., proteins and natural macromolecules) and the humic substances. The humic substances are divided into fulvic acid, humic acid and humin by their aqueous solubility; humic and fulvic acids are soluble in the normal pH range and humins are not. Fulvic and humic acids are distinguished by their solubility at low pH: fulvic acids are soluble in all pH, whereas humic acids precipitate at low pH. For the isolation and separation of the humic substances the procedure described by Swift et al. [33] is mostly used as the International Humic Substances Society recommends it.

Humic particles found in soil, sediment and water have an extreme structural complexity. In an overview Leenheer [34] discusses the successive approximations of model structures to molecular structures that have appeared in literature for dissolved humic particles. Present days insight is that the old “polyelectrolyte model” that represented the dissolved humic particles as randomly coiled macromolecules resulting from various chemical condensation and coupling reactions of smaller biomolecular constituents is no longer adequate. New structural models view dissolved humic particles as dynamic associations of relatively low molar mass components stabilized by hydrophobic interactions and hydrogen bonds [35] or as complex supramolecular assemblies of small molecules, oligomers, and polymers aggregated into supramolecular assemblies by non-covalent forces [36].

From physicochemical point of view the dynamic character of the aggregation [37], the presence of a diversity of functional groups that protrude in the aqueous phase [38] and the fact that the aggregates have an open structure [39] that allows the aqueous solution to partly permeate through the particles has to be taken into account. The functional groups can dissociate or associate with protons and this causes the primary charge of the particles that governs the electrostatic interactions. With physicochemical treatments humic particles should therefore be considered as amorphous, polydisperse, chemically complex and internally structured supramolecular particles that are held together by hydrophobic

attraction and hydrogen bonding and that are partly permeable by the aqueous solution. Through their structure and dissociation or association of the functional groups with protons the particles have in aqueous solutions a polyelectrolyte nature that can be classified as soft-colloidal matter and both their charging and electrokinetic behavior [40] are different from that of rigid solid particles. Due to their 'open structure' humic and fulvic acid have very large sorption capacities per kg of material. The main differences between humic and fulvic acids are their functional group density, average molar mass and hydrophobicity: fulvic acids have a relatively low molar mass, a relatively high functional group density and a relatively low hydrophobicity. Humin particles are only poorly investigated, but based on the isolation procedure it may be expected that they are solid like (much less permeable than humic acid) with a relatively low functional group density, have a large particle mass and are hydrophobic in nature.

For a further physicochemical characterization of humic and fulvic acids the proton binding characteristics of humic and fulvic acids are relevant. The heterogeneity of the proton binding groups of humic substances is considerable with, in general, two main classes of groups each with a wide distribution [41, 42]. The low proton affinity groups are mostly referred to as 'carboxylic' groups (pK_H around 3-4) and the high proton affinity groups as 'phenolic groups' (pK_H around 8-9). For the pH conditions in natural waters humic and fulvic acid are negatively charged and pH and ionic strength affect the proton charge density [43], the hydrodynamic radius of the humic particles [44] and their electrokinetic behavior [40]. Fig. 4 gives a typical example of proton binding to a humic acid at four different salt concentrations [45].

Much attention has been paid to modeling proton (and heavy metal ion) binding to humic and fulvic acids and the literature is reviewed in [46-50]. In general, models should (i) take explicitly into account the heterogeneity of the functional groups of humic and fulvic acids, (ii) distinguish between electrostatic and ion-specific binding and (iii) account for

competition for binding among ions. Models that confirm to these conditions are based on intrinsic parameters that are independent of the environmental conditions (e.g., pH, ionic strength). The two most successful models that suit the above conditions are Tipping's ion-binding Model VI/VII [51-53] and the NICA-Donnan model [38, 43, 54-56]. These models can be applied across a wide range of environmental conditions and be used to make predictions outside the calibration range. The heterogeneity of the humic substances is described in Model VI/VII with a wide discrete distribution of (intrinsic) proton affinity constants [47, 51] and in the NICA-Donnan model with a bi-modal continuous distribution [57, 58]. For the electrostatic interactions a simple Donnan model is used in the NICA-Donnan model [54] and recently also in Tipping's model [52, 53]. The Donnan models describe the electrostatic interaction with only one average smeared-out electrostatic Donnan potential at given environmental conditions [59]. The Donnan model leads to calculated Donnan potentials that are highly non-Nernstian, see [54]. This means that the Donnan potential is non-linear with a change in pH and that its value is also strongly ionic strength dependent. By considering a great deal of the existing data up to 2003, Milne et al. [55, 56] have been able to establish two sets of parameters that can describe the proton and other ion binding to, respectively, generic-HA and generic-FA. These generic-HS compounds can be used as substitutes when no detailed information is present on a specific HS to calculate the ion binding for many ions.

3.2 Silica and metal (hydr)oxides

In many parts of the world, silica (SiO_2) is the major constituent of sand and silt. The fine silica particles (<2 μm) are classified as clay. Oxides of iron and aluminum are most prominent in soils of the tropics but are widespread elsewhere. Silica has a number of distinct crystalline forms in addition to amorphous forms. Amongst the various crystallographic forms of silica, α-quartz is the most abundant, as it is the most stable

crystalline silica phase. Thus, α-quartz has been widely used as a model for the investigations of water/silica interface systems in environmental processes. Due to their coarse size, quartz particles have a low specific surface area and do not have colloidal properties, yet they exhibit adsorption. In contrast, amorphous silicas can be very fine and mostly have a large specific surface area. Also because their industrial uses, the adsorption properties of amorphous silicas (mostly synthetic) have attracted much attention.

The surface structure of silica is composed of siloxane sites (-Si-O-Si-) and silanol (-SiOH) sites. Siloxane sites are hydrophobic and silanol sites are hydrophilic; therefore, the higher the silanol content is, the larger is the hydrophilicity of the surface. The silanol groups can be subdivided into isolated (or single), geminal ($-Si(OH)_2$) and vicinal or bridged silanols. The vicinal OH groups are two nearest neighbors that are bound together by a hydrogen bond. The silanol sites are formed by hydroxylation of siloxane bridges. Based on dehydration studies, Zhuravlev [60] has shown that amorphous silica surfaces will contain predominantly single and geminal silanol groups and siloxane bridges, the relative content of each type of group depending on the temperature of dehydration and the subsequent rehydration conditions. Direct information on the distribution of silanol groups over isolated, geminal and vicinal groups can be obtained from NMR studies. Chuang and Maciel [61] have reported that the surface of amorphous silica powders have a roughly equal distribution of isolated and geminal silanols. Yang and Wang [62], who reviewed computational simulations, conclude that the normal siloxane bond is hard to be hydrolyzed because of the high reaction barrier, but siloxane surface structures with a large strain stress and surface defects are rather readily broken by water attack, especially with the aid of extra water molecules. The presence of silanols next to siloxane groups thus also follows from the simulation studies.

From hydration-dehydration and tritium and deuterium exchange studies it can be concluded that when an amorphous silica surface is hydroxylated to the maximum state the

silanol density is around 4.9 groups per nm^2 independent on the history of the sample [60]. This number is about two times smaller than the classical value of number of silanols of about 8 groups per nm^2 derived by Iler using the assumption that for each surface Si there is one OH group [63]. The difference can be explained by the fact that only half of the Si atoms are capable of holding OH groups [64]. Tamura et al. [65] give an overview of hydroxyl site densities of silicas and a range of metal oxides (Al, Fe, Mn, Ti, Sn, Zn, Mg). From the collected densities it follows that the hydroxyl content of silica is substantially lower than that of the metal oxide surfaces. The high hydroxyl content of the metal oxides explains that these surfaces are more hydrophilic than the silica surface.

The sites responsible for the charging of the aqueous interface of silica and metal oxides can be derived from the mineral structure. For *crystalline* minerals the structure is well known through X-ray diffraction measurements and in combination with electron microscopy also the dominant crystal faces that make up the surface can be detected. Using this information in combination with Pauling's bond valence concept [66] and its refinement [67-69] the protonation properties of the oxygen containing surface groups can be derived. In the bond valence concept, the charge of the central cation is distributed over the surrounding O-ligands and the sum of bond valences around oxygen should be equal to the oxygen valence. Hiemstra et al. [70, 71] have used the bond valence concept in the multi-site complexation (MUSIC) model to describe the protonation of mineral surfaces. The model allows differentiating various types of surface groups in terms of formal charge and takes into account that most metal oxide surfaces have multiple types of surface oxygen groups that can react with protons. The pK_H values of the groups can be predicted and the model has highlighted that the two pK_H values of two successive protonation steps on one and the same O-ligand differ by about 10 pK-units ($\Delta \log K_H \approx 10$). This implies that practically only one proton association or dissociation step per surface group can occur in the normal pH window. Other predictions are: (i) the inertness of double coordinated

surface groups on sesquioxides, which may result in non-charged perfect crystal faces for gibbsite [72, 73] and hematite [73, 74], and (ii) the difference in proton affinity for the two basic types of triply coordinated groups of goethite [71]. The MUSIC model may also account for changes in temperature as shown by Machesky et al. [75]. It should further be noted that the predicted ΔpK_H value of 10 provides evidence that the older description of the proton charging of mineral surfaces based on two protonation steps for each surface group ($\equiv SO^-$ to $\equiv SOH^0$ to $\equiv SOH_2^+$; 2-pK model) is fundamentally wrong.

It is instructive to discuss the primitive, but relevant, situation of a homogeneous silica and gibbsite surface; each containing singly coordinated surface hydroxyls only [76-78]. According to the bond valence concept, the silanol group has a formal charge of zero ($\equiv SiOH^0$), while the aluminol group has a formal charge of -1/2 ($\equiv AlOH^{-1/2}$). By varying the pH of the aqueous solution the $\equiv SiOH^0$ can release its proton and becomes $\equiv SiO^{-1}$, while the $\equiv AlOH^{-1/2}$ group may associate with a proton to form $\equiv AlOH_2^{+1/2}$; therefore, the silica surface is *acidic* and the gibbsite surface is *amphoteric*. This difference leads to a different type of point of zero net proton charge (pznpc): the silica charge approaches the pznpc asymptotically (all groups in the protonated form at low pH), while the charge of gibbsite changes linearly around the pznpc (equal numbers of $\equiv AlOH^{-1/2}$ and $\equiv AlOH_2^{+1/2}$). To be able to calculate the charge vs. pH curves at different ionic strength a further model is required that describes the electrical double layer. For flat surfaces the diffuse part of the electrical double layer can be described with the Debye-Hückel or the Gouy-Chapman model [79], but for a good description of the electrical double layer of silica, gibbsite and other mineral surfaces it is necessary to incorporate besides the diffuse layer also a Stern layer adjacent to the surface. The Stern layer accounts for the dimensions of the counterions close to the surface and allows the structure of water near the mineral surface to be different from bulk water [80]. The MUSIC model in combination with the double layer model provides the means to calculate the proton charge pH curves of silica and gibbsite. As a

consequence of protonation reactions and the different points of zero net proton charge, the shape of the proton charge curve as function of pH of silica is rather different from that of gibbsite. Also the surface potential behavior is different: the surface potential of silica is highly non-Nernstian (i.e. strongly dependent on the ionic strength and non-linear with a change in pH), while the surface potential of gibbsite is approximately Nernstian (linear with a pH change and nearly independent of the ionic strength) [76-78]. Other metal oxide surfaces have also fractional formal charges and react in a similar way as gibbsite. At constant pH also the surface potential of metal oxide surfaces is about constant and about independent of further solution conditions, therefore metal oxide surfaces are also called 'constant (surface) potential' surfaces. The fact that most surfaces have multiple types of surface oxygen groups that can react with protons makes the situation more complicated, but the principle difference between silica-type and gibbsite-type behavior remains. The proton charge vs. pH at different ionic strength values, as observed for gibbsite [81], silica [82] and hematite [83] is depicted in Fig. 5.

The multiple types of surface oxygen groups on silica and metal oxides and a detailed electrical double layer model are of most importance for a good understanding of ion binding other than protons, because these ions often do not react with all surface groups and/or may lose part of their hydration shell depending on the type of surface group (inner-sphere versus outer-sphere complex formation). Information on the type and structure of the adsorption complexes has to be derived from spectroscopic studies and can be used in the extended MUSIC model for ion binding, the CD-MUSIC model [84, 85], where CD stands for charge distribution of the bound ions. For goethite the available parameters allow calculations with many different ions and reliable predictions can be made based on 'model goethite' even in complex situations.

Concluding, silica and metal oxides have rather different surface properties: (i) silica contains both hydrophilic and hydrophobic sites (siloxanes), while the normal metal oxides

are hydrophilic, (ii) silica has an asymptotic point of zero net proton charge and a highly non-Nernstian surface potential, while the metal oxides charging curves are linear in the point of zero net proton charge and their surface potentials are close to Nernstian. Metal oxide surfaces can be called, to a good approximation, 'constant potential' surfaces. For ion adsorption to goethite accurate parameters are available for many ions so that reliable predictions can be made for soils dominated by goethite.

3.3 Silicate clays (alumino-silicates)

A very important fraction of soils are the clays or alumino-silicates. Clay particles are crystalline and found around the world but they are more widespread in temperate areas. A main difference with most metal oxides is that silicate clays have a layered structure [14, 86]. The basic structure is composed of a sheet of tetrahedrons of silicon atoms surrounded by oxygen atoms and a sheet of octahedrons in which an aluminum ion is surrounded by six hydroxyl groups or oxygen atoms. The tetrahedrons in a sheet are linked by three of the oxygens in the tetrahedron with adjacent tetrahedra and arranged in hexagonal rings, which allow the sheet to extend indefinitely in the plane direction; the remaining oxygen is linked to Al in the octahedral sheet. Also apical oxygen atoms are common to adjoining tetrahedral and octahedral sheets. Combinations of stacked tetrahedral and octahedral sheets are termed layers. Many layers are found in each crystal and in some clays the layers are separated by interlayers in which water and adsorbed cations are found. In nature, cations having nearly the same radius as Si^{4+} (e.g. Al^{3+}) can replace Si^{4+} in the tetrahedral sheet by isomorphous substitution. Isomorphous substitution can also take place in the octahedral sheet with Al^{3+} being replaced by a similar-sized cation (e.g. Mg^{2+}). The substitution finds mostly place with cations that have a lower valence than either Si^{4+} or Al^{3+} and this results in unsatisfied negative charges within the crystal, therefore isomorphous substitution is the primary source

411 of the negative charge of clay surfaces. The negative charges attract cations from the soil
412 solution.

413 Based on the number and arrangement of tetrahedral and octahedral sheets contained in
414 the crystal units or layers, silicate clays are classified into two different groups: i) 1:1 type
415 minerals in which the layers have a TO structure build up of one tetrahedral (T) sheet and
416 one octahedral (O) sheet and ii) 2:1 type minerals with a TOT layer structure. The stacking
417 of layers in a 1:1 type crystal leads to two different basal plates: a T-layer with surface
418 oxygens and an O-layer with surface hydroxyls. For a 2:1 type mineral both basal plates are
419 T-layers with surface oxygens. The surface oxygens of the tetrahedra in a T-surface layer
420 form a siloxane surface; in the centers of the 6-membered rings of the tetrahedra a cavity is
421 formed of about 0.23 nm that acts as a specific site for cations if their size matches the size
422 of the cavity [87]. Although the siloxane sites make the surface hydrophobic, the charged
423 sites that occur due to the isomorphic substitution and the presence of hydrated cations
424 make the surface considerably less hydrophobic than a neutral siloxane surface. The basal
425 surface of the T-layer is very common, it occurs for all clays; as different clays have
426 different degrees of isomorphous substitution the hydrophobicity-hydrophilicity of the
427 T-surface also varies, the higher the structural charge density, the lower the hydrophobicity.
428 The surface oxygens of the O-layer are similar to the double coordinated oxygens of the
429 planar 001 face of gibbsite and form surface hydroxyls that are fully charge satisfied and
430 unreactive with respect to protons. The structural surface charge and the presence of the
431 hydroxyls make the O-basal plate hydrophilic.

432 The edges of the clay particles have unsatisfied bonds that are quite reactive with respect
433 to protons. For the T-layer edge these are the silanol groups that can protonate: $\equiv SiO^- + H^+$
434 $= \equiv SiOH^0$. For the O-layers the edge face has doubly and singly coordinated oxygen groups.
435 The doubly coordinated $\equiv Al_2\text{-}OH^0$ groups are inert in the normal pH range, the singly
436 coordinated $\equiv AlOH^{1/2-}$ groups at the O-edges are the reactive groups; for their protonation

437 one can thus write $\equiv AlOH^{1/2-} + H^{+} = \equiv AlOH_2^{1/2+}$. Note that the site density of $\equiv SiO^{-}$ at the
438 edges for a 2:1 clay will be higher than that at the edges of a 1:1 clay. In the normal pH
439 range the silanol sites will be partly negative, partly neutral, while the aluminol sites will be
440 partly positive, partly negative, the edge surface is therefore amphoteric. The above is the
441 simplest representation of the edge, in practice the situation is more complicated because of
442 non-ideal structures and end effects that cause bond-length relaxation and charge
443 redistribution at the edge surface [88-90].

444 Proton binding to clays is considerably more complex than to silica or metal oxides;
445 protons will participate in the cation exchange at the basal planes and in the protonation or
446 deprotonation of the edges. Because of the presence of the structural charge on the basal
447 planes next to the variable charge of the edge, one deals with a patchwise heterogeneous
448 surface and for such surfaces the points of zero net proton charge are dependent on the
449 differences between the patches and the electrolyte concentration [83, 91]. One of the
450 complications is that the proton binding to the edges can be affected by the structural charge
451 due to ‘spillover’ of the electrostatic potential between basal and edge surface. In a
452 relatively simple model Avena et al. [92] incorporated both the structural charges that can
453 exhibit ion exchange and the variable edge charge that can change with pH according to a
454 simple proton association - dissociation reaction. The spillover of the potential is taken into
455 account by smearing-out the total particle charge over the entire surface. This model
456 captures the basic features of the proton charging and exchange reasonably well, but the
457 parameters have to be fitted. Fig. 6 depicts the measured proton charge curves for
458 montmorillonite that clearly show the shifts of the points of zero net proton charge, together
459 with the calculated curves [92].

460 When the spillover effect is calculated in a sophisticated way and the site structure and
461 reactivity are modeled with the MUSIC approach with predicted pK_H values the situation is
462 considerably more complicated. Bourg et al. [88] mention the various models that have been

used to describe the proton charging of montmorillonite and discuss the experimental results and the most promising sophisticated models.

It is also instructive to briefly discuss how the layers are held together for the main clay types. In the 1:1 type crystals, with kaolinite as most prominent example, the layers are held together by hydrogen bonds; as these bonds are strong, the layers are closely held together in stacks that are large in size, have no internal surfaces and do not swell when wetted. Also the isomorphous substitution is low, consequently, these minerals have a relatively low adsorption capacity for cations. The so-called *cation exchange capacity* or *CEC* is largely due to cation adsorption on the edges of the particles and therefore relatively strongly depending on the pH. The 2:1 clays can be subdivided in four general groups depending on how strongly the layers are bound together: micas, chlorites, vermiculites and smectites. In micas a relatively high fraction (~25%) of the silicon atoms in the tetrahedral sheets have been replaced by aluminum. The resulting large negative charge is satisfied by potassium ions held rigidly between the adjoining 2:1 layers and preventing expansion of the crystal. As a consequence of the strong binding they have a fairly large stacking of layers and are non-expanding. They resemble the 1:1 type clays somewhat and have a relatively low CEC that is also fairly pH dependent. The chlorites are also non-expansive, the adjacent negative layers are held together by a positively charged magnesium-dominated octahedral sheet in the interlayer between the two 2:1 layers. Chlorites have particle sizes, CECs, and physical properties similar to those of fine-grained micas. Vermiculites have a significant substitution of aluminum for silicon in the tetrahedral sheets as well as some substitution of magnesium for aluminum in the octahedral sheet, but lower than in micas. The individual 2:1 layers are held together only loosely by Mg^{2+} and Ca^{2+} ions that act as bridges between the structural charges in the adjoining layers. Water molecules are attracted between the layers and vermiculites expand when wet and shrink when dry. Due to the weak attraction between the layers the surfaces adjoining the interlayer are also available for adsorption and this leads to

a very large total interface and a large CEC. Due to the limited expansion and the high CEC, vermiculites have a high affinity for weakly hydrated cations such as K^+, NH^{4+} and Cs^+. The final group contains the smectites, with montmorillonite as well known member. In the smectites some magnesium has been substituted for aluminum in the octahedral sheet and some aluminum for silicon in the tetrahedral sheet, but the degree of substitution is less than in vermiculite and the interlayer is larger. Due to the relatively low structural negative charge, K^+ fixation is lower than in vermiculite. As in vermiculite, the cations in the interlayer are exchangeable and this gives rise to high CECs. It may be clear that also surfactant binding to non-expanding clays is far simpler than that to the expanding clays.

3.4. Concluding remarks

Comparing the ion binding models for metal oxides and silica with those of humic substances it follows that the electrostatic part of the model for metal oxides and silica is far more complicated than that of the humic substances, especially when the adsorption of ions other than protons is considered; for humic substances the heterogeneity is most important. Adequate understanding of proton adsorption to silicate clays is only possible when a distinction is made between the edges and the basal planes and considering the spillover of the electrostatic potential of the basal planes to the edges. For all systems the proton charging may change when another species is adsorbed (primary charge adjustment) due to generic electrostatic effects and/or site competition. The different particles also differ in hydrophobicity. Humic substances have many hydrophobic parts, the silica surface is partly hydrophobic and the metal oxides are hydrophilic. Furthermore, adsorption on silica should be distinguished from that on the metal oxides, because of the differences in proton charging behavior and hydrophobicity. With silicate clays the edges are hydrophilic and the basal planes of 2:1 clays are hydrophobic, but the hydrophobicity is weakened by the presence of the structural charge and the adsorbed cations. For kaolinite (1:1 clay) the basal

siloxane surface is fairly hydrophobic, but the basal aluminol surface is hydrophilic; with montmorillonite (2:1 clay) the two basal siloxane surfaces are less hydrophobic than the siloxane surface of kaolinite due to the greater degree of isomorphic substitution.

4. Surfactant binding to humic substances

4.1. Early experimental studies and isotherms measured with surfactant electrodes

The investigations of surfactant binding to humic and fulvic acids are relatively recent, still limited, and have not been reviewed. Therefore, the most important binding studies will be discussed. Early reports are of Tombacz [93, 94] who investigated alkylammonium - humate complexes with X-ray and interfacial tension measurements. Binding isotherms to dissolved humic substances were reported for the first time in 1996 by Traina et al. [95], who used an ultra-centrifugation technique and fluorescence quenching to obtain the binding characteristics of C10-, C12-, and C14-linear alkyl-benzene sulfonates (LAS; in 0.03M NaCl and 0.01M $CaCl_2$) to dissolved humic substances. By using pulse-field gradient NMR Otto et al. [96] found that humic substances enhance the aggregation of the anionic sodium dodecylsulfate (SDS) prior to micellization and that they form ion pairs with cationic C16-trimethylammonium bromide.

The first isotherms ranging from low surfactant concentrations till the CMC were reported by Koopal et al. [97], who used a potentiometric method with a surfactant electrode to measure the equilibrium surfactant concentration. Three surfactants were used, one anionic (SDS) and two cationic (C12- and C16-pyridinium chloride or C12PC and C16PC) and the binding to purified Aldrich humic acid (PAHA) was investigated at three pH values (5, 7, 10) at 0.025 M background electrolyte concentration. No binding could be observed for SDS under the given conditions. The isotherms of the cationic surfactants were independent of the humic acid (HA) content in solution (0.2-0.5 g/L), which indicates that

541 the results were not affected by possible dynamic aggregation/segregation of HA. The
542 observed isotherms for the cationic surfactants are depicted in Fig. 7; the binding is plotted
543 vs. c/CMC^0, where c is the surfactant concentration and CMC^0 is the CMC in the absence of
544 HA. The binding of C12PC and C16PC increased with increasing pH to maxima that
545 corresponded to the negative charge of the HA (arrows in Fig. 7). By plotting the binding vs.
546 log c/CMC^0 the isotherms of C12PC and C16PC merged largely, indicating that next to the
547 electrostatic attraction hydrophobic bonding is important. When the charge neutralization
548 point was reached the cationic surfactant–PAHA complexes precipitated, which occurred at
549 approximately 10% of the CMC. For C16PC, the precipitation was complete, but in the case
550 of C12PC, a noticeable fraction of PAHA remained in solution.

551 Subsequent binding studies were made by Yee et al. [98-101], Matsuada et al. [102] and
552 Ishiguro et al. [103], who all used the potentiometric technique with a surfactant electrode
553 to measure the equilibrium surfactant concentrations. Yee et al. [100] also investigated the
554 binding of SDS to HA using Aso HA (AHA) derived from the Aso area of Kyushu Island,
555 Japan. At pH 9.18 and low ionic strength (0.03M) no binding could be observed between
556 SDS and AHA with either the potentiometric or dynamic light scattering (DLS) method,
557 which confirmed the result of Koopal et al. [97]. However, with the DLS method some
558 interaction could be detected at pH 3.98 and high ionic strength (0.10M). The attraction can
559 be explained by the fact that at 0.1M the electrostatic repulsion is suppressed, but the
560 hydrophobic attraction remains the same and the net effect is a weak attraction. Temperature
561 studies of C12-pyridiniumbromide binding to Aso fulvic (AFA) and AHA at pH 9.18 and
562 ionic strength of 0.03M showed that the binding of $C12P^+$ with AFA was endothermic, i.e.
563 driven by a positive entropy [99], while the enthalpy of $C12P^+$ binding with AHA was
564 slightly negative [101]. For AFA different binding modes were observed at two pH regions,
565 i.e., cooperative binding at $pH > 7$ and non-cooperative binding at $pH < 7$, see Fig. 8 [99].

For the AHA-$C12P^+$ system no cooperative binding was observed, but the $C12P^+$ concentration at which the first binding was observed was much lower for AHA than for AFA [101]. The latter reflects that AHA is more hydrophobic than AFA because the acidic type of groups to which the surfactant head groups bind are very similar for FA and HA and the negative charge density of FA is in general larger than that of HA. The $C12P^+$ binding to AFA did rise steeply just before the CMC, i.e. AFA-$C12P^+$ cooperation occurred very close to the CMC. The isotherm of $C12P^+$ binding to AHA leveled-off just before the CMC as the binding was close to its maximum value. The behavior of the AFA-$C12P^+$ system at pH>7 could therefore also be caused by enhanced $C12P^+$ micellization in the presence of AFA, instead of typical $C12P^+$ binding to AFA. The stronger hydrophobicity of AHA than of AFA was confirmed by studying the effect of the aliphatic chain length (*n*) of the surfactant tail (*n*: 12, 14, 16) [98]; the results are plotted in Fig. 9. In all cases the comparable isotherms started for AHA at concentrations that were ~10x lower than for AFA. The isotherms shifted with increasing chain length roughly with the same factor as the CMC, but the shift was larger for AFA than for AHA. The results for AHA correspond with the observations of Koopal et al. [97] and Ishiguro et al. [103].

It should be realized that two different hydrophobic interactions have to be considered with surfactant-HS interaction: (i) the hydrophobic effect of transferring the hydrocarbon tail of surfactant into the hydrophobic parts of humic substances (HS) and (ii) the lateral hydrophobic attraction between bound surfactants; (i) contributes to the greater binding strength of HA than FA and (ii) may cause cooperative binding. However, when the hydrophobic effect of transfer of the tail into the hydrophobic parts of HS is large, than the extra effect of (ii) will be small. This explains why (ii) is larger for AFA than for AHA.

Yee et al. [99, 101] also investigated the role of the HS content (0.2-0.5g/L), pH and ionic strength. In accordance with Koopal et al. [97], no HS concentration dependence of binding was observed in both systems; possible self-aggregation of HS did not affect the

592 binding. The binding of $C12P^+$ increased with increasing pH, similarly as observed by
593 Koopal et al. [97] for $C12P^+$ and $C16P^+$, and this can be explained by the increase of the
594 negative charge of HS with increasing pH. The bound amount decreased with increasing
595 ionic strength, due to the screening of the electrostatic attraction between surfactant ions
596 and HS; the effect was larger for AHA than for AFA. With DLS the hydrodynamic radii of
597 the AHA-C12PB (PB = pyridinium bromide) and AFA-C12PB complexes were measured at
598 pH 9.2 at ionic strength values of 0.03M and 0.1M for a constant concentration of AFA or
599 AHA of 0.05 g/L. In the absence of surfactant no reliable average size could be measured,
600 but in the presence of surfactant good results were obtained. At low surfactant binding the
601 aggregate diameters were about 200 nm and with increasing surfactant binding up to ~4
602 mmol C12PB/g the aggregate sizes increased; at 0.1M the increase in aggregate size was
603 similar for AFA and AHA (~1400 nm), while at 0.03M the increase in size was somewhat
604 lower for AFA (~1200 nm) but considerably less for AHA (~500 nm). The difference might
605 be due to the fact that the particle concentration in the case of AFA is much higher; at high
606 ionic strength rapid aggregation may occur for both HS, while at 0.03M the kinetics are
607 important.

608 The binding of Cn-trimethylammonium ($CnTA^+$) ions to AFA and AHA has been studied
609 by Yee et al. [100] and Matsuda et al. [102]. Yee et al. compared the binding of $C12TA^+$
610 with that of $C12P^+$ at pH 9.2 and 0.03 M at 25 ^oC. The binding of $C12TA^+$ to AFA or AHA
611 was weaker than that of $C12P^+$, presumably due to the relatively large size of the headgroup
612 of $C12TA^+$, that prevents a close approach to the negative sites of HS. The differences
613 between the $CnTA^+$ isotherms for AFA and AHA were similar as in the case of
614 $C12P^+$-AFA/AHA A stronger interaction with HA than with FA for C16TAB was also
615 observed by Otto et al. [96] using NMR diffusion analysis. The surfactant head group
616 structure also affects the aggregation behavior: the hydrodynamic diameters of
617 AFA-C12TAB and AHA-C12TAB aggregates were smaller than those of AFA-C12PB and

618 AHA-C12PB aggregates. Similarly as for C12PB the aggregate size of the HS-C12TAB
619 aggregates increased with surfactant binding and the AFA-C12TAB aggregates were larger
620 than those of AHA-C12TAB. Thieme and Niemeyer [104] also observed an increase in size
621 of HS-C12TAB aggregates with increasing C12TAB binding.

622 Matsuda et al. [102] investigated first the binding of $C12TA^+$ and $C10TA^+$ surfactants to
623 PHA (derived from an HA-rich layer in Heilongjiang, China) at pH 8 and different NaCl
624 concentrations (0-50 mM) and subsequently that in the presence of divalent metal ions (Cu,
625 Cd, Zn, Pb, and Ca) at pH 8. With respect to $C16TA^+$ the binding curves of $C12TA^+$ were
626 shifted to higher surfactant concentrations; the shift was comparable to the shift in CMC. As
627 stated before, the stronger binding for C12TAB than C10TAB indicates the role of the
628 hydrophobic interaction between the tail of the surfactant ions and the hydrophobic parts of
629 PHA. The affinity of $C12TA^+$ for PHA decreased linearly with the square root of the NaCl
630 concentration. In the presence of 0.5 mM divalent metal salts, the PHA-$CnTA^+$ binding
631 decreased significantly, which can be explained by site competition and screening of the
632 electrostatic attraction. The effect of the different metal ions on C12TAB binding to PHA
633 was similar, but for C10TAB binding to PHA the effect decreases in the order Cd, Zn, Pb,
634 Ca, and Cu.

635 Ishiguro et al. [103] studied the binding of Cn-pyridinium chloride (C12PC and C16PC)
636 to purified Aldrich humic acid (PAHA), Dando humic acid (DHA, Japan), Inogashira humic
637 acid (IHA, Japan), Laurentian fulvic acid (LFA, Canada) and Strichen Bs fulvic acid (SFA,
638 Netherlands) at pH 5 and 0.005M NaCl, and C16PC binding to PAHA was also studied at
639 0.1M NaCl. Besides surfactant isotherms also titrations of HS with surfactant were carried
640 out using an automatic titrator combined with a Mütek particle charge detector (M-PCD)
641 [105, 106]. This M-PCD-method is well suited to measure the charge sign of colloidal
642 particles and in the case of titrations with a complexing agent of opposite charge the
643 iso-electric point (IEP) can be detected. The M-PCD titrations were used to determine the

charge of the HS samples at the given conditions (pH 5 and 0.005M NaCl) with poly-DADMAC (poly-diallyldimethylammonium chloride) a strong cationic polyelectrolyte [107, 108] and with $C16P^+$. For this charge determination the IEP is required. For the HA samples the charges determined with $C16P^+$ were slightly higher than those observed with poly-DADMAC, this could be explained by better screening and stronger charge adaptation in the case of $C16P^+$. For the two FA samples the charges obtained with $C16P^+$ were significantly larger than those measured with poly-DADMAC. This difference was explained by the relatively low hydrophobicity and corresponding relatively low affinity between FA and $C12P^+$. By binding of $C16P^+$ a surfactant-FA complex becomes more hydrophobic, this enhances the affinity and the isotherm becomes very steep; for such conditions the rate of titration was likely too fast and leading to too high IEPs. With $C12P^+$ the M-PCD method was only used to obtain at the given conditions the bound amount of surfactant at the IEP and the corresponding solution concentration of surfactant. Comparison of the $C16P^+$ results with those of $C12P^+$ showed that for PAHA the bound amounts (mol/g) of $C16P^+$ and $C12P^+$ were the same, i.e. at the IEP the charge associated with the HS was neutralized by bound surfactant ions. For the other HS samples the bound amount of $C12P^+$/C12PC at the IEP was larger than that of $C16P^+$. This must indicate that at the IEP some C12PC was included in the complex, as there is no reason to believe that the screening of the HS charge by $C12P^+$ is better than that by $C16P^+$ when the HS-$C12P^+$ affinity is weaker. Chloride inclusion is most likely caused by the fact that around the IEP the C12PC concentration in solution is relatively high. The behavior of CnP^+ surfactants often shows a dependence on the type of counterion, indicating incomplete dissociation [109]. With C16PC the affinity for HS is so high that the amount of C16PC left in solution is very low. Therefore, binding of uncharged C16PC to HS is insignificant for C16PC. The M-PCD titrations with the surfactants also reveal that the surfactant–HS complexes reached their IEP before the CMC was reached. Around the IEP some flocculation of the complexes

could be observed, and upon continuation of the titration charge reversal of the aggregated complexes occurred. This may have lead to partial re-dispersion of the aggregates. Shang and Rice [110] and Subbiah and Mishra [111] investigated HA-C16TB complexes by, respectively, small-angle X-ray scattering and synchronous and excitation emission matrix fluorescence, both found (partially) reversible flocculation around the CMC. Shang and Rice used a purified peat HA; Subbiah and Mishra, who used Aldrich HA that was purified by two filtration steps, also investigated SDS and Triton-X100 (t-Octyl-C_6H_4-$(OCH_2CH_2)_x$OH, x=9-10), a nonionic surfactant, and found only very weak interactions for these surfactants.

Binding isotherms of $C16P^+$ to PAHA at two ionic strength values reported in [103] are reproduced in Fig. 10. The binding is plotted in panel a) vs. log c_{eq}(surfactant) and in panel b) the same result is depicted but now as double logarithmic plot. The horizontal dashed line indicates the bound amount of $C16P^+$ and the approximate concentration at the IEP as measured with the M-PCD. The thin vertical lines in the top of the figures indicate the CMC values. In panel a) also the proton release due to $C16P^+$ binding is included. Two striking effects can be observed: (i) the isotherms at different salt concentration intersect at the IEP of the complex and (ii) close to or at the CMC the isotherms rise steeply. The latter is an artifact; it is binding of surfactant in micelles, not to PAHA. At the common intersection point (CIP = IEP) the charge of PAHA is neutralized by $C16P^+$. The CIP occurs at a surfactant concentration smaller than the CMC and the $C16P^+$ binding continues till the CMC because of hydrophobic attraction. Binding above the CIP=IEP indicates that $C16P^+$ binds super-equivalently to PAHA. Before the CIP, where the complex is negative, the salt concentration screens the negative charge of the complex and this diminishes the head group surface attraction, at the CIP the complex is net uncharged and salt has no effect, beyond the CIP the complex is positive and the salt concentration screens the repulsion between the head groups. As a consequence the salt concentration dependence inverses at the CIP=IEP. The proton release is up to the CIP very small, $C16P^+$ binding occurs on

already dissociated groups; beyond the CIP the proton release increases and is only slightly smaller than the increase in surfactant binding, so most of the increment in surfactant charge is balanced by proton release.

For sake of comparison the binding of $C12P^+$ to sodium polystyrene sulfonate (SPSS), a flexible linear anionic polyelectrolyte, is also plotted in Fig. 10, panels c) and d) [112]. The $C12P^+$ isotherms of SPSS at the three different ionic strength values merge before the CMC (the measurements are not accurate enough to observe a CIP); however, for SPSS-$C16P^+$ a clear CIP could be detected [112]. The double logarithmic plots (b and d) are best suited to investigate cooperativity of binding. It should be remarked that sometimes the S-shape of single logarithmic plots is used to indicate cooperativity, but this leads easily to erroneous results, because the Langmuir isotherm (no cooperativity) also has an S-shape in these plots. Firstly, the binding of $C12P^+$ to SPSS is considered as this system shows the various aspects most clearly (this is the reason that in Fig. 10 SPSS-$C12P^+$ was preferred above SPSS-$C16P^+$). Along the isotherm four regions can be distinguished. Region I, at the very low surfactant binding (or surfactant concentration) is the region where the slope of the isotherm is unity, this is the “Henry region” where binding and concentration are proportional; the surfactant is ideally bound on isolated sites of equal energy. For SPSS-$C16P^+$, region I cannot be observed; the slope is very steep from the start due to the strong cooperativity [112]. In region II, the slope of isotherms becomes larger than unity, which clearly indicates cooperativity. The transition point of region I and II is defined as the *critical association concentration* (CAC); at the CAC aggregation of surfactant starts. In region II the number of aggregates along the polyelectrolyte chain increases with increasing surfactant concentration. In region III the slope of the isotherms gradually lowers and becomes smaller than unity due to three factors: 1) the attractive electrostatic interaction becomes smaller due to the decrease of the negative charge of SPSS-$C12P^+$ complex, 2) the mixing entropy of “free” and $C12P^+$-occupied sites decreases and 3) polymer chain

conformations become more restricted. The last factor will be of little importance for HS, which is internally structured. The CIP marks the end of region III and the start of region IV, the negative charge of the polymer is compensated by the positive charge of bound surfactant. In region IV the aggregates grow slightly further and the SPSS-$C12P^+$ complex becomes increasingly positive.

Let's now return to the PAHA-$C16P^+$ system [103]; in the double logarithmic plot the 'Henry slope' is indicated by the dashed line. At 0.005M NaCl a CAC and cooperativity cannot be observed, but there is a slight kink in the isotherm that could be the transition point between regions I and II. Region III (up to the CIP) and region IV beyond the CIP can be clearly observed. At 0.1M the isotherm starts with a slope higher than unity, that implies some cooperativity is observed at low surfactant concentration, but the CAC cannot be established. The increase in cooperativity with increasing electrolyte concentration occurs because the electrostatic repulsion between the bound surfactants decreases.

In Fig. 11 the binding at 0.005 M NaCl of $C16P^+$ is compared to that of $C12P^+$. The influence of carbon chain length on binding can be clearly observed. The $C16P^+$ binds at much lower surfactant concentrations than $C12P^+$ and the isotherm is somewhat steeper. The larger affinity for $C16P^+$ is largely due to the fact that $C16P^+$ 'hates' the aqueous solution more than $C12P^+$, because the shift of the two isotherms is similar to that of the CMC. This reveals the importance of the hydrophobic effect for the binding.

The $C12P^+$ binding isotherms for the different humic and fulvic acids at 0.005 M NaCl are compared in Fig. 12. The shape of the binding isotherms to the humic acids is distinctly different from that of the fulvic acids and the $C12P^+$ binding decreases in the order of PAHA>>IHA≈ DHA>>SFA≈LFA. The order ranks the HS with respect to hydrophobicity, PAHA is most hydrophobic the FA's the least. Cooperativity is not observed at pH 5 and 0.005 M NaCl because the slopes of the curves are almost unity or smaller than unity. These results correspond with the findings of Yee et al. [98, 100, 101] discussed above.

748

749 *4.2. Surfactant binding measured by solid-phase micro-extraction*

750 Recently, Chen et al. [113] have demonstrated that polyacrylate (PA) coated microfiber
751 sorbs organic cations via ion exchange at the carboxylic groups. When the binding isotherm
752 is known, it can be used to determine the freely dissolved concentration of the given
753 cationic surfactants. The free surfactant concentration in a HS-surfactant system can be
754 obtained by extracting the surfactant bound to PA and determine the extracted amount by
755 HPLC, hereafter the calibration line gives the equilibrium surfactant concentration. The
756 method is called solid-phase micro-extraction (SPME). The method will work well when
757 the surfactant binding to PA is negligible compared to the binding to HS. The double
758 logarithmic representation of the surfactant isotherm to PA fiber is used as calibration curve
759 for the dissolved surfactant, because in this way the isotherm is linear in the low
760 concentration range. Binding isotherms of hexadecyl-trimethylammonium chloride
761 (C16TAC) and benzyldimethyl-dodecyl-ammonium chloride (C12BDAC) to PA are
762 reported as examples; the isotherms of these two surfactants coincide, while their CMCs
763 differ by more than a factor 10. Based on the difference in hydrophobicity this must imply
764 that PA is strongly hydrophilic and that there is-no hydrophobic contribution to the specific
765 affinity for the PA-carboxylic groups, mainly the surfactant head group chemistry seems
766 important. The linear part of the log-log isotherms of the two surfactants cover a
767 concentration range from about 10^{-10} to $10^{-6.5}$ M. The upper limit of this range is 10^{3} to 10^{4}
768 times smaller than the CMCs. This implies that accurate measurements are only possible in
769 an equilibrium surfactant concentration range considerably below the CMC, for higher
770 concentrations the sensitivity lowers with increasing concentration. Therefore, the method is
771 most valuable for the linear part of the log-log surfactant HS isotherms. The preliminary
772 conclusion is that the PA-SPME will be of substantial added value in the low surfactant
773 concentration range, but that the surfactant electrode will be superior in the higher

774 concentration range (>10^{-3}CMC). Anyhow, this new technique is highly welcome and will
775 promote further research of cationic surfactant binding. As example a series of binding
776 isotherms of C12BDAC to purified Aldrich humic acid (purified AHA) at pH 6 and
777 different salts and salt concentrations were measured. Chen et al. [114] continued the latter
778 study in a subsequent paper in which the pH range of the measurements was extended to pH
779 3, some results are reproduced in Fig. 13.
780
781 *4.3. Modeling surfactant - humic substance interaction*
782 Ishiguro and Koopal [115] modeled the results of C12PC and C16PC to different humic
783 and fulvic acids with the NICA-Donnan model [38, 43, 54-56] (see also section 7) under the
784 assumption that the surfactant (*s*) was dominant: $(k_s c_s)^{ns} \approx \Sigma(k_i c_i)^{ni}$ with k_i the intrinsic
785 affinity, c_i the concentration and *ni* the stoichiometry of component *i*. This implies that only
786 the low affinity or carboxylic groups were considered and that the surfactant binding to
787 these groups was larger than the proton binding. For these conditions the NICA equation
788 simplifies to a Hill type equation, but the cooperativity parameter, *m*, includes the
789 cooperativity *ns* and the site heterogeneity parameter, *p*: $m=ns \bullet p$. This Hill-type equation is
790 complemented with the Donnan model that accounts in a simple way for the electrostatic
791 interactions by assuming that for a given set of conditions there is only one electrostatic
792 potential that governs the behavior in the Donnan phase. With the combined model the
793 experimental results for the binding of the different surfactants to the different HAs at
794 different salt concentration and pH could be well described. For the FAs only the linear part
795 of the log-log isotherms could be described well.
796 Chen et al. [114] also modeled the surfactant isotherms with the NICA-Donnan model.
797 As the measured isotherms were restricted to the linear range, they made the assumption
798 that the *total* binding was hardly or not affected by the surfactant (*s*) binding: $(k_s c_s)^{ns} << \Sigma(k_i c_i)^{ni}$ with k_i the intrinsic affinity, c_i the concentration and *ni* the stoichiometry of
799

component *i*. In this limit the NICA equation becomes a Hill-type equation ($m=ns$) for which $(k_s c_s)^{ns} << 1$, which has the same form as the classical Freundlich equation. By combining this equation with the Donnan model to incorporate the electrostatics and using the generic description of HA as provided by Milne et al. [55, 56] the salt effects at pH 6 could all be explained well.

By considering the successful modeling attempts by Ishiguro and Koopal [115] and Chen et al. [114] and the fact that two different limiting forms of the NICA equation both lead to a Hill type equation also explains the success of the use of the Hill equation in the work of Yee et al. [98-101]. However, as the Donnan (electrostatic) part was omitted by Yee et al. no explanation could be provided for pH and salt effects. For more information on the NICA-Donnan equation section 7 should be consulted.

4.4. Sorption of organic cations and risk assessment

Droge and Goss [116] studied the sorption of organic cations to soil organic matter (SOM) using dynamic column experiments (peat mixed with silicium carbide) with different compositions of electrolytes in aqueous eluents. The sorption affinity of the organic cations to Pahokee peat soil (i) strongly decreased with increasing electrolyte concentration, (ii) was higher in NaCl solutions than in $CaCl_2$ solutions of similar ionic strength, and (iii) was more sensitive to a decrease in NaCl than to a decrease in $CaCl_2$. Based on the results of this comprehensive study the authors made three remarks. (1) The mass action law equations for ion-exchange reactions predicted trends in a qualitative but not in a quantitative way. (2) Complex models, such as the NICA-Donnan model, are required to fully account for the contributions of ionic interactions to the sorption of organic cations to SOM. (3) The results imply that risk assessment models for organic bases should take ion-exchange processes adequately into account when estimating soil sorption coefficients and bioavailability. These findings indicate that, in general, the NICA-Donnan

826 model can play an important role in the description of organic cation exchange with soil
827 organic matter.
828
829 **5. Surfactant adsorption to metal (hydr)oxides and silicas**
830
831 *5.1 General aspects and reviews*
832 In contrast to the binding of surfactants to HS, the adsorption of surfactants to mineral
833 surfaces has received much attention, because insight in the structure that adsorbed
834 surfactants adopt is vital for practical applications. In older studies most attention was
835 focused on adsorption isotherms and their description. The typical isotherm of ionic
836 surfactants on oppositely charged metal oxides, when depicted as logarithm adsorbed
837 amount vs. logarithm concentration$_{eq}$ (as done in the section on surfactant binding to SPSS
838 and HS), can be subdivided into four regions. Somasundaran and Fuerstenau [117] have
839 introduced this “four-regions” concept and it has been followed in many studies. Typically,
840 the four-regions isotherm extends over about three decades in concentration and adsorbed
841 amount; two examples of the four-regions isotherm are presented in Fig. 14(a), the isotherm
842 to the left depicts the adsorption of an anionic surfactant (sodium C9-benzene sulfonate) on
843 rutile at low pH, the isotherm at the right shows the adsorption of a cationic surfactant
844 (C12-pyridinium chloride) on rutile at high pH; for sake of comparison the same isotherms
845 are presented in Fig. 14(b) as semi-logarithmic plot that provides better insight in the higher
846 adsorbed amounts close to the CMC [118].
847 To interpret the four-regions isotherm, the adsorption is best described with the relation
848 $\Gamma = Kc^n$, where Γ is the adsorbed amount, c the concentration divided by the standard state
849 concentration (1 mol/L), K the effective affinity constant and n the cooperativity. In region I
850 isolated surfactant molecules adsorb and slope-I =1 or close to unity, which implies n_I =1
851 and ideal behavior. In region II, which starts at low amounts adsorbed, slope-II is mostly >1

852 and thus $n_{II} > 1$ which is due to cooperative association of adsorbed molecules caused by
853 hydrophobic attraction. For $n_{II} > n_I$ the transition I/II is called the *critical surface*
854 *association concentration* (CSAC). At transition II/III the slope of the log-log isotherm
855 mostly decreases, i.e. $n_{III} < n_{II}$; for $n_{III} > 1$ there is still cooperative adsorption but the
856 cooperation is less than in region II; for $n_{III} < 1$ there is negative cooperativity likely caused
857 by a decrease in configurational entropy due to high surfactant adsorption. Region IV
858 begins at the CMC, beyond which the chemical potential of the monomeric surfactant
859 remains approximately constant, therefore also the adsorption is constant. In some cases, e.g.
860 for cationic surfactant adsorption on silica at low ionic strength, a four-regions isotherm is
861 observed that does not confirm to the above picture: $n_{II} < n_I$ (=1) and $n_{II} < n_{III}$ with $n_{III} > 1$,
862 thus region III has the steepest slope. In that case the concentration at which the transition
863 II/III occurs is the CSAC. Although the four-region-type isotherm is well established,
864 especially the interpretation of transition II/III is debated together with the structure of the
865 adsorbed molecules in both adjoining regions. This discussion is enhanced by the results of
866 modern techniques that give information on the adsorbed layer structures. An important
867 contribution to the discussion has been the paper of Manne et al. [119] in which convincing
868 evidence, based on atomic force microscopy (AFM), was presented that surfactants tend to
869 self-assemble at surfaces to form analogues of the micelles in bulk solution. Since then the
870 attention has shifted from adsorption isotherms to modern techniques that provide
871 information on the adsorbed structures. Most reviews of ionic surfactant adsorption pay
872 attention to the four-regions isotherms, but the debate around the four-regions isotherm is
873 still not fully settled and in reviews different views may be expressed. We will return to the
874 four-regions isotherm when the measured isotherms on silica and the metal oxides at
875 constant pH and different ionic strength values will be discussed. First, the various reviews
876 on surfactant adsorption to silica and metal oxides will be briefly introduced.

Several authors have reviewed the state of art of surfactant adsorption, mostly with emphasis to their specialism in the field. The older studies are reviewed in [120, 121] and Rosen's book [24] provides a general review of surfactants and surfactant adsorption with emphasis on surfactants and their mixtures both in solution and at interfaces and on the modification of the surface properties by surfactants. After the pioneering work of Manne et al. [119, 122] to directly visualize the structure of aggregates formed on surfaces using high resolution scanning probe and atomic force microscopy (AFM), these techniques have been used regularly. This work has been reviewed in [123] and in [119]. Johnson and Nagarajan have presented a theory of surfactant self-assembly on isotropic hydrophobic and hydrophilic surfaces [124, 125]. The theory is extending the treatment of self-assembly in solution [28, 126] with an additional term that accounts for the replacement of the solid surface-water contact by the solid surface-aggregate contact. This contribution depends on the surfactant and surface properties and can be calculated for an *assumed* geometrical shape of the aggregate; for hydrophobic surfaces and nonionic surfactants it is the Gibbs energy change of replacing surface-water contact by solid surface-aggregate core contact, while for hydrophilic surfaces and ionic surfactants it is (i) the electrostatic interaction between the charged surfactant head groups and the hydrophilic surface, if the surface is charged, plus (ii) the Gibbs energy change associated with displacing water by the surfactant head groups wherever aggregate solid surface contact occurs. The CSAC and the aggregate morphology can be predicted by computing the equilibrium Gibbs energy of formation for a range of assumed geometrical structures and selecting the structure with the lowest Gibbs energy. The CSAC is always predicted to be lower than the bulk phase CMC and a variety of aggregate morphologies are predicted. Morphological transformations of surface aggregates to less energetically favorable structures will occur when the surfactant concentration increases. For hydrophobic surfaces the morphologies include hemispheres, hemicylinders, finite disks, and continuous monolayers depending upon surfactant, solid

surface and surfactant concentration. For hydrophilic surfaces the situation is more complex and in addition to full spheres and cylinders a series of composite structures are proposed which are composed of monolayers oriented with head groups in contact with the surface and covered with either hemispheres, hemicylinders, finite disks, or another monolayer (making the full structure a bilayer). It should be noted that the authors have assumed that monolayer structures with head groups in contact with the surface are instable and transform in composite structures of covered monolayers. This is only correct for surfactant concentrations close to the CMC. Stability and wetting studies have shown that beyond the CSAC the instability and contact angle still increase up to the point where surfactant charge and surface charge compensate each other [127], which points to largely uncovered monolayer type structures or teepee-micelles [128]. Nevertheless, the model provides basic insight in surface aggregation and allows a better judgment of the AMF images that are mostly obtained around or above the CMC.

Derived from results obtained with modern measurement techniques Tiberg et al. [129] have discussed in a comprehensive way the adsorption mechanisms and interfacial structures of nonionic and ionic surfactants for both hydrophobic and hydrophilic surfaces. It is an excellent review for a good orientation on surfactant adsorption.

Atkin et al. [128] have given a follow-up on this review with emphasis on the adsorption process for ionic surfactants. Traditional equilibrium data (including the four-regions isotherms), discrete aggregation on the substrate (mainly silica), and the morphology of the aggregates are thoroughly discussed. As the AFM is most useful at detecting periodicity, surfactant–substrate combinations that produce highly regular morphologies produce the clearest AFM images. The hydrophobic cleavage plane of graphite orients the adsorbed surfactant structures more strongly than any other substrate, and hemi-cylindrical structures are formed for surfactant chains with more than 10 carbon atoms, smaller chains result in a laterally featureless adsorbed layer. The hydrophilic, crystalline mica substrate also orients

the adsorbed surfactant structures, but not as strongly as graphite. The alkyl trimethyl-ammonium surfactants form cylindrical admicelles, which were stable at relatively high ionic strength, but less stable at low ionic strength. The morphology of adsorbed gemini surfactants on mica depend strongly on the geometry of the surfactant monomer. On silica surfactants are less strongly oriented, due to a lower surface charge and the amorphous state of the substrate. The adsorbed configuration of C16TAB was concentration dependent, with short rods at 0.9*CMC and worms at 10*CMC. Similar structures have been observed for C14TAB and C12TAB on silica. For C16TAC, only spheroidal structures were present. In all cases there was little or no long range ordering of the adsorbed aggregates. By sequentially increasing the substrate hydrophobicity the structure of adsorbed *nonionic* surfactants can be changed in a controlled manner from diffuse adsorbed micelles on the least hydrophobic interface, to densely packed micelles, to a bilayer, to a monolayer on the most hydrophobic interface. The information gained by AFM, fluorescence quenching and neutron reflectivity is discussed and with this knowledge, kinetic data obtained from ellipsometry and optical reflectometry, are analyzed. In the summary the likely mechanisms of adsorption along the four-regions isotherm are proposed.

Zhmud and Tiberg [130] discuss applications of modern techniques (tensiometry, ellipsometry, photon correlation spectroscopy, and neutron reflectivity) with emphasis on the physical principles and theoretical aspects related to the adsorption and desorption kinetics, interfacial structure development, wetting enhancement, and interfacial dynamics. The review includes mathematical derivations that demonstrate how raw data can be transformed into sought layer characteristics. After the discussion of the techniques the intermolecular interactions in aggregated surfactant complexes are discussed and experimental studies on the dynamics and structure of adsorbed surfactant layers are briefly reviewed. The discussion of the isotherm for ionic surfactants is somewhat confusing because two surface association concentrations are considered, the hemi-micelle

concentration and the critical surface association concentration. Although different names have been used for the concentration at which aggregation starts, there is for a given system only one concentration where the four-region isotherm steeply increases. In the last part of the review wetting enhancement by surfactants and the effect of surfactants on the damping of capillary waves are discussed.

A topical review on *in-situ* surface-enhanced infrared and non-linear vibrational sum-frequency spectroscopy in relation to a better understanding of adsorption at mineral–water interfaces is presented by Schrödle and Richmond [131]. Particular consideration is given to organic adsorbates including surfactants. The authors conclude that non-linear optical methods greatly extend the well-established linear IR techniques and provide many opportunities to advance our understanding of the structure and dynamics of mineral–water interfaces. This will be true, but, as the material is quite complex, help of an expert will be required for the data analysis.

Many of the experimental results discussed in the above reviews are obtained on graphite, mica, quartz and silica and these surfaces are different from the metal oxide surfaces. Reviews that put more emphasis on metal oxide surfaces are those of Paria and Khilar [132] and Zhang and Somasundaran [133]. Paria and Khilar discuss the four-regions isotherms of ionic surfactants on oppositely charged metal oxides, and pay special attention to region IV, that occurs for surfactant concentrations > CMC, where some anomalies have been observed. Influences of molecular structure, temperature, salt concentration that are very important in surfactant adsorption are reviewed for both nonionic and ionic surfactants and the state of aggregation of the adsorbed surfactants is discussed on the basis of AFM and fluorescence measurements. Also the adsorption behavior and mechanism of different mixed surfactant systems (anionic–cationic, anionic–nonionic and cationic–nonionic) are reviewed. Mixtures of surface-active materials can show synergistic interactions, which can be manifested as enhanced surface activity, spreading, foaming and detergency.

The review of Zhang and Somasundaran [133] is concerned with adsorption of single surfactants as well as mixtures of various types and provides lists of systems (surfactant / surface / method) that have been studied for both ionic and nonionic surfactants. Also zwitterionic surfactants are briefly discussed. The information derived from the isotherms, combined with fluorescence spectroscopies, electron spin resonance (ESR), Raman spectroscopies, small angle neutron scattering, neutron reflectivity and AFM, has been used to discuss the structural properties of the surface aggregates along the isotherms. Compared to the adsorption of single surfactants, adsorption of mixtures of anionic– cationic, anionic– nonionic, cationic– nonionic, cationic– zwitterionic and nonionic– nonionic types generally exhibit synergy at interfaces. To predict the shape of mixed aggregates of nonionic surfactant mixtures a new model of the critical packing parameter is derived that takes into account the mole fractions of adsorbed surfactants.

5.2 Surfactant adsorption and charge regulation

In the next sections the adsorption isotherms of ionic surfactants to rutile (TiO_2) and silica measured at *constant pH* and *different background 1-1 electrolyte concentrations* will be critically examined, together with the *adaptation of the surface charge* as a result of the surfactant adsorption. Results for rutile are taken from [118, 134-136], those for silica from [137, 138]. It will be shown that these surfaces behave differently with respect to surfactant adsorption. A strictly constant pH allows the calculation of the surface charge regulation (adaptation) and measurements at different ionic strength at constant pH can be of help with unraveling the orientation of the adsorbed surfactant. In order to keep the pH constant, the pH is regularly checked during the course of adsorption and restored to its initial value. The amounts of alkali or acid to restore the pH are used to calculate the proton charge adaptation of the surface. The surface charge adjustment is important in itself (in many studies the effect of a change in surface charge is simply ignored), but it can also help to create a

picture of the adsorption behavior. It is also required for full understanding of specific co-ion and counterion effects on surfactant adsorption. A combination of surfactant adsorption and surface charge (adjustment) results makes it possible to differentiate between (i) adsorbed surfactant molecules with the head groups adjacent to the surface *('head-on'* adsorption) which may occur with a counterbalancing (de)protonation of the surface, and (ii) molecules with an oppositely orientation, i.e. with their head group at the solution side (*'head-out'* adsorption) which will not affect the surface charge. To discriminate between different aggregate structures monolayer type aggregates of *head-on* adsorbed molecules will be called *'teepee'-micelles* [128] and local bilayer type structures (*head-on* + *head-out* adsorbed molecules) *ad-micelles*. Knowledge about the prevailing molecular orientation and or aggregate structure is of direct importance for wetting and stability behavior of the particles [25, 127].

5.3. Ionic surfactant adsorption on rutile.

Rutile is chosen because it allows studying anionic surfactant adsorption on positive rutile at the acidic side of the pH of zero net proton charge ($pH<pH_{pznpc}$) and cationic surfactant adsorption on negative rutile at the alkaline side ($pH> pH_{pznpc}$). Rutile is not of direct importance for soil systems but at the same ionic strength the adsorption behavior of surfactants on rutile is very similar to that on aluminum oxides and hematite when $\Delta pH = pH\text{-}pH_{pznpc}$ is considered as parameter that characterizes the charge density [134, 139-141]. At *similar pH* values the adsorption isotherms and admicelle structures of a given surfactant on different metal oxides surfaces will strongly depend on $pH\text{-}pH_{pznpc}$, i.e., on the type of metal oxide surface [142]. Nonionic adsorption on rutile will not be discussed.

In Fig. 15 adsorption isotherms of sodium nonyl-benzene-sulfonate (SNBS) on rutile at pH 4.1 and three salt concentrations are depicted as log-log (a) and lin-log (b) plots [134]. In region I the coverage is too low for the adsorbed molecules to interact with each other,

the slope is about unity. Mutual attraction starts in region II, where the coverage is still very low: roughly between 0.03 and 3% of the maximum coverage. The concentration at the transition point between region I and II is the critical surface association concentration or CSAC. A straight line with a slope of about four fits the data points in region II, indicating a strongly positive cooperativity of the adsorption and proof for surfactant self-assembly. The slope in region III is considerably lower than that of region II and it depends notably on the salt concentration. It is less than unity for low salt concentrations and somewhat higher than unity for 0.1M salt. Salt addition promotes the adsorption in region III by screening the head group repulsion. The transition between regions II and III is more pronounced for low salt concentrations, which also indicates that at low salt concentrations the repulsion between head groups becomes important in region III. The CMC marks the transition to region IV, where the plateau is reached.

Due to the fact that isotherms at three salt concentrations are plotted another important phenomenon occurs: the three isotherms at different salt concentration intersect in a *common intersection point* or CIP. The presence of such a CIP was first noted by De Keizer et al. [143] who also showed that in the absence of specific adsorption of other ions and/or activity effects the CIP should correspond to the IEP of the particles covered with surfactant. In Fig. 15(b), the lin-log plot, the strong cooperativity present at low coverage is evident at low salt concentrations as a weak shoulder in the isotherms. The lin-log isotherms show much better than the log-log isotherms that the ‘bulk’ of the adsorption occurs in region III. Also the position of the (near) CIP is clearly shown. The plateau values reached in region IV are about the same for the different salt concentrations.

The adsorption of SNBS and surface charge of rutile are shown in Fig. 16 as function of the surfactant concentration at three pH values and two salt concentrations [134]. To facilitate the comparison the surface charge is divided by F, the Faraday, so that proton excess, $\Gamma(0)$, and adsorbed amount of surfactant, Γs (SNBS), are both expressed in $\mu mol/m^2$.

Information about the structure of the adsorbed layer can be obtained by comparing Γ(0) and Γs. For a given pH, see e.g. pH 4.1 (Fig. 16, panel a and b), head-on adsorbed surfactant ions may either have displaced adsorbed Cl^- ions or caused the formation of new proton charges at the surface to counter balance the surfactant charge and the latter increases Γ(0) . Head-out adsorption will not affect the surface charge. Therefore, as long as the surface charge adjusts to the surfactant adsorption head-on adsorption occurs. Initially Γ(0) > Γ(SNBS) because the surface charge is already present (best seen at 0.1 M NaCl) but at somewhat larger surfactant concentrations Γ(0) < Γ(SNBS). Beyond the intersection point the difference between Γs and Γ(0) is due to head-out adsorption plus some head-on adsorption of molecules that are accompanied by a counter ion; therefore, head-out adsorption is about proportional to Γs-Γ(0) but not necessarily equal to this difference. The proton uptake due to surfactant adsorption is the strongest at low surfactant adsorption and low salt concentrations: with almost every adsorbing surfactant molecule a proton is adsorbed, indicating that all surfactant ions will be adsorbed head-on. At higher salt concentrations the initial surface charge is higher, therefore the initial slope of the Γ(0) curve is less, surfactant ions cause displacement of Cl^- ions at the surface by NBS^- ions and proton adsorption. At high amounts adsorbed the surface charge becomes almost independent of the salt concentration: the surfactant is responsible for the screening of the surface charge. Very similar results are obtained at pH 5.1 and 6.0. At pH 6 the pure rutile surface is slightly negative (pH_{pznpc} rutile 5.85); however, the specific affinity of the head group for the surface is sufficient to overcome the coulomb repulsion and the surfactant adsorption induces a positive charge on the surface. Therefore, only positive surface charges are observed once surfactant is present, and the two curves coincide at low surfactant concentrations.

In general, the proton adsorption tends to level off after the CIP in the isotherms. The CIP corresponds for SNBS with the IEP and with the point where the surface charge and the

surfactant charge balance, the equivalence point. The strong surface charge adjustment before the CIP in combination with the observed steep slope of region II of the isotherms indicates that teepee-micelles are formed at the surface. Teepee-micelle formation is promoted by the ‘flexibility’ of the surface charge. Changes in surface charge due to SNBS adsorption still occur beyond the CIP. This demonstrates that the head-on adsorption is not completed at the CIP. The substantial difference between Γs and Γ(0) beyond the CIP indicates that a large part of the additionally adsorbing molecules is oriented head-out: after the CIP the formation of admicelles is dominant. The rate of transition from teepee- to ad-micelles depends strongly on the salt concentration; the higher the salt concentration the sharper becomes the transition. The SNBS adsorption around the CMC depends only weakly on the salt concentration, increasing the salt concentration increases the adsorption somewhat due to the better screening of the head group charges.

Comparing the behavior at the three pH values (Fig. 16) it can be observed that the pH effect on the SNBS adsorption is most strongly at the initial part of the isotherm (region I and II): the smaller $\Delta pH = pH\text{-}pH_{pznpc}$ is, the lower is the affinity of the surfactant for the surface. However, the pH may also affect the admicelle structure because an increase in surface charge density can lead to a reduction in the effective headgroup area of the adsorbed surfactant and this may decrease the critical packing parameter [142]. Further adsorption studies on positively charged rutile with four sodium p-dodecylbenzene sulfonate isomers (3SDBS, ISDBS, 5SDBS, 6SDBS) [135] to study the effects of aliphatic chain length and architecture, revealed that the adsorption increases with chain length and decreases if the point of attachment of the aliphatic chain to the hydrophilic part of the molecule is shifted from a terminal to a medial position.

The adsorption on negative rutile was studied by using two pyridinium surfactants (C12, C14) and the results were compared with those of SNBS (see Fig. 14) [118, 136]. The four-regions isotherm and the CIP are found also for the anionic surfactant adsorption on

positive rutile, but for the weakly adsorbing CnP^+ ions the situation is considerably more complicated than for the strongly adsorbing NBS^- ion. Due to the relatively weak CnP^+ adsorption, the competition with the salt cations (K^+) becomes noticeable and the 'CIP' is no longer 'sharp', the IEP shifts with the salt concentration and differs from the 'CIP'. However, the 'CIP' remains the transition point for tepee- to ad-micelle formation. For more details and a further discussion of surfactant adsorption on rutile or the metal hydroxides in general the quoted references should be consulted.

5.4. Ionic surfactant adsorption on silica

The adsorption of cationic surfactants on silica (negative) is far greater than the adsorption of anionic surfactants. Nevskaia et al. [144] have shown that small amounts of anionic surfactants (C_9H_{19}-phenol-$(OCH_2$-$CH_2)_n$-$SO4^-$ Na^+, with n = 4 and 10) could be adsorbed on quartz but the relevance is very limited. Therefore, no further attention will be paid to anionic adsorption to silica.

The adsorption isotherms for C12PC on Aerosil, measured at pH 9 and two salt concentrations are shown in Fig. 17(a) as log-log plot and in Fig. 17(b) as lin-log plot [137]. The isotherms at low and high salt concentrations have different shapes. At low salt concentration the adsorption shows a 'hesitation' in the both the lin-log and log-log plot. This is usually observed for adsorption of cationic surfactants on silica in the absence of salt or at low salt concentrations [145-148]. At both low and high salt concentrations four regions may be distinguished in the log-log plots and for low salt concentration the different regions can also be observed in the lin-log plot. The slope in region I of the C12PC isotherms is equal to unity within experimental error. In this region specific and coloumbic attraction between surface and surfactant ions take place, but the adsorbed molecules don't interact with each other. In region II, the slope of isotherms, measured at low salt concentration, is less than unity. This demonstrates that surfactant self-assembly still does not occur! Self-assembly is

counteracted by mutual head group repulsion and by the partial hydrophobicity of the pyrogenic silica surface that interacts with the surfactant tails by hydrophobic attraction. This behavior deviates strongly from that observed for adsorption of C12PC on rutile [118, 136] and in general from surfactant adsorption on the crystalline metal oxides. On silica surfactant molecules adsorb, at low salt concentration, without appreciable lateral interaction up to the end of region II. In the same concentration range the surface charge adapts strongly to the surfactant adsorption. Therefore, the mutual repulsion between the headgroups will be modest and most likely the tail-surface interaction is the main reason for the absence of self-assembly. Evidence for tail-surface interaction was obtained from both comparison of the effect of C16TAB and tetramethyl-ammonium bromide on the charging behavior of Aerosil [138] and theoretical calculations using the SCFA model [137]. The surfactant concentration has to increase to about 0.1*CMC before region III begins and the aggregation starts. Due to lateral hydrophobic attraction the slope of the isotherm in region III is steeper than that in II and the CSAC is located at the transition of region II to region III.

Increasing the salt concentration increases the slope of region II due to the higher initial surface charge and a better screening of the lateral head group repulsion. At 0.1M salt the slope of region II is larger than that at region I; therefore, the CSAC now occurs at the transition from region I to region II. A relatively high salt concentration leads to a relatively high surface charge due to the presence of many counterions close to the surface, and this reduces the surface hydrophobicity. Consequently, not only the mutual head group repulsion is diminished, but also the tail-surface attraction, therefore surfactant self-assembly occurs at a much earlier stage than at low salt concentration. The slope in region III depends only weakly on the salt concentration and is now smaller than in region II. The transition to region IV is observed at the CMC. An increase in the salt concentration leads to a rise of the plateau value and small decrease of concentration (CMC), where plateau is reached: diminishing the lateral repulsion allows a closer packing of the molecules and/or a higher aggregate density.

The isotherms show a CIP in region II, the concentration at which the intersection occurs, corresponds well with the point where the surfactant charge and the surface charge balance, the equivalence point. The fact that CIP and equivalence point coincide is direct evidence that the binding of $C12P^+$ to Aerosil is much stronger than that of K^+. The much stronger binding of C12PC to silica than to rutile [118, 136] is also likely due to the tail-surface affinity in the case of silica. The reasons for the CIP are the same as those mentioned for SNBS adsorption on rutile. The difference with the SNBS-rutile case is that the CIP is located in region II instead of in region III of the isotherm.

The effect of C12PC adsorption on the surface charge of Aerosil at pH 9 is shown in Fig. 18 for two salt concentrations (0.001 M and 0.1M KCl) [138, 149]. To allow easy comparison of the adsorbed amount of surfactant, Γs, and the surface charge the latter is divided by F, the Faraday, an indicated as, Γ(0); they are both expressed in μmol/m^2. The maximum change in surface charge occurs at low surfactant and low salt concentrations, where the adsorption and surface charge isotherms almost coincide. It means, that at low salt concentrations with almost every adsorbing surfactant ion a proton is desorbed and practically all adsorbed surfactant ions will adsorb head-on. After compensation of the surface charge by surfactant (the equivalence point) the surface charge continues to increase weakly whereas the surfactant adsorption increases substantially. This indicates that locally adsorption of surfactant in head-out position starts, i.e. head group directed to the solution. The weak increase of Γ(0) shows that some of the additionally adsorbing molecules are still head-on adsorbed. On top of this some other surfactant ions may adsorb head-on if they are accompanied with a counter-ion. In general, one may conclude that small admicelles are formed around the initially head-on adsorbed (isolated) molecules. This representation of the surface aggregate corresponds with that suggested by Zhu et al. [150, 151].

At high salt concentration the changes in surface charge due to the surfactant adsorption are much less, evidently $C12P^+/K^+$ exchange is important. The high salt concentration

screens the surface charge fairly well and it is difficult for the surfactant to start its adsorption. Once the adsorption starts it increases strongly over a rather small concentration range and a sharp intersection point with the Γ(0) isotherm is found. This equivalence point corresponds with the CIP of the C12PC isotherms. Before the equivalence point $C12P^+$ adsorption occurs by exchange of K^+, beyond the equivalence point the adsorbing surfactant ions bring their 'own' counter ions to compensate their charge. These adsorption mechanisms have been indicated before by Bijsterbosch [148]. The super-equivalent adsorption indicates admicelle (head-on + head-out adsorption) formation. The effect of a high salt concentration is twofold: (1) before the CIP teepee-micelles are formed (steep slope of region II of the log-log isotherm) and (2) the transition from head-on adsorbed molecules to admicelles becomes very sharp. In summary, below the CIP head-on adsorption occurs: at low salt concentration as isolated molecules, at high salt concentration as teepee-micelles, above the CIP head-out adsorption and ad-micelle formation occurs at all salt concentrations. Increasing the salt concentration increases the packing density of the adsorbed surfactants, but the values of the Γ(0) at the CMC hardly depend on the salt concentration. This indicates that the admicelles become more asymmetric and that around the CMC the screening of the surface charge is almost entirely done by surfactant.

Goloub et al. [137] also studied the adsorption behavior of C16PC and the effect of the pH on both C12PC and C16PC; in general the behavior for C16PC is very similar but the isotherms are shifted to lower concentrations, which makes it difficult to study the lower regions of the four-regions isotherms. Lowering the pH to 7 or 5 also makes the study of the isotherm more difficult because less adsorption occurs when the negative surface charge is relatively low. For a further discussion the original papers should be consulted.

The experimental results for both rutile and silica have also been compared with calculations using the Self-Consistent-Field Adsorption (SCFA) model [25, 134, 135, 137, 152, 153] (see also section 7) both SCFA theory and experiments show that the course of the

isotherms is dependent on the salt concentration and the charge characteristics of the surface. Also the SCFA model isotherms obtained at different salt concentrations show a CIP, and also here the CIP marks the point where the coulombic interaction vanishes and the surfactant orientation of the newly adsorbing molecules changes form mainly head-on to predominantly head-out. Although the SCFA theory is not perfect, it definitely can help to understand surfactant adsorption and to design experiments to gain further insight in the adsorption behavior.

The surfactant orientations in the adsorbed layer as deducted from the present analysis relate very well to experimentally observed maximums in hydrophobicity [154-157] and flotation recovery [158, 159] of particles as a function of surfactant concentration: at low adsorbed amounts the particles are hydrophobized, whereas at high adsorbed amounts the presence of head groups at the solution side make the particles more hydrophilic again [1]. The results also indicate that around the CIP the colloidal stability will be at its minimum, not only because the particles plus adsorbed layer are uncharged, but also because the particles are hydrophobized [127].

5.5. Nonionic surfactant adsorption on silica

The adsorption of nonionic surfactants of the oligo(oxyethylene) n-alkyl ether [Cn(EO)m] or oligo(oxyethylene) n-alkylphenyl ether [CnΦ(EO)m] type at the solid/aqueous interface has been the subject of much experimental and theoretical research, see the review of Tiberg et al. [129] and the cited references. The vast majority of adsorption studies of nonionic surfactants have been performed on silica. A classical set of adsorption isotherms of nonionic surfactants with different polar head group is shown in Fig. 19 [160]. From Fig. 19 it follows that the affinity increases with EO chain length, but that the adsorption level around the CMC strongly decreases.

The main experimental evidence shows that the adsorbed nonionic surfactants aggregate

strongly on hydrophilic surfaces such as silica. Oxyethylene (EO) groups bind initially to the silanol groups by hydrogen bonding and this initiates strong adsorption at the CSAC through self-assembly. Contrary to ionic surfactants, nonionics do not readily make hydrophilic particles very hydrophobic because the head-on adsorption (monolayer-type) is relatively low. With limited EO chain length pronounced adsorption on silica starts at the CSAC, because the affinity of the EO segments to the surface is relatively weak. In the case of surfactants having short EO chains relative to the length of the aliphatic chain part, bilayers are formed on the surface and when the EO chain is long the adsorbed layer consists of small admicelle type aggregates.

Denoyel and Rouquerol [161] have shown that different silicas (Spherosil, Aerosil and quartz) show quite different adsorption levels ($\mu mol/m^2$), but that the adsorption mechanism is the same on the silicas despite the great differences in adsorption. The initial anchoring of molecules is exothermal on the three samples (but with a different magnitude of the corresponding enthalpy) and the subsequent surfactant aggregation is endothermal and tends for all three surfaces towards a value equal to the micellization enthalpy. This two-step mechanism involves weak hydrophobization of the surface at low surfactant concentration followed by hydrophilzation at concentrations still below the CMC. Such a transition has been confirmed for the quartz-nonionic surfactant system by contact angle measurements [162].

For a good understanding of the behavior accurate experiments come in the first place, but modeling experiments can help to explain the behavior and reveal trends that govern the adsorption. SCFA model calculations [152] have been used to analyze the results of Levitz et al. [160, 163, 164] on the adsorption of a series of alkyl-phenol polyoxyethylene glycols on silica. This work was followed by a detailed experimental study of the adsorption of C12(EO)6, C12(EO)25 and the oligomer (EO)122 on different silicas [153]. To be able to apply the various techniques, different silica surfaces had to be used. To some extent this

was a disadvantage, but by comparing the results, trends emerged, and these could be studied with the 1D and 2D versions of the SCFA theory and in this way a better insight was gained. Recently the SCFA theory has been applied to investigate the experimentally observed pH and salt concentration dependence of Cn(EO)m adsorption to silica [165]. The parameter choices and some aspects of the model were refined as compared to the older SCFA modeling; the calculations contributed to detailed insight in the mechanisms of the pH and salt effects. At high ionic strength, the solvent quality for the surfactant head groups is affected, which changes both bulk solution and adsorption behavior of the surfactant. Nonionic surfactants adsorb above the CSAC, which is a function of surfactant and surface properties. Therefore, the CSAC varies with both the ionic strength and the pH. The model predicts that with increasing ionic strength, the CSAC will first slightly increase but then drop substantially. The charge on the surface is pH dependent, and as the head groups bind through H-bonding to the silanol groups, the CSAC increases with increasing pH. The predictions follow experimental findings, which shows that the molecularly realistic SCFA model can reveal a rich interfacial behavior.

6. Surfactant adsorption to clays

6.1 General aspects and outline

An analysis of surfactant adsorption on clays is faced with several difficulties: (1) clay surfaces have basal plates and edges that make the surfaces patchwise heterogeneous, (2) for swelling clays surfactants may also intercalate between the layers and (3) the anionic surfactants tend to precipitate in the presence of multivalent cations. The patchwise nature of the clay surface is a fact that has to be considered in all cases of surfactant adsorption to clays. For expanding clays the adsorption is far more complicated than for non-expanding clays. For instance, the adsorption of anionic (SDS), nonionic (Triton X100) and cationic

(C18TAB) surfactants did not modify the X-ray diffraction diagrams of kaolinite and sepiolite (non-expanding clay types), but the interlayer space of montmorillonite (expanding clay type) increased through nonionic and cationic surfactant adsorption [166]. When the interlayer spacing expands upon surfactant adsorption the adsorption capacity becomes a function of the amount adsorbed and this leads to complex shaped adsorption isotherms that do not follow classical behavior. A further complication with anionic surfactant adsorption is that cations bound to the clay surface may exchange with the counterions of the anionic surfactant and this can lead to precipitation of the anionic surfactant, especially when the clay charge is (partially) compensated by multivalent cations [167]. Furthermore, at relatively low pH leaching of Al^{3+} ions from the clay may occur and can be promoted by the presence of anionic surfactants through Al^{3+} complexation with the anionic surfactant followed by surfactant precipitation [168-170]. Any precipitation of the surfactant obscures the pure adsorption results.

The most studied non-expanding clay with respect to surfactant adsorption is kaolinite and cat-, an- and nonionic surfactant adsorption to kaolinite will be discussed in the next sections, with emphasis to cationic surfactants. Subsequently, surfactant adsorption to montmorillonite will be discussed at surfactant concentrations up to the CMC. The situation of surfactant binding to expanding clays to produce organo-clays for various specific applications is a field in itself. For reviews of this field we refer to [171-174] and to some original papers [175-178].

6.2 Cationic Surfactant adsorption on kaolinite

De Keizer et al. [143, 179, 180] have made a very thorough study of the adsorption of cationic surfactant adsorption (C16TAB and C12PC) on kaolinite (Sigma Chemicals) by investigating the adsorption behavior at different pH values and salt concentrations as a function of temperature. Adsorption isotherms (lin-log) of C16TAB and C12PC at different

electrolyte concentrations show a well-defined CIP where the adsorption is independent of the electrolyte concentration [143, 179], see Fig. 20. The CIP coincided with the IEP of the particles with adsorbed surfactant, indicating that at this point the surface charge is compensated by the surfactant charge, including any counter-charge that may be present within the slip layer. The presence of a CIP and the correspondence with the IEP seems to be a general property for adsorption of organic ions on a surface with an opposite charge. Very similar behavior occurred for the surfactant adsorption on silica and rutile (metal oxides). Also for kaolinite head-out (second layer) adsorption driven by hydrophobic attraction starts after the CIP. This view is supported by the effect of the temperature on the adsorption. Below the CIP, adsorption is independent of temperature, whereas after the CIP it has a maximum as a function of temperature. With increasing temperature the adsorption changes from endothermic to exothermic, as for micellization. The CIP occurred for both surfactants at about 32 μmol/g, roughly 40% of the maximally attained value. In the CIP=IEP the charged surfactant groups just compensate the surface charge. Therefore, the above value may also be compared with the cation-exchange capacity (CEC). The CEC according to the silver-thiourea method was 57 μmol/g (exchange on plates plus edges), while the CEC with the ammonium acetate method at pH 7 was 30 μmol/g (cation exchange on the plates). This provided evidence that C16TAB and C12PC adsorption took place essentially on the plate surfaces.

In part 3 of the study [180] the investigations were complemented with micro-calorimetric measurements of the adsorption enthalpies of C12PC on Na-kaolinite at two electrolyte concentrations (5 and 100 mM NaCl) and three temperatures (6, 20 and 60 °C). Curves of cumulative adsorption enthalpies against amount adsorbed show a break around the CIP adsorption. The curves are about linear both before and after the break, and result in partial molar adsorption enthalpy values that are independent of surface coverage, confirming that the surface is homogeneous with respect to the C12PC adsorption. This is

additional evidence that the surfactant is hardly adsorbed on the edges. The isotherms are independent of temperature up to CIP coverage, implying a zero isosteric adsorption enthalpy, but upon formation of the second layer (head-out mode) the adsorption has a maximum at about 23 ^{o}C, implying a transition from an endothermic to an exothermic process. The calorimetric adsorption enthalpies change sign at T ≈ 24-30 ^{o}C. In this respect, the adsorption process is very similar to micellization [181]. The electrolyte concentration has a minor effect on the adsorption enthalpies of the first (head-on adsorption) and second (head-out adsorption) layers. The directly measured heats agree qualitatively with the isosteric heats.

In the last paper [180] the isotherms were also modeled with a simple two-layer model based on the Frumkin-Fowler-Guggenheim model that takes into account both the interaction with the surface and the lateral interaction, therefore the standard Gibbs energies have two contributions: $\Delta G^0_{surface}$ and ΔG^0_{lat}. For the first layer it is assumed that the molecules adsorb head-on to the mineral surface with their tails at the solution side, for adsorption in the second layer the 'surface' is made-up of the tails of the first layer and the molecules adsorb head-out with their tails contacting the new 'surface'. Since the adsorption on kaolinite particles involves chemical and electrical contributions, the changes in the standard Gibbs energies can be written as $\Delta G^0 = \Delta G^0_{chem} + \Delta G^0_{el}$. ΔG^0_{el} accounts for the generic interactions due to the 'smeared-out' electrostatic potentials, ΔG^0_{chem} contains chemical (specific), hydrophobic and 'local' electrostatic interactions (local self-atmosphere potentials). Because of their special nature and important role the hydrophobic attractions are separately indicated. The standard Gibbs energy of adsorption in contact with the surface (layer: 1, surface: s), $\Delta G^0_{1,s}$ can then be written as $\Delta G^0_{1,s} = \Delta G^0_{1,s\text{-spec}} + \Delta G^0_{1,s\text{-hydrophobic}} + \Delta G^0_{1,s\text{-el}}$); $\Delta G^0_{1,s}$ becomes less negative with increasing electrolyte concentration, because salt addition decreases the electrostatic attraction part $\Delta G^0_{1,s\text{-el}}$. The effect of salt addition on $\Delta G^0_{1,s}$ is opposite to that on $\Delta G^0_{1,lat}$, because for $\Delta G^0_{1,lat}$

(=$\Delta G^0_{1,lat\text{-}hydrophobic}$ + $\Delta G^0_{1,lat\text{-}el}$) the salt effect is favorable (repulsion between surfactant head groups decreases). The two salt effects compensate each other at the CIP. The $\Delta G^0_{2,s}$ (second layer) values are hardly dependent on the salt level, because the second layer starts when the particle potential is close to zero (CIP ≈ IEP); therefore, to a good approximation, $\Delta G^0_{2,s} \approx \Delta G^0_{2,s\text{-}chem} \approx \Delta G^0_{2,s\text{-}hydrophobic}$, the standard hydrophobic attraction between layer 2 and layer 1 (which is the new s). However, the lateral attraction in layer 2, $\Delta G^0_{2,lat}$, (=$\Delta G^0_{2,lat\text{-}hydrophobic}$ + $\Delta G^0_{2,lat\text{-}el}$) also contributes and increasing the salt concentration from 20 to 100 mM causes a decrease of $\Delta G^0_{2,lat\text{-}el}$ as a result of a decrease in the electrostatic repulsion between the head groups and, in turn, this increases net attraction and hence the adsorption.

The sum ($\Delta G^0_{1,s}$ + $\Delta G^0_{1,lat}$) turns out to be hardly temperature dependent. This shows that the independence of the temperature of the adsorption in the first layer is caused by internal compensation. As a result, according to the Gibbs-Helmholtz equation, $\Delta H^0_{1,s} \approx 0$. However, for the second layer the sum ($\Delta G^0_{2,s}$ + $\Delta G^0_{2,lat}$) is smaller at 20 °C than at 60 ^oC, in line with the exothermic nature of the process over this temperature range. At 20 °C the adsorption enthalpies, $\Delta H_{1,s}$, are much smaller than $\Delta G^0_{1,s}$ indicating that entropic contributions dominate at both electrolyte concentrations. Apparently, for both layers the enthalpies of hydrophobic bonding of the tails and those due to interactions of the head group and/or change of hydration at the surface compensate. At 60 °C the entropy has decreased, but the (exothermic) enthalpy renders the standard Gibbs energies virtually temperature independent. This is another example of enthalpy entropy compensation which is characteristic for hydrophobic bonding and which has also been found for the solubility of alkanes in aqueous solution [182, 183].

Xu and Boyd [184] have obtained very similar C16TAC isotherms (lin-log) on kaolinite (Source Clay Minerals Repository, University of Missouri, Columbia) at pH 6.5 and two salt concentrations (2 and 42 mM), see Fig. 21. The (C)IP of the isotherms is found at about 20 μmol/g (0.5CEC). The reported CEC value at pH 6.5 was 40 $\mu mol_e/g$; this would imply

that about 50 % of the CEC is due to the plate surfaces. Although the authors measured electrophoretic mobilities and dispersion stability of montmorillonite, it is a pity that they did not state such results for kaolinite, because this might have shown the correspondence of their (C)IP with the IEP or the minimum in dispersion stability.

Wang et al. [185] studied the adsorption of a series of alkyl-trimethylammonium bromides ($RR_1N(CH_3)Br$) with different chain lengths on sodium kaolinite (Source Clay Minerals Repository, University of Missouri, Columbia) by micro-electrophoresis and adsorption isotherms. The isotherms (lin-log) were measured over a relatively large concentration range and have a similar shape than those measured by de Keizer et al. [143], Mehrian et al. [179] and Xu and Boyd [184]. At very low concentrations the adsorbed amount increased only slowly with increasing surfactant concentration; the second stage of adsorption occurred at higher surfactant concentrations below the CMC and a sharp increase of adsorption was observed. Adsorption in the second stage is accompanied by a sharp change in the ζ-potential, charge reversal and second layer formation. The third region is located around the CMC with a constant adsorption above the CMC, where the monomer concentration and the adsorption remain constant. For all surfactants the amount adsorbed at the IEP is about 10-12 μmol/g. Though kaolinite came from the same source as that of Xu and Boyd [184], this value is about half the value reported by Xu and Boyd [184]. The CEC of the kaolinite is not reported in the paper so no further comparison can be made between the adsorption at the IEP and the CEC. An increase in the number of CH_2 groups in the shorter alkyl chain of the double chain surfactant, or the introduction of another kind of alkylgroup (phenyl group), was found to have much less effect on the adsorption behavior than changing the length of the alkyl chain in the single-chain surfactants. This corresponds with the trend in CMCs and with the findings of Böhmer et al. [135] for surfactant adsorption on rutile. Intra-molecular association reduces the effective hydrophobicity of the shorter chains in the double-chain surfactants.

A further study on chain architecture and adsorption on kaolinite was made by Qi et al. [186] who compared the adsorption of C16TAB with a C16-2-C16 gemini surfactant of similar structure (2 CH_2 segments as spacer) at pH 6 and a ionic strength of about 0.02 M salt. Compared to C16TAB the affinity of the gemini surfactant was higher and the isotherm was steeper, but the maximum adsorptions in μmol/g at the CMC were rather similar. The maximum adsorption was about 1.4CEC, so well above the charge compensation point, which provides evidence for the presence of the second layer.

An alternative approach to detect the onset of the head-out adsorption and the ratio head-out / head-on adsorption (maximum adsorbed amount in the second ‘layer’ relative to that in the first ‘layer’) has been introduced by Li et al. [187-189]. The somewhat simplified notion of the adsorption behavior is that first complete cation exchange occurs due to head-on surfactant adsorption (maximum first layer surfactant adsorption = CEC) and that subsequently further surfactant is adsorbed in the head-out mode by hydrophobic attraction (second layer adsorption). In the absence of added background electrolyte, surfactant bound head-on by ion exchange will loose its counterion and the cations that were adsorbed to the negative sites on basal planes will be released. For the second layer, formed by hydrophobic attraction, the mechanism is different: it leads to head-out surfactant adsorption and these surfactant ions will still require counter ions in the diffuse layer to compensate their charge and as the surfactant counterion is the only negative ion present except for some OH^-, the surfactant ion adsorption will be accompanied by adsorption of its counterion. Thus, by comparing the surfactant adsorption with the counterion release from the clay (or with the CEC) and with the surfactant counterion co-adsorption a distinction can be made between first layer and second layer surfactant adsorption. This type of investigation goes back to the classical study of Bijsterbosch [148] of the counterion binding to C16TAB and C12TAB on silica.

Li and Bowman [187] studied kaolinite (KGa-1; Source Clay Minerals Repository, University of Missouri, Columbia, MO) and a zeolite, clinoptilolite, and observed (1) that the maximum adsorption of C16TAX (X= Br^-, Cl^- or HSO_4^-) was in all cases larger than the CECs of the minerals, which implied that the adsorption was in excess of ion exchange and (2) that the maximum adsorption increased in the order $HSO_4^-<Cl^-<Br^-$ which showed the surfactant counterion effect for the adsorption in the second layer. At the adsorption maximum the ratio surfactant counterion adsorption / surfactant adsorption ranged from 0.33 to 0.55 in going from HSO_4^- to Br^-, which is a clear indication of the formation of a second layer and that the counterion affects the amount of surfactant that is adsorbed head-out.

In a subsequent study Li and Gallus [188, 189] investigated C16TAB adsorption on two kaolinites, KGa-1b and KGa-2 (Clay Mineral Repository; Purdue University, West Lafayette, IN, USA); the CECs determined by an ammonia method were 30 and 37 mmol/g, respectively. Relatively crude surfactant and counterion isotherms were measured, together with the accumulative cation desorption The discussion of the results is not always convincing, but the cation release as function of the surfactant adsorption provides clear information about the situation up to the CMC. Around the CMC the maximum amounts of $C16TA^+$ adsorbed of about 58 and 85 μmol/g were reached and the corresponding amounts of cation released were about 18±2 $\mu mol_e/g$ and 11±2 $\mu mol_e/g$ for KGa-1b and KGa-2, respectively. However, at about 10 μmol/g surfactant adsorption the total cation release was already about 90% of the maximum release, and at 30-40 μmol/g nearly all the cations were released. This indicates that the adsorption in the second layer started at adsorption values of about 10-15 μmol/g; upon further surfactant adsorption a small fraction of the ions will still be head-on adsorbed, but the majority of surfactant ions was adsorbed head-out (second layer). Therefore, the head-out adsorption started at surfactant concentrations clearly below the CMC and the contribution of the head-out adsorption (by hydrophobic attraction) was

far greater than that of the head-on adsorption (by cation exchange) and this means that asymmetric admicelles were formed. In the kinetic experiments the adsorption of bromide ions differed by about 15 μmol/g from the surfactant adsorption, which is close to the above estimate of the head-on adsorption. FTIR measurements showed a consistent shift of C–C symmetric and asymmetric vibration from high to low frequencies, which supported the view of a transition from head-on adsorbed monomers to admicelles as the C16TAB adsorption increased.

Li and Gallus [189] also investigated the effect of surfactant chain length (C12TAB and C16TAB) and surfactant mixtures on kaolinite. As expected the surfactant chain length had no effect on the head-on adsorption (= cation exchange or first layer adsorption), but it did affect the adsorbed amount in the head-out mode (second layer). For C16TAB the head-out adsorption was considerably larger than the head-on adsorption, but for C12TAB the situation was reversed. For the 50/50 mixture the adsorbed amounts in head-on and head-out mode were comparable. Regardless of how much alkyl-ammonium adsorbed at the adsorption plateau, the amounts of cations desorbed were 15-18 $\mu mol_e/g$ for KGa-1b and 9-11 $\mu mol_e/g$ for KGa-2, respectively. Therefore, the CEC of KGa-1b and KGa-2 as determined by alkyl-ammonium adsorption/cation desorption will be 15-18 $\mu mol_e/g$, and 9-11 $\mu mol_e/g$, respectively. These values are much less than the values determined by an ammonia method [190] or the reference values listed on Clay Mineralogical Society website (http://cms.lanl.gov/ chem.htm). However, the value of cations desorbed from KGa-1b through surfactant adsorption was similar to the CEC values of KGa-1 determined by a complexation method using copper bisethylenediamine and copper triethylenetetramine in the presence and absence of the buffer tris(hydroxymethyl)- aminomethane [191]. Comparing this with the results of Mehrian et al. [179] would imply that the difference should be related to the CEC of the plates as compared to the total CEC (plates + edges).

Recently, Malek and Ramli. [192] investigated C16PB on kaolinite with respect to antibacterial activity. Based on X-ray diffraction they first concluded that the structure of kaolinite was not affected by the surfactant adsorption. Although the interpretation of the results by the authors contains several errors, it is interesting that the antibacterial activity started after the IEP, i.e., when the surfactant started to adsorb in the head-out mode that made the overall particle charge positive, which must have caused the action of $C16P^+$ against the bacteria cells.

6.3 Anionic surfactant adsorption on kaolinite

Adsorption of anionic surfactants to kaolinite also occurs and for this adsorption the amphoteric edge sites are crucial. The point of zero net proton charge of the edge of kaolinite depends on the ionic strength and kaolinite composition, and is found to be in the pH range 4 to 7 [193]. Therefore, the net proton charge of the edge is positive at relatively low pH and negative at relatively high pH. The investigations of anion adsorption have mainly been carried out at relatively low pH, which can lead to some dissolution of kaolinite and surfactant precipitation so that next to surfactant adsorption also surfactant (surface) precipitation occurs. The total amount of surfactant removed from the solution is therefore called the *surfactant abstraction*. Somasundaran et al. [168-170, 194, 195] have investigated these aspects in detail in their studies of sodium dodecyl benzenesulfonate and sodium dodecyl sulfonate abstraction by kaolinite. Results obtained under various ionic strengths and pH values indicated a complex abstraction mechanism involving surfactant adsorption by ion exchange and hydrophobic attraction and metal activated adsorption and surface precipitation of surfactant, all depending on the solution pH. The precipitation of sulfonate with dissolved mineral species results in an adsorption maximum in micellar solutions. The dissolution of kaolinite and the resulting solution speciation can be found in [169]. Results for the abstraction of sodium dodecyl benzenesulfonate on Na-kaolinite

(Georgia kaolinite from the clay repository at University of Missouri subjected to an ion-exchange treatment) as a function of pH at 0.1 M NaCl and 25 ^{o}C as obtained by Siracusa and Somasundaran [195] are summarized in Fig. 22. The authors made the following remarks concerning the abstraction (adsorption) mechanisms. (1) At acidic pH levels below pH 3.7 significant precipitation of the dodecylbenzene sulfonate with cationic dissolved aluminum species occurs and subsequent re-dissolution of the aluminum-sulfonate precipitates above the CMC produces an abstraction maximum. (2) At or near pH 4.4 (the pznpc of the sample) a reduction in the concentration of dissolved cationic aluminum species results in decreased precipitation such that the adsorption maximum is no longer observed. However, some contribution of aluminum-sulfonate precipitation is still present. (3) At pH levels above pH 4.4, both in the neutral region (pH 7.9) and the alkaline region (pH 10.8), incongruent dissolution of kaolinite can result in phase transformations to gibbsite; therefore, adsorption occurs at levels governed not only by the surface of the kaolinite, but also by that of gibbsite.

Very similar pH dependent results have been obtained by Torn et al. [196] for the dodecylbenzenesulfonate / Na-Kaolinite (Sigma Company) system at 0.01 M NaCl and 25 ^{o}C, but in this case the abstraction maximum occurred at pH 4.8-4.9. Proton titrations of the kaolinite sample suggested a pznpc of about 7 [197], which is higher than the pznpc of the kaolinite used by Siracusa and this might explain the shift of the maximum. Torn et al. [196] concluded that both electrostatic and hydrophobic interactions play a role in the adsorption of the sulfonate surfactant to kaolinite.

Poirer and Cases [167] have studied the effect of chain length (C14 and C12) and the presence of a benzene ring in the apolar chain (C10Φ) of the sulfonate surfactants on their adsorption to kaolinite. The adsorption isotherms at 28 ^{o}C showed a sharp increase in abstraction close to the saturation concentration of the surfactants, which was due to the precipitation of the sulfonates. The isotherms were shifted toward lower equilibrium

surfactant concentrations as the hydrophobic moiety of the surfactant increased. The shifts were due to the increase in hydrophobic attraction and corresponded with the differences in CMC with surfactant structure. The benzene ring was about equivalent to three methylene groups. Del Hoyo et al. [166] investigated the adsorption of SDS on kaolinite by FTIR measurements and observed modification of the CH stretching wavenumbers of SDS indicating a re-arrangement of the adsorbed surfactant molecules and hydrophobic attraction between the hydrocarbon chains of the surfactant.

How the structure of the adsorbed surfactant layer evolved as a function of the surfactant concentration has not been discussed in the above mentioned studies, but most likely also in this case head-on adsorption occurs at low adsorption values and head-out adsorption at surfactant concentrations closer to the CMC.

6.4 Nonionic surfactant adsorption on kaolinite

The adsorption of nonionic surfactants on kaolinite resembles that on silica. Also on kaolinite the surfactant monomers adsorb by hydrogen bonding between the polyoxyethylene segments and the hydroxyl groups on the surface. In addition interaction may occur with the hydrated cations on the siloxane basal plate as is observed for montmorillonites [198]. The energy involved in the initial adsorption process is somewhat stronger than with silica. Similar as for silica, the energetic balance at the beginning of the adsorption is exothermic, because contacts between the surface and the ethoxy segments of the polar chains are enthalpically favorable. When the coverage of the surface increases, the enthalpy decreases down to the appearance of an endothermic regime. In the latter regime the molar enthalpy of adsorption is comparable to that of micellization in aqueous solution and this is characteristic for the presence of surfactant admicelles (or two adsorption layers) on the surface [161]. The temperature dependence of the adsorption [161, 199] is in agreement with this adsorption mechanism. Two steps can be observed along the adsorption

isotherms [144, 161, 199, 200], some typical isotherms are depicted in Fig. 23. The first pseudo-step occurs at low coverage and is followed by a rapid but gradual rise of the adsorption up to the CMC, somewhat above the CMC the adsorption plateau is reached. Due to the polydispersity of most nonionic surfactants the plateau starts somewhat beyond the CMC. The second step corresponds with a cooperative adsorption mechanism and the formation of admicelles. The relative importance of the first step increases with the EO chain length (stronger adsorption), but the adsorption level at the CMC strongly decreases with EO chain length because the large head group makes it more difficult for the apolar chains to associate by hydrophobic attraction. The plateau adsorption is reached at higher surfactant concentrations for longer EO chains. The reason for this is that when oxyethylene length rises, the monomer solubility in water is higher and, thus, the CMC is also higher.

For different kaolinite samples (Supreme, Charentes, Aldrich, Sigma) the isotherms have a similar shape, but the adsorption levels of the first step and the final plateau around the CMC differ [200], which implies that the structural organization of the surface aggregates is dependent on the surface heterogeneity of the kaolin crystals. Based on the characteristics of the kaolinite samples and the adsorption results no final conclusion could be reached regarding the role of the edge surfaces and the basal surfaces.

6.5 Anionic surfactant adsorption on montmorillonite

The adsorption of surfactants to montmorillonite differs from that of kaolinite for two reasons. (1) Kaolinite has two different basal plate surfaces and a relatively large edge surface, while the basal plate surfaces for montmorillonite are the same and the edge area is relatively small. (2) Montmorillonite is an expanding clay-type, which implies that the adsorption capacity may increase with increasing surfactant adsorption, depending on the conditions. Anionic surfactant adsorption will mainly occur on the edges and the anions will not easily intercalate between the clay platelets, this and the relatively small edge area of

montmorillonite make anionic surfactant adsorption on pure montmorillonite relatively unimportant. Similarly as for kaolinite, adsorption of anionic surfactants to montmorillonite is complicated by surfactant precipitation when multivalent ions are present as counterions of the negative clay charge and by partial clay dissolution and precipitation phenomena as described for kaolinite. For instance, Yang et al. [201] have shown that the abstraction (adsorption + precipitation) of sodium dodecylbenzene sulfonate (SDBS) by montmorillonite was affected by the presence of Ca^{2+} ions. They observed that: (i) SDBS was abstracted significantly by montmorillonite saturated with Ca^{2+}, but little by Na-saturated montmorillonite; (ii) the amount of SDBS abstracted by Ca-montmorillonite was enhanced by NaCl; and (iii) no significant intercalation of SDBS into Ca-montmorillonite was observed by X-ray diffraction analysis. Therefore the abstraction for the Ca-montmorillonite was largely due to surfactant precipitation with Ca released by ion exchange.

6.6 Cationic surfactant adsorption on montmorillonite

The binding of cationic surfactants on montmorillonite is dominated by adsorption at the plate surfaces, therefore, for these surfactants adsorption in the interlayers plays an important role. The adsorption behavior at the external surface of montmorillonite will be similar to that on silica and/or kaolinite, but the adsorbed amount and the conformation of adsorbed molecules in the interlayer space are affected by the two neighboring surfaces and the distance between these surfaces (the interlayer distance). In fact one deals with adsorption in a narrow slit pore with the complication that the slit width increases step wise with increasing surfactant adsorption. The interaction between the platelet surfaces and, therefore, the interlayer distance, are affected by the surfactant adsorption and vice versa. In other words, the interlayer distance, the adsorbed amount of surfactant and the conformation

of the adsorbed surfactant molecules are mutually related and this makes the adsorption behavior complicated.

To unravel cationic surfactant adsorption in practice, next to information on the adsorbed amount, at least, also information is required on the interlayer distance and/or the conformation of the adsorbed surfactant molecules in the interlayer. Somewhat similar to Mehrian et al. [180], Pan et al. [202] measured C12TA+/C12TAB isotherms and adsorption enthalpies for Na- and Al-montmorillonites in a wide pH range; the results support the two-stage adsorption above the IEP. Very illustrative experimental results on the adsorption of hexadecyl-trimethylammonium ($C16TA^+$ = HDTMA) on montmorillonite (Wyoming montmorillonite, SWy-1; CEC = 900 $\mu mol_e/g$) and kaolinite (Na-kaolinite, CEC = 40 $\mu mol_e/g$ at pH 6.5) are provided by Xu and Boyd [184, 203]. They studied the adsorption by combining adsorption isotherms, electrophoretic mobility, colloidal stability and X-ray diffraction to determine the effects of clay type and solution composition on the adsorption of cationic surfactants and to unravel the orientation and/or conformation of the adsorbed surfactants on the external and internal (interlayer) surfaces and the dispersion stability of surfactant-clay complexes. Some of their results are depicted in Figs. 24 and 25. Fig. 24 shows the isotherms of C16TAC on three different clays; isotherms provide information on the total surfactant adsorption. With a single isotherm further information is required to make a distinction between the adsorptions on external and internal surfaces. The C16TAC adsorption isotherm on Ca-montmorillonite (Ca-SWy-1) follows the ‘normal’ isotherm pattern and is similar to that on Na-kaolinite (non-swelling), but the adsorption isotherm on Na-montmorillonite (Na-SWy-1) differs from the other isotherms with its peculiar S-shape at relatively low C16TAC adsorption (< 1CEC). The fact that the shape of the C16TAC isotherms on Na-kaolinite and Ca-SWy-1 are rather similar indicates that the swelling of C16TA/Ca-SWy-1 due to surfactant adsorption is negligible small. The peculiar S-shape of the of C16TA/Na-SWy-1 system with different adsorption values for one equilibrium

concentration must be due to interlayer expansion due to surfactant adsorption. The behavior of the C16TA+/Na+-montmorillonite clay is further illustrated in Fig. 25 to provide proof for this behavior.

The $C16TA^+$/C16TAC isotherm on Na-SWy-1 (Fig. 25a) can be divided into four distinct regions. Region 1 (0-0.75 CEC) is non-monotonic and characterized by an equivalence of Na release and $C16TA^+$ adsorption, resulting in superimposable $C16TA^+$ adsorption and cation release curves. In regions 2 and 3, the adsorption isotherm is monotonic and the adsorbed amount of $C16TA^+$/C16TAC is greater than the corresponding Na^+ release; this implies that the head-on adsorption (ion exchange) slows down and the head-out adsorption increases (difference between the $C16TA^+$/C16TAC and Na^+ isotherms). The head-out adsorption is due to surfactant adsorption to already adsorbed surfactants by hydrophobic attraction between the surfactant tails. The slope of the $C16TA^+$/C16TAC adsorption isotherm in region 3 is much larger than in region 2, which indicates cooperative adsorption in region 3. Moreover, the difference between the $C16TA^+$/C16TAC and the Na isotherms increases strongly, indicating that head-out adsorption to already adsorbed surfactants increases much stronger than the ion exchange. At the CMC the $C16TA^+$/C16TAC and Na isotherms reach a plateau (region 4).

Fig. 25b shows the behavior of the electrophoretic mobility with increasing surfactant adsorption; it reflects the situation at the external surface of the clay. In region 1 Na^+ exchanges for $C16TA^+$, therefore it is to be expected that the electrophoretic mobility of the C16TA/Na-SWy-1 particles remains the same as for homoionic Na-SWy-1; this is indeed the case. In region 2 (0.75 CEC to 1.0 CEC) the net particle charge is relatively low; more $C16TA^+$ is adsorbed than Na^+ is released and the electrophoretic mobility increases rapidly, it passes the IEP (particle charge changes sign) and reaches a maximum value at 1CEC, the end of region 2. The fact that the IEP is reached before $C16TA^+$ (ads) = CEC implies that the Na+ ions also contribute to the charge neutralization at the IEP. The fact that the

mobility changes sign confirms that the surfactant adsorption is super-equivalent and this implies that beyond the IEP head-out adsorption by hydrophobic attraction starts. The mobility is very sensitive to changes in charge around the IEP where the particle charge is low, therefore the information in region 2 is directly related to the charge situation of the clay complex and provides valuable information. In region 3 the mobility decreases slightly and stays constant in region 4. Somewhat outside the IEP (zeta potentials > 50 mV) retardation and relaxation effects can easily lead to only small changes in mobility with particle charge [204]. Moreover, the changing particle (aggregate) sizes (see the stability) further complicate the situation. Therefore, further interpretation of the mobilities in regions 1 and 3 or 4 is not feasible.

The adsorption behavior at the external surface was further investigated by dispersion stability measurements (optical density of the clay suspension), see Fig. 25b. The degree of clay dispersion decreases with increasing surfactant adsorption till the IEP is reached. This is due to (i) the decrease of the net negative charge of the C16TA/Na-SWy-1 particles, so that the electrostatic repulsion between the particles decreases and (ii) at the same time the hydrophobicity of the particles increases because the surfactant tails point to the solution (ion exchange and head-on surfactant adsorption) and this increases the inter-particle (hydrophobic) attraction. The stability has a minimum around the IEP because the net particle charge is zero and the amount of unscreened surfactant tails pointing towards the solution is at its maximum, which makes the particles maximally hydrophobic. Beyond the IEP further $C16TA^+$ adsorption in the head-out mode makes the $C16TA^+$-SWy-1 particles positive and increases the particle hydrophilicity, together this results in a strong increase in the dispersion stability.

In Fig. 25c d(001)-spacings obtained by X-ray diffraction are shown for water saturated, partially wet (dried at 95% relative humidity, RH), and dry (dried at 5% RH) $C16TA^+/Na^+$-SWy-1 as function of the $C16TA^+$ adsorption. These results reflect the

situation at the interlayer surfaces. The clays are nearly identical at high $C16TA^+$ adsorption, but completely different at low $C16TA^+$ loadings (< 1CEC). As the $C16TA^+$ loading increased from 0.1 CEC to 0.75 CEC (region 1), the d-spacings of wet (100% RH) clay samples ($C16TA^+/Na^+$-SWy-1) increased gradually from 1.76 to 2.21 nm. No further change in the d-spacing was observed at higher $C16TA^+$ adsorption. Partial air-drying (95% RH) or drying (5% RH) of the clays decreases the d-spacings and results in stepwise d-spacing vs. $C16TA^+$ loading curves. At loading levels up to 0.3 CEC, the d-spacing was around 1.4 nm. The first step occurs between 0.3 and 0.5 CEC and raises the spacing to about 1.8 nm, the second step occurs at $C16TA^+$ loadings of 0.5 to 0.8 CEC leads to a final d-spacing of about 2.2 nm. The steps are sharp for the dry clay. The step-wise behavior of the d-spacing indicates that the conformation of the adsorbed surfactant ions changes stepwise. Confining the interlayer to lower values of the d-spacing by drying allows only specific surfactant conformations and sudden conformational changes result. However, at 100% RH the d-spacing increases gradually, therefore the capacity for surfactant adsorption increases gradually and the actual conformation of the adsorbed surfactant is more random than for the (partially) dried clays.

With the C16TA/Ca-SWy-1 system and adsorption values of about 0.25 CEC to 0.8 CEC the d-spacing stays around 1.8 nm and then increases gradually with higher loadings to 2.16 nm (not shown). The higher charge of the Ca^{2+} ions keeps the two interlayer surfaces better together and only close to $C16TA^+$ adsorption values = 1CEC some swelling is observed and the isotherm has a similar shape as the $C16TA^+$ isotherm to kaolinite. The peculiar shape of the $C16TA^+$ isotherm for Na-SWy-1 and the ‘normal’ shape of the isotherm for Ca-SWy-1 is thus due to the fact that in the adsorption range 0-0.8 CEC swelling occurs for Na-SWy-1 and no swelling for Ca-SWy-1. Due to swelling and a concomitant change of the adsorption capacity in the case of the C16TA/Na-SWy-1 system different adsorption values can occur at one equilibrium surfactant concentration.

When for the C16TA/*Na*-SWy-1 system the ionic strength is increased by increasing the NaCl concentration, the isotherms gradually change to the 'normal' shape at about 42 mmol/L NaCl. At this ionic strength the d-spacing stays about constant up to 0.8 CEC. Around loadings close to the CEC the isotherms at different NaCl concentration intersect and after the intersection point (loadings larger than the CEC) the adsorption increases with increasing NaCl concentration. The residual water in the interlayer allows salt ions to enter the interlayer, and similarly as at the external surface, this leads to an increased screening of the lateral repulsion between the charged head-groups of super-equivalently bound surfactant ions and an increase in adsorption. For the same reason also surfactant counterions that partially associate with the surfactant ions increase the surfactant adsorption for loadings beyond the CEC. The NaCl concentration has little effect on the C16TA/*Ca*-SWy-1 system at $C16TA^+$ loadings up to the CEC and after the CEC the behavior is similar to than of the C16TA/Na-SWy-1 system.

Concluding, based on the results of Xu and Boyd [184] it follows that the swelling of expanding clays due to cationic surfactant adsorption depends on the strength at which the clay layers are held together. It is well known that the attraction between the clay layers depends on the degree of isomorphic substitution, the valence and size of the counterions of the clay charge and the ionic strength [205]. Therefore, also the swelling of clays due to cationic surfactant adsorption is depending on these variables. Swelling occurs when the surfactant isotherm shows a peculiar S-shape for surfactant loadings up to 0.8 CEC; the adsorption capacity is a function of the adsorbed amount and this makes it possible that different adsorption values may occur at one equilibrium surfactant concentration. The surfactant adsorption at the external surface of expanding clays shows a very similar behavior to that at kaolinite. Up to loadings close to the IEP of the external particle surface (roughly corresponding with a loading approaching 1 CEC) the surfactant adsorption occurs by ion exchange and head-on adsorption. Beyond the IEP of the external surface (or

loadings ≥1 CEC), adsorption of the surfactant by hydrophobic attraction starts and this adsorption increases strongly with further surfactant loading. The adsorption beyond the 1 CEC increases with increasing ionic strength and is sensitive to the kind of surfactant counterion. The clay stability is strongly affected by this adsorption behavior. The minimum dispersion (colloidal) stability occurs at the IEP of the external surface where the net particle charge is zero and the hydrophobicity of the particles is at its maximum due to the unscreened surfactant tails protruding into the solution. The results of Xu and Boyd are largely supported by Tahani et al. [206] who investigated the adsorption of the benzyldimethyl dodecyl ammonium chloride on a Na-montmorillonite by various techniques.

An interesting complementary study, specifically oriented towards the structural characteristics of the surfactant adsorbed in clay interlayers, has been presented by Zhu et al. [207] who studied the interlayer aggregates of $C16TA^{+}$/C16TAB in a bentonite (> 95% pure montmorillonite, < 5% quartz; CEC 1084 $\mu mol_e/g$) for different surfactant loading levels (0.20 CEC to 2.56 CEC), using *in situ* X-ray diffraction (XRD) and Fourier Transform Infra Red (FTIR) spectroscopy on samples in the hydrated state. For the dried and hydrated organo-bentonites, the measured basal spacings depended on surfactant loadings and indicated that the water molecules present play an important role in regulating the microenvironment, even at high surfactant loads. In the presence of water the surfactant tails formed aggregate structures in the interlayer space due to hydrophobic attraction. As a result, the values of the d001 spacing increased gradually with increase in surfactant loading. *In situ* FTIR spectra indicated that the surfactant intercalated at high loading had a more ordered and compact structure than the associates at low surfactant sorption density: the surfactant state in wet organic bentonites changed from a liquid-like (disordered) state to a solid-like (ordered) state.

Based on the FTIR results, the XRD data, and the dimensions of the C16TAB surfactant in moist organo-bentonites with different surfactant loading, Zhu et al. proposed that $C16TA^+$/C16TAB arrangements in wet organo-bentonites were different from that in dried organo-bentonites. For the wet organo-bentonites the interlayer spacing around 0.2 CEC is 1.02 nm and the $C16TA^+$ ions lie about parallel to the silicate interlayer surfaces. Then a smooth step in the interlayer spacing occurs and at 0.4 to 1.2 CEC the spacings of 2.0 - 2.5 nm are roughly the length of $C16TA^+$. Therefore, a possible arrangement could involve the $C16TA^+$ head groups being adsorbed on the two interlayer surfaces and the 'interfingered' long alkyl chains roughly perpendicular to the interlayer surfaces. When the loading level further increases (1.2 to 2.6 CEC), a next smooth step in interlayer spacing occurs to about 3.3 nm and the $C16TA^+$ ions (ion exchanged) and C16TAB molecules (hydrophobically attracted) form a partly 'interfingered' admicellar type layer. With these surfactant conformations at loadings > 0.4 CEC the surfactant phase in the interlayer is divided into three regions: region 1 and 3 are adjacent to the two interlayer surfaces, each extending to about 0.5 nm from the surface, containing H_2O, surfactant head groups and, if loaded in excess of the CEC, also the surfactant counterions (Br-), and region 2 with a thickness of about 2 nm in the center of the interlayer space, containing the aggregated tails of the alkyl chains and residual water. The total structure is bilayer-like and/or resembles flattened admicelles. The core region with the tails becomes more aliphatic and less aqueous as the surfactant loading increases from 0.40 to 2.6 CEC. With increasing surfactant loading the core region becomes more hydrophobic, but induced steric hindrances increase and the space left for ad-solubilization decreases; therefore, the partitioning of organic contaminants shows a maximum around loading levels of 1 CEC. This maximum corresponds roughly with the maximum hydrophobicity of the surfactant layer at the external surfaces of the clay around loadings of 1 CEC, but the structure of the external surfactant layer is rather

different (head-on monolayer type and/or teepee-like micelles) from that in the interlayer (flattened admicelle-like).

The specific behavior of surfactant adsorption in confined space has also been investigated theoretically by Molecular Dynamics studies. Initially these studies modeled dry organo-clays [177, 208-210] but in later studies water was included in the simulations [211, 212]. The latter are most relevant with respect to understanding the adsorbed surfactant conformations in the interlayer space. The introduction of the paper by Liu et al. [178] provides a brief overview of the history of MD calculations on organo-clays and the force fields used; in that of Zhou et al. [213] the most relevant experimental results and the recent MD simulations are mentioned. Liu et al. [178] discuss the structure and dynamics of alkylammonium-intercalated wet SWy-type montmorillonite with emphasis to the alkyl chain length; the paper is complementary to the recent paper of Zhou et al. [213], which will be discussed here. The study of Zhou et al. [213] on $C16TA^+$/C16TAB intercalated Ca-montmorillonites (Mt) in the water-saturated condition largely mimics the experimental system of Zhu et al. [207] discussed above, and provides a good illustration of the information that can be gained by MD simulations.

The simulation results of Zhou et al. [213] show that, as the surfactant adsorption on montmorillonite (CEC 1060 μmol/g) increases, the arrangement of $C16TA^+$/C16TAB transforms from flat bilayer-type to inclined paraffin-type with a large amount of water in the interlayer space. This configuration is different from that in dry systems; for dry samples the surfactant conformation changes from monolayer to bilayer and to pseudo-trilayer as surfactant loading increases [171, 175]. Compared to the dry models, the percentage of gauche conformations of $C16TA^+$ decreases in the water saturated condition. The head groups of $C16TA^+$ are located close to the centers of the six-member rings of the silicate surfaces and coordinated with 4–6 water molecules. Their mobility is low due to the electrostatic interactions, while the alkyl chains show a higher mobility. Montmorillonite

with a high CEC (1310 μmol/g) has a stronger confining effect on both $C16TA^+$/C16TAB and water, which reduces the mobility of alkyl chains and water molecules within the interlayer space.

A general impression of the surfactant conformations in the interlayer space as function of surfactant loading is provided by the density distributions for ammonium N, alkyl C, Ca^{2+}, Br^- and water O [213]. The calculated density distributions for montmorillonite with a CEC of 1060 $\mu mol_e/g$ are depicted in Fig. 26 for different loading levels relative to the CEC as indicated in the figure. Corresponding snapshots of $C16TA^+$ intercalated in the interlayer that further visualize the distribution are presented in Fig. 27. For Mt-0.25CEC-1nm (= montmorillonite with a C16TA+/C16TAB loading equal to 0.25 CEC and an interlayer spacing of about 1 nm) both ammonium N and alkyl C are arranged in two layers according to the two clear peaks of the density distributions, indicating a bilayer structure, see Figs. 26a and 27a. As the surfactant loading level increases (Mt-0.5CEC-2nm; Figs. 26b and 27b), the density distribution of ammonium N remains two peaks close to the silicate surface due to the strong electrostatic attraction between the negative charge site and the cationic ammonium N. The distribution of alkyl C is rather different from that at 0.25 CEC, it transforms to one broad peak in the center and the arrangement of alkyl chains is inclined to the Mt surface. In these two incomplete cation exchange cases Ca^{2+} displays a symmetrical distribution with ammonium N to balance the residual negative charge. Ca^{2+} plays no role for surfactant loadings > 1.0 CEC, but in this case the negative surfactant counterion (Br^-) comes into play. For Mt-1.0CEC-2.2nm (Figs. 26c and 27c), the situation is similar as for Mt-0.5CEC-2nm, but more pronounced. The broad central peak of alkyl is larger, indicating strong association of the alkyl chains in the interlayer space; the arrangement of alkyl chains is still inclined to the Mt surface. In the excessive surfactant loading case (Mt-2.0CEC-3nm; Figs. 26d and 27d), most N is still close to the surfaces, but part of N is distributed over the core of the interlayer. The N distribution is roughly paralleled by the Br distribution, but

close to the surface N and Br occupy separate layers. The magnitudes of the N and Br peaks close to the surface indicate that a large part of head groups that did not participate in the ion exchange is also located close to the surface. The small peaks of ammonium N in the interlayer space are balanced with Br in the core of the interlayer space. The alkyl chains are connected closely, reflecting the association by hydrophobic attraction. In all cases, the density of water near the Mt surfaces is somewhat higher than in the center, which is probably related to the hydration of the accumulated ions and ammonium head groups close to the surface. The hydrophilicity of the interlayer surfaces is somewhat questionable, because a siloxane surface without charge is fairly hydrophobic. The density distributions of interlayer species for Mt with a high CEC (1310 μmol/g) are in most cases similar as those shown here. However, for the Mt-0.25CEC-1nm system, the alkyl C forms several peaks near the center of the interlayer space instead of two peaks. The ammonium head groups close to the surface cause most likely obstruction of the orientation of the alkyl chains parallel to the surface. To sum up, under the water saturated condition and low surfactant loading the surfactant alkyl chains are oriented roughly parallel to the surface; at loadings ≥ 0.5 CEC alkyl chains are concentrated in the center of the Mt interlayer space and most head groups are close to the surface. The calculated results are consistent with the experimental results of Zhu et al. [207] and the density profiles are subtler versions of the schematic models suggested by Zhu et al.

An alternative way of modeling surfactant binding from aqueous solutions in confined space is by Self-Consistent Field calculations with the SCFA model [214-217]. With the SCFA model surfactant isotherms can be calculated for two surfaces at a given distance and the interlayer spacing can only be changed by discrete step of about the diameter of a water molecule; simultaneous with the adsorption isotherm the interaction force between the two surfaces can be calculated. Calculations made [214-217] have not addressed the specific clay-surfactant systems, but some knowledge of the obtained results is still useful for a

better understanding of the complications that occur with surfactant adsorption in confined space. For charged hydrophilic surfaces the SCFA calculations have provided insight in the adsorption behavior below and above the charge compensation point [214, 215]. The confined space drives the adsorbed surfactant layer toward a structure similar to that obtained at the charge compensation point. At solid-solid separations where the surfactant layers on each surface begin to merge with each other (proximal adsorption), there is a confinement-induced phase transition leading to complex adsorption and interaction behavior at very small separations. In addition, calculations show that the interaction between surfactant tails is a key contributor to both the magnitude of proximal adsorption and the exchange between surfactant and co-ions at the surface. For (charged) hydrophobic surfaces [216, 217] a first-order phase transition takes place when the slit width approaches the thickness of the two surfactant layers; the transition is driven by the unfavorable hydrophobic-water contacts. At the transition, the average orientation of the surfactants switches from a high concentration of tails at the surface and head groups in the center to a bilayer configuration where the tail profiles from both sides merge in the center and the head groups are in the vicinity but slightly away from the surface. For more information the original papers should be consulted.

6.7 Nonionic surfactant adsorption on montmorillonite

Similarly as with cationic surfactants the binding of nonionic surfactants on montmorillonite is dominated by adsorption at the plate surfaces, therefore, also for these surfactants adsorption in the interlayers plays an important role. Detailed results on the adsorption of nonionic surfactants on montmorillonite at low surfactant concentrations are scarce; recent results mainly concentrate on concentrations around and above the CMC because the interest is on preparation of organo-clays made with nonionic surfactants. Rheinländer et al. [218] have investigated C12(EO)8 on four different clays

(Na-montmorillonite = Na-Mt, Ca-bentonite (95% montmorillonite) = Ca-Mt, Na-kaolinite and Na-illite) based on adsorption isotherms and for the swelling clay minerals (Na-Mt and Ca-Mt) microcalorimetry and X-ray diffraction. The measured isotherms were presented as double logarithmic plots that are reproduced in Fig. 28. The isotherm on Na-kaolinite runs below that on Na-illite, and both isotherms (mmol/g) are clearly below those on the swelling minerals. However, when the adsorbed amount is expressed per m^2 the maximum adsorption values on the Na-clays are similar and about twice as high as that on Ca-Mt. The isotherms for Na-Mt and Ca-Mt are similar; however, the adsorption for Ca-Mt is stronger at low concentrations than that of Na-Mt, but at high concentrations the situation is reversed (maximum adsorptions Na-Mt and Ca-Mt, respectively, 0.94 and 0.35 mmol/g). A greater (exothermic) initial differential molar enthalpy (heat) of adsorption confirms the higher affinity of C12(EO)8 for Ca-Mt than for Na-Mt. The heat of adsorption of the two clays decreases about linearly with surfactant loading and becomes zero above 0.26 mmol/g, which is below the adsorption maximum of the two clays. The behavior of the heat of adsorption indicates two steps in the adsorption process: (i) adsorption due to interaction with the surface and (ii) adsorption by mainly hydrophobic attraction with already adsorbed surfactant. The observations that zero heat of adsorption to Ca-Mt and Na-Mt is reached at the same loading (mmol/g), but that the maximum amounts adsorbed are rather different indicates that the second adsorption step is larger for Na-Mt than for Ca-Mt. Although the adsorption process contains two steps, the shape of the log-log isotherms indicates that there is no critical surface association concentration (CSAC), all isotherms show a gradual increase in adsorption and the slope is of the isotherms is always ≤ 1. Therefore, the transition of the first to the second adsorption process is gradual. This is the case for all four clay samples studied.

The X-ray diffraction results showed that the basal (d001) spacing of pure *air-dried* Na-Mt of about 1.25 nm differed significantly from that of Ca-Mt of 1.5 nm due to stronger hydration of the Ca^{2+} than of Na^{+}. The basal spacing of Na-Mt with surfactant goes from

1938 1.25 nm to 1.4 nm for 0.1-0.35 mmol/g and to about 1.8 nm for higher adsorption values.
1939 For Ca-Mt the spacing changes from 1.5 to 1.8 nm between 0.2 and 0.3 mmol/g. These
1940 values are for both swelling clay minerals indicative of the formation of flat-lying
1941 C12(EO)8 molecules in the first adsorption step and of the formation of a 'flat' bilayer
1942 structure in the second adsorption step. As the spacings are derived from air-dried samples,
1943 the distances will be likely different in the water saturated situation (and therefore the
1944 surfactant conformation), but the two steps in the adsorption process are reflected in the
1945 measured values. The stronger hydration of Ca^{2+} than of Na^{+} has, most likely, also caused
1946 the higher affinity of C12(EO)8 for Ca-Mt than for Na-Mt.

1947 Sonon and Thompson [219] investigated the adsorption of C12(EO)<23> (=Brij 35; the
1948 notation <n> indicates that the EO chain length is polydisperse) on two smectites (Wyoming
1949 montmorillonite and Panther Creek smectite) that were brought in the K and Ca form. For
1950 both smectites the adsorption affinity and adsorption plateau were somewhat larger for the
1951 Ca-smectite than the K-smectites. The d001 values of both air-dried K-saturated smectites
1952 increased in two steps from 1.11 nm to about 1.7 nm as more surfactant was sorbed, while
1953 the d001 spacing of the air-dried Ca-smectites increased gradually from 1.47 nm to about
1954 1.7 nm. These results confirm those of Rheinländer et al. [218].

1955 Backhaus et al. [220] continued the work of Rheinländer and investigated the adsorption of
1956 the octylphenol poly(ethylene oxide)s [(C8Φ(EO)<n>], TX100 (<n> = 9.5), TX-165 (<n> =
1957 16) and TX-305 (<n> = 30), on Ca-Mt and silica. Note that the hydrophobic character of a
1958 C8Φ group is very similar to that of a C12 group. The adsorption isotherms of
1959 C8Φ(EO)<9.5> (= TX100) on Ca-Mt at pH 4 and pH 9 in 10^{-2} mol/L $CaCl_2$ showed only
1960 small differences, which indicated that the share of the edge surfaces to the surfactant
1961 adsorption on Ca-Mt is small. Furthermore, the affinity (measured by the initial slope of the
1962 isotherm) of C8Φ(EO)<9.5> at pH 4 to Ca-Mt was higher than that on silica, which point to a
1963 different binding mechanism. With silica the EO segments mainly bind to the silanol groups

by H-bonds, but with expanding layered silicates these groups are hardly present and the binding mechanism is most likely H-bonds with the hydration water of the bound counterions on the clay surfaces. The interlayer spacings of Ca-Mt with adsorbed C8Φ(EO)<9.5> in the dried and moist state show a similar behavior as in the case of C12(EO)8 [218], but the spacings for the moist sample are even at the largest adsorption values considerably (2nm) larger than the spacings of the air-dried sample. This indicates again that in aqueous solution the interlayer spacings will be different from that of the air-dried samples.

The isotherms (non-logarithmic) of the three surfactants (TX100, TX-165, TX-305) [220] were all L2-type [221], i.e. a steep rise towards the maximum adsorption. For TX-100 adsorption on montmorillonite or bentonite the L2 type isotherm has also been observed by [218, 222, 223]. Somewhat above the CMC the isotherms show a plateau that decreases with increasing EO head group length. The fact that the plateau adsorption is reached beyond the CMC is due to the fact that head group polydispersity leads to a relatively low CMC and a maximum adsorption at relatively high concentration [224]. The lack of the S-shaped course and thus of cooperative effects suggests that, unlike in the case of silica gel, no aggregate formation took place on the surface at low surfactant concentrations. This behavior is to be expected when the affinity of the surfactant molecules to the surface (hydrated Ca ions) is greater than the hydrophobic attraction between the surfactant molecules. With the relatively small interlayer spacing, the second step caused by hydrophobic attraction will be largely lateral (tail-tail) attraction. For steric reasons the lateral hydrophobic attraction decreases by the head group size and this explains the decreasing plateau adsorption with increasing head group size.

A decrease in the adsorption with increasing head group size for a given alkyl chain length has also been observed by Shen [225] who measured the adsorption of C9(EO)<10>, C9(EO)<20> and C18(EO)<20> (= Brij 78) on bentonite at pH 6-7 and 0.01 M NaCl. Doubling the alkyl chain length at a given degree of ethoxylation increased the adsorption

maximum also but the effect was much smaller than that of doubling the head group size, especially when the adsorption was expressed as mmol/g. Deng et al. [226] who studied the adsorption of C16(EO)<10> (= Brij-56) and C9Φ(EO)<12> (= Igepal-CO720) on Ca-bentonite found somewhat larger adsorption for the surfactant with the smaller head group in line with the results of Shen [225]. However, the proposed surfactant conformation for the freeze-dried composites with EO segments in the interlayer and the alkyl chains sticking-out in air, is highly unlikely for water saturated samples and for the situation of the intercalated smectite in contact with an aqueous surfactant solution, because in this case hydrophobic attraction comes into play and the proposed conformation would lead to many unfavorable CH_2-water contacts which can be avoided when the alkyl chains associate in the interlayer space. Therefore, it is to be expected that with adsorption from solution the conformation will be somewhat similar to that of cationic surfactants in the interlayer as described in the previous section.

To unravel the EO binding mechanism and the EO chain conformation of intercalated polymeric nonionic surfactants Deng et al. [198] also investigated the intercalation of bentonites (with different cations) by: C16(EO)<10> (= Brij 56), C18(EO)<100> (= Brij 700), C2(CH2-CH2)<15>(EO)<40> (= polyethylene-polyethylene oxide or PE-PEO) and (EO)<76> (= PEO). The surfactants and the organo-bentonites were characterized with X-ray diffraction (XRD) and Fourier transform infrared (FT-IR) spectroscopy. The surfactants intercalated the bentonite and expanded the d001 spacing of the freeze-dried samples to nearly 1.8 nm. The shapes and positions of the IR bands of interlayer surfactants resembled amorphous PEO. The EO segments of the surfactants were arranged in a distorted and extended form in the interlayer, instead of in the favored helical conformation of the crystalline state. The shifts of the C–O–C stretching bands of the intercalated surfactants pointed to H-bonding of the EO oxygen atom with water in the hydration shell of the exchangeable cations, or to direct coordination or ion–dipole interaction between the

exchangeable cations and the oxygen atoms. The type of exchangeable cations (Na^+ , K^+ , Ca^{2+} , Mg^{2+} , Cu^{2+} , Ni^{2+} , H^+) in the interlayer of smectite did not affect the conformation of the EO chain of the intercalated surfactants. These results give valuable information on the binding mechanisms and indicate clearly that the (EO)<n> conformations in the interlayer of the freeze-dried samples are more disordered than in the crystalline state. However, as indicated above, in the case of water-saturated samples the conformation of the EO chains is likely more random and affected by the presence of the apolar segments in the interlayer, because the apolar segments will locally associate due to hydrophobic attraction and not protrude into the aqueous solution.

The studies by Guégan [227, 228] on the intercalation of C10(EO)3 in the interlayers of Ca- and Na-montmorillonite (SWy-2) also deserve some attention because this surfactant easily forms in solution somewhat above the CMC a lamellar phase that consists of the stacking of molecules by hydrophobic attraction and it is well known that relatively small Cn(EO)m surfactants with m<n, such as C12(EO)6, adsorb on silica with a condensation step just before the CMC in a bilayer arrangement [153, 164]. With Ca-Mt the adsorption isotherm of C10(EO)8 was high affinity with a pseudo plateau reached at about the CMC. X-ray diffraction and FT-IR measurements on samples dried at 70 ^oC indicated an expansion of the basal spacing to 1.7 nm and adsorption in two adsorbed monolayers parallel to the clay surface [227]. In a subsequent study [228] intercalation of Na-Mt by C10(EO)3 was investigated, the Na-Mt suspension was well swollen and showed a stable hydration state in which silicate layers were widely expanded and already opened when the surfactant solution was added, thus allowing an easier adsorption. Moreover initial solution concentrations of C10(EO)3 were selected that where several times the CMC which already displayed the Lα-lamellar phase. The adsorption values that where reached were similar and somewhat higher (40%) than those in the Ca-Mt system. The results obtained with small angle X-ray scattering and with FT-IR (samples dried at 70 ^oC) however revealed d001

spacings from 1.1 nm for Na-Mt and 3.8 nm for the loaded samples and in the interlayer space a well-ordered surfactant bilayer, with a structure similar to that of the lamellar phase. The X-ray diffraction patterns further indicated that the C10E3 molecules were not aggregated on the external clay surfaces. Although the translation of these results to the surfactant conformations that are adopted with adsorption from solution is not straight forward, it seems plausible that a kind of bilayer with a hydrophobic core in the interlayer space might also be possible with simple C10(EO)3 adsorption. Calculations with the SCFA model might provide further insight; calculations for nonionic surfaces have been made before [152, 153, 165] and can be extended to adsorption in a confined space as has been done for ionic surfactants [214-217].

7. Surfactant adsorption modeling

7.1 General remarks

Surfactant adsorption isotherms have been qualitatively and (semi-) quantitatively interpreted using several adsorption models, ranging from the Langmuir equation to very sophisticated models. For a review of the models used to describe surfactant adsorption, including those specifically designed for surfactant adsorption to solid-liquid interfaces, the reader is referred to [25], where also references can be found. Here some classical models are briefly discussed in relation to surfactant adsorption. In general two types of modeling can be distinguished, (i) mean-field models in which the adsorbed layer is assumed to be smeared-out homogeneously over the surface and (ii) aggregation models in which the surfactants are adsorbed as aggregated, micellar type structures. Simple examples of the first category are the Langmuir-, the Frumkin-Fowler-Guggenheim- and the Freundlich -equation;. examples of the aggregate models are the Hill- and the Gu-equation.

7.2 Mean-field models of monocomponent solute adsorption

The famous Langmuir model applies to sorption from an ideally dilute solution of non-interacting molecules on homogeneous binding sites. The binding sites should be attached to particles, but the geometry of the particles and precise location of the sites is not relevant, only the homogeneity of the sites is important. The Langmuir (L) Eq. can be written as:

$$\frac{\theta}{1-\theta} = Kc \qquad (1)$$

where θ is the fraction of the sites covered with the adsorbate, c the equilibrium concentration and K the equilibrium affinity constant accounting for all types of interactions with the sites. Preferably, the concentration, c, is expressed as *normalized concentration*, i.e., with respect to a chosen standard state: $c = c' / c^*$, therefore, as both c' and c^* should have the same units, c is dimensionless. When the concentration c' is expressed in mol/L a convenient standard state is $c^* = 1$ mol/L. For a good understanding of the obtained parameter values the standard state should be indicated. In the case of a normalized concentration also the affinity constant K is dimensionless and can be expressed as a Boltzmann factor containing the standard molar Gibbs energy of adsorption: $K = \exp(-\Delta G^0/RT)$, the surface covered with water (considered as a continuum) is taken as the standard state for the energy difference, R is the universal gas constant and T the absolute temperature. The site coverage can be expressed as the covered amount of sites divided by the total amount of sites, or, as is done most often in practice, the adsorption, Γ, divided by the maximum adsorption, Γ_m, and in that case the L-equation becomes

$$\Gamma = \frac{\Gamma_m Kc}{1+Kc} \qquad (2)$$

As the L-eq. applies to ideal sorption it will, in general, not be able to describe surfactant adsorption, but when it does, the obtained parameters K and Γ_m are conditional, that is to say, depending on the conditions of the experiment (surfactant concentration range and environmental conditions). Literature examples of reasonable fits of the L-eq. for surfactant

adsorption are mostly based a limited surfactant concentration range around the CMC where the plateau adsorption is reached.

The Frumkin-Fowler-Guggenheim (FFG) equation is an extension of the L-eq. in which lateral interaction between the adsorbed molecules is taken into account; it can be written as

$$\frac{\theta}{1-\theta} = Kc\,\exp\left(-b\theta\right) \qquad \text{with } \theta = \frac{\Gamma}{\Gamma_m} \tag{3}$$

where b is a dimensionless lateral interaction parameter: $b = \Delta G^0_{lat} / RT$ with ΔG^0_{lat} the standard Gibbs energy of lateral interaction. This equation is more realistic for surfactant adsorption than the L-eq. because next to the interaction with the surface (K), the lateral hydrophobic attraction is included explicitly; the parameter b can be expressed as linearly dependent on the alkyl chain length. In many studies of surfactant adsorption FFG-type models have been used to qualitatively understand the role of surface-surfactant attraction as compared to the lateral hydrophobic attraction.

When the binding sites are heterogeneous and randomly or regularly mixed the adsorption isotherm can be obtained by solving the integral adsorption equation that contains both the local isotherm for binding on equal energy sites and the heterogeneity distribution. A Freundlich-type isotherm equation is obtained when the local isotherm is L-type and the heterogeneity distribution is given by a quasi-Gaussian distribution function [57]:

$$\frac{\theta}{1-\theta} = \left(\tilde{K}c\right)^p \qquad \text{with } \theta = \frac{\Gamma}{\Gamma_m} \tag{4}$$

where $\tilde{K}$ is the median value of the affinity and p ($0 < p \leq 1$) is a measure of the width of the distribution, for p =1 the surface is homogeneous. The quasi-Gaussian distribution function is called ‘Sips-distribution’ after Sips [229, 230] who derived Eq. 4. Eq. 4 is called the Langmuir-Freundlich equation, for p = 1 it reduces to the L-eq.. Because of the presence of an exponent in the equation the use of a dimensionless solute concentration is a must, it makes the interpretation of K possible. For sorbed amounts much lower than Γ_m Eq. 4

reduces to the common Freundlich equation, $\Gamma = \Gamma_m \left(\tilde{K}c\right)^p = K^* c^p$, where K^* is a composite parameter that can be indicated as the effective affinity constant; it has the same dimension as Γ, (provided c is normalized) but information on Γ_m cannot be obtained. Freundlich type equations are more 'flexible' than the L-eq.; therefore, they have been mainly applied when the L-eq. did not fit the results well. The interpretation of the obtained parameters is however not so easy. Below we return to this aspect.

So far electrostatic interactions are not considered explicitly; in mean-field models these interactions can be formally introduced in the mentioned models by replacing the (normalized) equilibrium concentration of solute by the equilibrium solute concentration adjacent to the adsorption site:

$$c_s = c_b \exp\left(\frac{-zF\psi_s}{RT}\right) \qquad (5)$$

where c_s is the solute-ion concentration at the location of the binding site, c_b the normalized equilibrium solute concentration in the dilute bulk solution, the Boltzmann factor accounts for the smeared-out electrostatic interaction at the location of the binding sites (mostly the surface) that the solute ion experiences, z is the valence of the solute ion and ψ_s is the electrostatic potential at the location of the site. The value of c_b can be multiplied by the activity coefficient calculated with, for instance the Debye-Hückel or Davis model [231], when the ionic strength is such that activity corrections are necessary.

A problem with Eq. 5 is that mostly no adequate information is present on ψ_s. For low and moderate ionic strength values the zeta-potential, obtained with one of the electrokinetic methods [204], can be used as approximation for ψ_s. Alternatively, a model can be used that the relates the particle charge to ψ_s, For flat surfaces and not too high surface potentials the Debye-Hückel model can be used [79], it relates ψ_s to the total (net) surface charge density, σ_t (C/m2):

$$\psi_s = \frac{\sigma_t}{\varepsilon_0 \varepsilon_r \kappa} \tag{6}$$

where κ is the inverse Debye length, ε_0 the permittivity in vacuum and ε_r the relative permittivity of water. The value of κ is determined by the ionic strength of the solution, at room temperature and a *z*-*z* electrolyte of concentration c_z

$$\kappa = (10 c_z z_z^2)^{0.5} \quad \text{with } \kappa \text{ in nm}^{-1} \text{ and } c_z \text{ in mol/L} \tag{7}$$

Substitution of Eqs. 5-7 in Eq. 3 provides an equation that explicitly takes into account the specific interaction with the surface, the electrostatic interactions both with the surface and in the adsorbed layer and the lateral interactions:

$$\frac{\theta}{1-\theta} = Kc \exp\left(-b\theta - \frac{zF\sigma_p + z^2F^2\Gamma_m\theta}{RT\varepsilon\kappa}\right) \tag{8}$$

where use has been made of the fact that the total (net) particle charge density $\sigma_t = \sigma_p + zF\Gamma_m\theta$ with σ_p the primary surface charge density and $zF\Gamma_m\theta$ the charge density contribution due to the ionic solute adsorption. This type of equation can be used to explain the presence of a common intersection point (CIP) of ionic surfactant isotherms measured at different ionic strength values. At the CIP the electrostatic interaction vanishes, as there is no effect of the salt concentration on the adsorption. This must mean that $zF\sigma_p + z^2F^2\Gamma_m\theta = 0$, i.e., the adsorbed surfactant charge just compensates the primary surface charge. For concentrations below the CIP the primary particle charge dominates and an increase in ionic strength (increase in κ) decreases the electrostatic surface-surfactant attraction, therefore the adsorption decreases with increasing ionic strength. For concentrations beyond the CIP the surfactant adsorption dominates the electrostatic interaction and with an increase in ionic strength the repulsion between the charged surfactant head groups decreases, therefore the adsorption increases with increasing ionic strength. From the above equations Eq. 8 is best equipped to understand qualitative or

(semi)-quantitative ionic surfactant adsorption behavior. Eq. 8 is a FFG-type equation this can be shown by regrouping the various terms:

$$\frac{\theta}{1-\theta} = KK_{el}c\,\exp\left(-b\theta - b_{el}\theta\right) \qquad (9)$$

where $K_{el} = exp\left(-zF\sigma_p / RT\varepsilon\kappa\right)$ and $b_{el} = \exp\left(-z^2F^2\Gamma_m / RT\varepsilon\kappa\right)$. Eq. 9 shows that when the electrostatic interactions are not explicitly considered with ionic surfactant adsorption and the simple FFG- Eq. (3) is applied, that both the affinity and the lateral interaction parameter contain an electrostatic contribution. Further extensions of Eqs. 3, 6, 8 and 9 are discussed in [232, 233].

Ionic surfactant adsorption is often at least partly due to ion exchange and/or accompanied by adaptation of the primary surface charge. None of the above equations considers the multicomponent nature or the competition. This implies that when the equations are applied in practice they are conditional, or stated differently, the fitted parameters are no longer adequate when the concentration of the competing ion (e.g., H^+ or OH^-) is changed. This can be illustrated by using the multicomponent Langmuir equation:

$$\theta_1 = \frac{K_1c_1}{1+K_1c_1+K_2c_2} = \frac{K_1^c c_1}{1+K_1^c c_1} \quad \text{with } K_1^c = \frac{K_1}{1+K_2c_2} \qquad (10)$$

where K_1^c is the conditional affinity, which is only constant at constant c_2. Eq. 10 is also Langmuir-type but it provides information on how K_1^c changes with changing conditions. A condition for the application of Eq. 10 is that Γ_m should be the same for both components; otherwise also the stoichiometry of the exchange has to be taken into account.

With ionic surfactants and charged surfaces adsorption is often a two-step process. The first step is binding to the charged surface, where some kind ion exchange and lateral hydrophobic attraction play a role, and the second step is governed by hydrophobic attraction to already adsorbed molecules and lateral hydrophobic and electrostatic

interaction in the second layer. With the above single layer models this distinction is not made, which implies that the second layer adsorption can only be due to lateral interaction. As a result the *b* parameter has a composite character, it accounts for both the layer-layer and the lateral hydrophobic attraction. A simple model that tries to avoid this problem is the FFG two-layer model of Mehrian et al. [180] in which not only the affinities for the first and second layer are different but also the lateral interactions, however the electrostatic interactions are not made explicit. The results of this model are discussed in the section on cationic surfactant adsorption to kaolinite. Scamehorn et al. [234] also used a two-layer FFG equation without treating the electrostatic interactions explicitly. With their parameter choice the affinity for the first and second layer differed, but the lateral interactions were assumed to be the same. With the chosen parameter values the model predicted a strong 2D phase transition at low surfactant concentrations and heterogeneity was invoked to explain the experimental isotherms. As explained above for the FFG-eq., also a two-layer FFG model, that does not treat electrostatics explicitly, is only suited for the description of experiments done at constant pH and constant salt concentration.

7.3 Aggregation models for monocomponent solute adsorption

The second group of adsorption models starts with the Hill equation that describes the formation of homogeneous aggregates containing *n* solute molecules on N_s homogeneous binding sites:

$$\frac{\theta_n}{1-\theta_n} = \left(Kc\right)^n \quad \text{with} \quad \theta_n = \frac{\Gamma_n}{\Gamma_t} = \frac{\Gamma_n}{nN_s} \tag{11}$$

where θ_n is the fraction of sites covered with *n* molecules, *K* is the affinity of the binding of 1 molecule, K^n that of the *n* molecules, *c* the normalized solute concentration, the actual adsorption equals Γ_n, and the total (maximum) adsorption Γ_t is equal to nN_s. The process of adsorption is *cooperative* because one adsorption step brings *n* molecules to a site, *n* is

therefore also called the cooperativity parameter. The Hill-eq. reduces to the L-eq. for $n = 1$; isotherms for $n > 1$ are somewhat S-shaped and the isotherm is steeper than the L-isotherm (*positive* cooperativity); for high n the steepness of the adsorption isotherm is large and close to a two-dimensional (2D) phase transition. It is also possible to derive the Hill-eq. for the situation that one molecule occupies n^* sites (n^*-dentate adsorption), so that on one site only $1/n^*$ molecules are adsorbed. In this case $n = 1/n^*$ or $n < 1$, i.e., for $n = 1/2$ the adsorption is bidentate. For $n < 1$ there is negative cooperativity and the isotherm is less steep than the Langmuir isotherm because it more difficult to find n^* sites than 1 site. Instead of calling n the cooperativity parameter, n can thus also be called the *stoichiometry parameter*: $n > 1$ more than 1 molecule per site, $n < 1$ more than 1 site required to adsorb 1 molecule.

It should be noted that the mathematical forms of the Hill-eq. and the Langmuir-Freundlich-eq. are identical; in terms of the Hill-eq. heterogeneity is a form of negative cooperativity, where adsorption becomes more difficult when the coverage increases. When the Hill-eq. or the LF-equation is applied in a practical situation the cooperativity parameter might therefore be affected by site heterogeneity, and the heterogeneity parameter by the cooperativity.

Zhu and Gu [150, 151] have proposed an extension of the Hill-eq., they make a distinction between a first and second step in the adsorption process. In the first step solute molecules are bound to the sites and in the second steps these bound molecules act as nuclei for an aggregation step or positive cooperative adsorption. The adsorbed amount in the first state equals

$$\Gamma_1 = N_s\theta_1 = N_s\frac{\kappa Kc}{1+\kappa Kc+\kappa(Kc)^n}$$

that in the second state

$$\Gamma_n = N_s n\theta_n = N_s \frac{n\kappa(Kc)^n}{1+\kappa Kc+\kappa(Kc)^n}$$

and the total adsorption is obtained by summation of the two contributions

$$\Gamma_t = N_s \frac{kKc+nk(Kc)^n}{1+kKc+k(Kc)^n} \qquad (12)$$

In these equations k is the ratio between the affinities of the first and second state, K the affinity of the second state, therefore, kK is the binding affinity for the first state. For $k = 1$ the affinities for the first and the second state are equal, but the nuclei formation is initially stronger than the aggregation because there are more free sites than nuclei. For $k >> 1$ the isotherm is typical stepwise, the first step is pronounced at low concentration and the second step occurs at somewhat higher concentrations. The parameter n is in this case equal to the ratio of the first adsorption plateau over the second. For $k <<1$ the equation becomes similar to the Hill equation and the isotherm depicts one step. Eq. 12 is often called the Gu-equation, it is a very 'flexible' equation and regularly used to describe quantitatively the adsorption of both nonionic and ionic surfactants.

In the case of ionic surfactants the description is conditional, because for each change in solution conditions (pH and ionic strength) new parameters are required. Moreover, the affinity for the first step is for ionic surfactants determined by both the specific and electrostatic interaction and lateral interactions, the parameter k accounts for the first two interactions, K for the lateral attraction. Ion competition for the surface sites is not considered. The affinity in the second step comprises the hydrophobic affinity for the nuclei and the lateral interactions; the latter contain for ionic surfactants not only the hydrophobic attraction but also the electrostatic repulsion. Part of the lateral interaction for the second step is however also incorporated in the value of n. It is therefore difficult to give a more detailed interpretation of the parameter values. The main advantage of the Eq. 12 is that a distinction can be made between the overall affinities for the first and the second step.

When it is assumed that the adsorbed states are governed by the same electrostatic adsorption potential it is possible to incorporate the electrostatic interactions in the Gu-eq. in the same way as illustrated above for the FFG-eq., but this has not been done.

Two sophisticated models for surfactant adsorption that take aggregation into account are that of Rudzinski et al. [235, 236] and Li and Ruckenstein [237]. The model by Li and Ruckenstein [237] is most advanced, it has much in common with the description of micellization of ionic surfactants but it also reflects the scaled particle theory used by Rudzinski et al. [235, 236]. Solvent molecules, surfactant monomers and two types of surfactant aggregates of various sizes cover the surface. The competition between the enthalpic and entropic contributions to the Gibbs energy in the adsorbed phase is responsible for the composition of the adsorbed phase; the standard Gibbs energy change in going from the solution to the surface aggregates is calculated by considering five contributions: hydrophobic, conformational, electrostatic, steric and interfacial. The electrostatic contributions are treated within the framework of the Poisson-Boltzmann equation for flat plates. The model can well predict the four-region isotherms, but no predictions have been made of ionic strength effects.

7.4 SCFA model for surfactant adsorption

The SCFA or Self-Consistent-Field theory for Adsorption model is a sophisticated model in which the structure and properties of the components present in the system are explicitly taken into account by considering them as composed of different segments that are linked together. The type and number of segments of a molecule, their charge and the way they are linked determine the structure and the properties of a molecule. Most molecules in the system are composed of just one or a few segments, but the molecular structure of the surfactant molecules is mimicked as closely as possible. The flat surface is also composed of segments that characterize the surface, for charged surfaces a part of the

segments can associate or dissociate a proton. The model is an extension of the theory of polymer solutions by Flory [107] to systems that have inhomogeneities in one direction (1D SCFA), i.e. perpendicular to the surface or the center of the lattice, or in two directions (2D SCFA), i.e. perpendicular to the surface and in concentric rings parallel to the surface. In the 1D SCFA option a mean field approximation is used in every lattice layer around to the center of the lattice or parallel to the surface. In the 2D case the mean field approximation is used in every ring. The interactions between the segments are calculated using Flory-Huggins interaction parameters, similarly as in the Flory theory. Starting from system characteristics such as the structure of the surface, the number of different types of molecules, the amount of each of them, their structure and properties, and the interactions between the various segments, the equilibrium distribution of molecules in the adsorbed layer is calculated. The conformational statistics of the chains in the layer are evaluated using Boltzmann statistics, i.e., each step of the walk is weighted with a Boltzmann factor that accounts for the interactions that the segment experiences in the adsorbed layer. The electrostatic interactions in the adsorbed layer are calculated using a multi-plate condenser model. In the absence of surfactants the electrostatic potential profiles correspond with the potential calculated with the Stern-Gouy-Chapman model. The detailed equilibrium distribution of surfactant segments within the adsorbed layer, i.e. within a potential field exerted by the presence of the surfactant molecules themselves and the surface, is calculated by an iterative minimization of the Gibbs energy of the system. At equilibrium the segment density distribution in the adsorbed layer and the potential field exerted by the segments and the surface are fully in accordance with each other (field is self-consistent). Once this is achieved the structure of the adsorbed layer and the thermodynamic properties of the system can be obtained. Similarly as in the model of Li and Ruckenstein [237], the SCFA theory has a closely related variant for self-assembly in solution [238, 239] so that the surfactant micellization can also be predicted. When micellization of a given surfactant is predicted

with a certain set of parameters, the same set of parameters should be used to predict the adsorption. The only new parameters for the adsorption calculation are in that case those that describe the interactions of the segments with the solid surface. As mentioned in the text on several places, the SCFA model has been very helpful for a better understanding of the surfactant adsorption behavior. Reference [25] is a fairly recent review in which experimental surfactant adsorption results obtained for metal oxides and silicas are compared with SCFA calculations. More recent results for surfactant adsorption in confined space can be found in the section on cationic surfactant adsorption on montmorillonite. For the SCF calculations a computer code, the SF-box, is available; for further information and/or application of the SF-Box see [240].

7.5 NICA-Donnan model applied to surfactant sorption on humic and fulvic acids

Surfactant sorption to humic and fulvic acids can be described with the NICA-Donnan model as an ion exchange process. In this model the humic substance is considered as a collection of particles that contain the binding sites and that are permeable for solvent and solute. The particles form the Donnan phase in which the electrostatic interactions are governed by a smeared-out electrostatic potential that is the result of the fixed charges and the mobile charges in the Donnan phase. The binding to the heterogeneous sites is described by the NICA model, which is based on the multicomponent Hill equation as local isotherm in combination with the Sips distribution and can be written as [57, 58]

$$Q_i = Q_H^{\max}\left(\frac{\tilde{n}_i}{\tilde{n}_H}\right)\frac{(\tilde{K}_i c_{D,i})^{\tilde{n}_i}}{\sum_i (\tilde{K}_i c_{D,i})^{\tilde{n}_i}} \cdot \frac{\left(\sum_i (\tilde{K}_i c_{D,i})^{\tilde{n}_i}\right)^p}{1+\left(\sum_i (\tilde{K}_i c_{D,i})^{\tilde{n}_i}\right)^p} \qquad (13)$$

where $Q_H^{\max}$ is the maximum sorption of protons, $\tilde{n}_i$ the Hill-parameter that accounts for the average stoichiometry of component *i* with the proton sites, $\tilde{K}_i$ is the median affinity of

component *i* for the sites and *p* the heterogeneity parameter. It is assumed that the first characterization of the humic substance is done through proton sorption, therefore this ion is used as reference for the total number of sites (Q_H^{max}) and the factor $\tilde{n}_i / \tilde{n}_H$ accounts for the fact that the maximum sorption of *i* can be different from that of the proton. The concentration $c_{D,i}$ is the concentration of *i* in the Donnan phase that can be obtained from the bulk solution concentration using Eq. 5 with $\psi_s = \psi_D$. In the Donnan model the charge of the humic particles is neutralized by counter- and co-ions within the Donnan volume, the latter is calculated with a simple empirical relation. Based on this electroneutrality the Donnan potential can be calculated and $c_{D,i}$ can be obtained for all ions present [38]. The NICA equation is a master equation that reduces to the multicomponent Langmuir equation for all $\tilde{n}_i$=1, and *p* =1, to the multicomponent Langmuir -Freundlich eq. for all $\tilde{n}_i$=1 and to the multicomponent Hill eq. for *p* = 1.

The last quotient in Eq.13 is the total coverage of the sites with all types of ions present in the system, the second quotient is the fraction of the total coverage that is occupied by component *i*. Therefore, in the case of sorption of a trace component, *j*, ($\left(\tilde{K}_j c_{D,j}\right)^{\tilde{n}_j} << \sum_i \left(\tilde{K}_i c_{D,i}\right)^{\tilde{n}_i}$) the total coverage is hardly affected by the binding of species *j* and the NICA eq. reduces to

$$Q_j = \Omega (\tilde{K}_j c_{D,j})^{\tilde{n}_j} \quad \text{with} \quad \Omega = Q_H^{max} \left(\frac{\tilde{n}_i}{\tilde{n}_H}\right) \frac{1}{\sum_i (\tilde{K}_i c_{D,i})^{\tilde{n}_i}} \cdot \frac{\left(\sum_i (\tilde{K}_i c_{D,i})^{\tilde{n}_i}\right)^p}{1+\left(\sum_i (\tilde{K}_i c_{D,i})^{\tilde{n}_i}\right)^p} \quad (14)$$

where Ω is considered to be constant. When the total adsorption is constant, then also the Donnan potential will be constant and the electrostatic interactions do not significantly change with sorption of *j*, thus also $c_{D,j}$ can be replaced by c_j (Boltzmann factor becomes included in Ω). Therefore, at low solute concentrations in a multicomponent system the sorption equation of a trace ionic component to the active sites of the humic substance, at

otherwise constant solution conditions (pH, ionic composition and ionic strength) is ruled by a simple equation that resembles the monocomponent Hill-eq. for low loadings. Because the sorption of *j* is low, the site heterogeneity is not detected but the cooperativity / stoichiometry ($\tilde{n}_j$) is relevant. When the humic substance is well studied, Ω is known and the changes of Ω with changing solution conditions (e.g., change of pH) can be calculated, therefore the behavior of the trace component with changing solution conditions can be predicted, once $\tilde{K}_j$ and $\tilde{n}_j$ are known. When no information is present on the humic acid, the generic humic acid proposed by Milne et al. [55, 56] can be used to represent the unknown humic acid and by using the parameters collected by Milne the total sorption can be calculated under the given conditions. Thus also in this case Eq. 14 can be used in combination with Eq. 5 to investigate trace component sorption and how it is affected by, e.g., pH.

In the case of metal ion binding a double NICA-Donnan equation has been used, where the first equation accounts for the low proton affinity sites ('carboxylic') and the second for the high affinity proton sites ('phenolic'). The above way of analyzing trace component binding is still relevant as long as the total sorption on both the phenolic and carboxylic type of groups is constant. In most cases the trace sorption will occur with either the carboxylic or the phenolic groups and in this case the type of groups that do not participate can be neglected.

For the surfactant binding only a limiting cases of the single NICA-Donnan equation have been used. As discussed in the section 'Modeling surfactant - humic substance interaction' Chen et al. [114] used Eq. 14 to unravel the surfactant binding and the Hill equations used by Yee et al. [98-101] are identical to Eq. 14. Ishiguro and Koopal [115] made a different simplification for their analysis of surfactant adsorption to various humic

acids; they assumed that the surfactant sorption was dominant, i.e., $\left(\tilde{K}_j c_{D,j}\right)^{\tilde{n}_j} \approx \sum_i \left(\tilde{K}_i c_{D,i}\right)^{\tilde{n}_i}$. In that case the NICA eq. reduces to

$$Q_j = Q_j^{max} \frac{\left(\tilde{K}_j c_{D,j}\right)^m}{1+\left(\tilde{K}_j c_{D,j}\right)^m} \qquad \text{with} \quad m = \tilde{n}_j p \tag{15}$$

Eq. 15 is mathematically equivalent to the Langmuir-Freundlich equation, but here the exponent is a composite parameter that reflects both the cooperativity and the heterogeneity. Because the surfactant sorption covered the entire sorption range up to Q_j^{max} the exponent in Eq. 15 is also affected by the heterogeneity. For the calculation of the Donnan potential the total (net) charge of the humic acids was used and the proton charge adjustment due to the surfactant adsorption was accounted for. When the charge adjustments are not known and a computer code for NICA-Donnan calculations is available, a good method is to use the full (single) NICA-Donna equation together with humic substance specific parameters or generic humic substance parameters [55, 56], because then the charge adjustments are automatically taken into account. Computer codes that include the NICA-Donnan model are ECOSAT [241] and Visual MINTEQ ver. 3.0 / 3.1 [242]. Furthermore, the computer code 'Fit' [243] is designed to fit experimental results to a range of adsorption isotherm equations.

8. Surfactant adsorption on soils

8.1 General considerations and trends

Soils are composed of organic and inorganic components each with different adsorption characteristics as discussed in the previous sections. Therefore, the adsorption of a surfactant on a soil sample will depend on both the types of soil constituents and their relative proportions. This has also been stated in literature [244]. The overall surfactant

adsorption to a given soil can be thus be approximated by a weighted summation of the adsorptions to the individual constituents, or oppositely, the soil composition has to be known to be able to understand the surfactant adsorption behavior. Yet, the overall adsorption is not necessarily equal to the sum of the adsorptions to the different components because the soil components may mutually interact and this interaction will affect the adsorption. The mutual interaction is especially relevant and strong in the case of net positively charged metal oxides or layered silicates and the negatively charged humic and fulvic acids [245-249]. A similar situation is encountered with trace element binding to soils [50].

Some general trends have also been observed for surfactant adsorption to soils. Hydrophobic interaction is important with surfactant adsorption. Due to increasing hydrophobic attraction surfactant adsorption increases, in general, with increasing organic matter content of the soils [250-256]. Treatment of a soil with H_2O_2 to remove the organic matter will therefore, in general, decrease the surfactant adsorption [228, 229], but the contrary has also been observed [231]. Nonionic surfactants bind to soil surfaces with hydrogen bonding on the –OH sites of soils besides hydrophobic interaction [257], but hydrogen bonding is also possible to the hydrated cations on siloxane basal planes [198]. Longer alkyl chains lead to stronger lateral hydrophobic attraction, this explains that there is also a positive correlation between aliphatic chain length and surfactant adsorption on soils. An example of this behavior has been presented by Westall et al. [255] who showed that linear alkylbenzene sulfonates with longer carbon chains adsorbed stronger on a sediment (Fig. 29). Adsorption studies comparing linear and branched aliphatic chain structures have also been performed for soils and alumina [258-261]. For surfactants with the same number of CH_2 segments, branching leads to lower adsorbed amounts at the same surfactant concentration. This is largely due to a decrease of the hydrophobic attraction; the decrease in adsorption corresponds with the increase in CMC with branching [261].

Soils possess both permanent and pH-dependent charges [262, 263]. The contents of those charges differ among soils and affect the adsorption of charged surfactants strongly. Soils and sediments generally have negative charges, therefore, the adsorption of anionic surfactants on soils and sediments is much lower than that of nonionic and cationic surfactants [251, 255, 256, 264, 265]. Bera et al. [266] showed that surfactant adsorption on a sand was in the order of cationic > nonionic > anionic (Fig. 30). For surfactants with a similar alkyl chain the adsorption of the cationic surfactant is largest because of the electrostatic attraction between surface and surfactant and that of the anionic surfactant is smallest because of the electrostatic repulsion. An example where the relatively low anionic surfactant adsorption to sand is applied is surfactant-enhanced soil remediation. With surfactant-enhanced soil remediation, surfactant adsorption to the soil particles increases the surfactant use and this decreases the efficiency. Therefore, anionic surfactants have usually been chosen in these technologies [267-269]. However, nonionic surfactants are also often used for the remediation because of their lower CMC compared to ionic surfactants, higher degree of surface tension reduction, and relatively constant properties in the presence of salt [268, 269].

A positive correlation is observed between cationic surfactant adsorption and the soil CEC because the CEC characterizes the soil negative charge density and the latter generates the electrostatic attraction with cationic surfactants [270]. For the soils which possess variable charges the pH also affects the adsorption as shown in Fig. 31 [266]. Anionic surfactant adsorption decreases as pH increases [254, 255, 258-260, 266, 271] because the soil negative charge increases and/or the positive charge decreases. On the other hand, the opposite occurs for cationic surfactant adsorption as shown in Fig. 31 [266]. When after sodium citrate - bicarbonate - dithionite treatment the fraction amorphous oxides in soils is decreased, the adsorption of anionic surfactant also decreases because the density of positively charged sites of the soils decreases [260]. Nonionic surfactant adsorption

increases as pH decreases at low pH and remains almost constant at high pH (Fig. 31) [266]. The increase at low pH resulted from the increase of the surface hydroxyl sites (due to protonation of the surface oxygens) to which the EO segments of the nonionics can bind by hydrogen bonding.

The electrolyte concentration also affects ionic surfactant adsorption. It is observed that anionic surfactant adsorption on negatively charged soils increases, in general, with the increase of electrolyte concentration [255, 258, 266]. This must be due to a larger screening of both the electrostatic repulsion between surface and surfactant and the mutual electrostatic repulsion between the adsorbed surfactant ions. Increase of cationic surfactant adsorption on negatively charged soils with the increase of electrolyte concentration is also observed [272, 273]. This is caused by the screening of the electrostatic repulsion between the head-out adsorbed head groups of the cationic surfactants. This situation occurs for bilayer and/or admicelle adsorption where part of the head groups are directed to the soil solution; this part of the surfactants is adsorbed by hydrophobic attraction to the carbon chains of the surfactants adsorbed in the first layer. In this case, the cationic surfactant adsorption is also affected by the type of anion of the electrolyte. The surfactant adsorption increases in the order of SO_4^{2-}>Br^->Cl^- because the screening effect increases in this order [272]. The influence of the electrolyte concentration becomes reverse for ionic surfactants adsorbed in direct contact with the oppositely charged soil surface (head-on adsorption). The adsorption decreases with the increase of electrolyte concentration due to the screening of the electrostatic surfactant-surface attraction.

An example of the influence of the electrolyte concentration on the sorption of dodecyl benzene sulfonate (DBS) on a humic soil is depicted in Fig. 32 [258]. The adsorption decreases with decreasing electrolyte concentration because the electrostatic repulsion increases. The influence of the (smeared-out) electrostatic potential at the location of the adsorption sites can be evaluated by using the Langmuir-Donnan model. In this model it is

assumed that the soil particles are covered with humic substances and that the surfactant binds to the sites in the humic layer according to a Langmuir equation that is extended by including the electrostatic attraction by a Boltzmann factor, exp(-$zF\psi_D/RT$), where ψ_D is the Donnan potential in the humic layer (see section 7):

$$Q_j = Q_j^{\max} \frac{K' c_{D,j}}{1 + K' c_{D,j}} \qquad (16)$$

$$c_{D,j} = c_{b,j} \exp\left(\frac{-z_j F \psi_D}{RT} \right) \qquad (17)$$

where, Q_j is the surfactant adsorption, Q_j^{max} the maximum surfactant adsorption, K' the specific or chemical affinity constant (surface-surfactant), , z_j the valence of the surfactant ion, $c_{D,j}$ the surfactant concentration in the Donnan phase and $c_{b,j}$ the surfactant concentration in the bulk solution. When for all salt concentrations the value of Q_j^{max} is put equal to the surfactant sorption at the CMC (estimated to be 20 μmol/g), the affinity constant, K', and the Donnan potentials, ψ_D, can be obtained by fitting Eq. 16+17 to the experimental data in the region where the slope of the double logarithmic plots is about equal to unity (region where Eq. 16 applies). The fitted adsorption isotherms and obtained Donnan potentials are depicted in Fig. 32. The negative value of Donnan potential increases at constant salt concentration due to the fact that DBS sorption increases the negative charge of the particles. Increasing the salt concentration at a given DBS sorption has the opposite effect: the salt ions screen the particle charge; therefore, the repulsive Donnan potential decreases with increasing the salt concentration. At the lowest surfactant concentrations the isotherms rise very steeply; this likely indicates strong sorption to some highly active sites of the soil sample.

8.2 Fate of surfactants in soils; degradation, hysteresis and precipitation

When the fate of surfactants in soil and water environments is considered, surfactant degradation is important, as well as adsorption. However, different classes of surfactants have different degradation behavior in the environment [264]. Sodium dodecylsulfate (SDS) easily degrades, especially in humic soil. Therefore, the influence of degradation on adsorption experiments is significant. Results of some batch experiments of SDS in the presence of a highly humic non-allophanic andosol are depicted in Fig. 33 [274]; the sum of adsorption and degradation corresponds to the SDS decay in the soil solution. The "adsorption + degradation" amount at intermediate SDS concentrations increases with time due to increasing of degradation. The initial steep increase is somewhat puzzling; the irregular behavior suggests that either or both degradation and cooperative adsorption are important in this region [274].

The environment also affects the degradation; sodium dodecylbenzenesulfonate with a linear carbon chain (L-DBS) degrades in river water with a half-life of less than 3 days, but its degradation in aerobic soil with a half-life of 7–33 days is much longer [264]. In general, adsorption restricts L-DBS degradation, especially in soils with allophane and amorphous metal oxides [260], which adsorb the anionic surfactant by electrostatic attraction.

Hysteresis of adsorption, which implies different adsorbed amounts for the adsorption and the desorption isotherm [168, 169, 275], must be also considered as a distinctive phenomenon. In general, the adsorbed amount with desorption is larger than that of adsorption [169, 275]. The hysteresis can, in general, be due to kinetic and/or multicomponent adsorption effects. An important kinetic reason for the difference between the adsorption and desorption isotherm is that the kinetics of desorption become very slow when the adsorption isotherm is rather steep [276]. In this case the adsorption isotherm is the true isotherm, the desorption isotherm is an artifact. In multicomponent systems the adsorption conditions are often not the same as the desorption conditions. This is especially the case in the presence of impurities adsorbed to the solid and when the solid area to

solution volume ratio is different in the ad- and desorption experiment. In the case of adsorption by ion exchange (‘first layer’ adsorption) and hydrophobic attraction (admicelle formation or ‘second layer’ adsorption), desorption of the ‘second layer’ shows no hysteresis. This has, for instance, been observed for cationic surfactant adsorption on vermiculitic soil with a negative charge [272].

Ionic surfactant insolubility must be considered when the Krafft temperature is larger than the temperature under the conditions of the adsorption [201, 277, 278]. The Krafft temperature or *Krafft point* is the minimum temperature at which surfactants can form micelles, below the Krafft temperature surfactant added to a solution with a monomer concentration close to the CMC remains in the crystalline form. Therefore, micelles are not formed when the temperature is lower than the Krafft point. The Krafft point becomes higher when the coion of the surfactant is multivalent.

8.3 Influence of surfactant adsorption on soil structure and permeability

Because surfactants modify the surface characteristics of solids, they affect the structure of soils and this affects the water permeability and gas diffusion in soils [279-283]. Proper permeability and gas diffusion are required for crop growth; therefore, a good soil structure must be maintained in crop fields. When a soil disperses and swells during the irrigation or rainfall, dispersed soil particles clog the macro-pores (water transmission pores) in the soil and permeability is decreased. A change in soil structure that leads to a decrease in permeability is a negative factor in relation to agriculture and soil- water environment. Moreover, sometimes flooded water conveys soils and causes erosion; important soil is lost and the nutrients or chemicals in the eroded soil cause water contamination. The soil dispersion is generally caused by clays and the reduction of hydraulic conductivity is larger when the clay content in the soil is larger [280]. When the soil organic matter content is

reduced, the reduction of hydraulic conductivity becomes larger because clays in soils with a high organic content are not easily dispersed [279].

A review on soil structure can be found in [284]. Soil and clay structural changes with changing inter-particle interaction have been described in [263, 285-288]. In general, repulsive inter-particle interaction allows the particles to slip along each other, which leads to relatively dense structures; with attractive inter-particle interactions the particles stick together which retards further individual movement and the clustering leads to a relatively open structure. It is general knowledge that a settling stable dispersion forms a compact structure and a settling unstable dispersion forms an open structure. The use of surfactants for soil washing to remove low-solubility organic contaminants, such as oils, also changes the inter-particle interactions and can result in a significant change in the hydraulic conductivity of porous media [279, 283]. Electrolyte concentration, pH and specific ions that all likely affect the particle-particle interaction may also change the soil permeability [263, 288-297]. An example of the effect of surfactant adsorption on soil stability is depicted in Fig. 34 [272], which shows the adsorption isotherm of hexadecyltrimethylammonium (HDTMA=$C16TA^+$), on two vermiculitic soils (Na and Ca), and the corresponding effects on the electrophoretic mobility of the soil particles and the optical density of the soil suspension. When the soil is better dispersed, the optical density becomes larger. For the Na-soil, the shape of the isotherm in region I indicates that the vermiculite is expanding upon adsorption. Up to about adsorbed amounts equal to 1.0 CEC, the soil gradually flocculates with increasing surfactant adsorption and the electrophoretic mobility changes from negative to zero at the IEP, where the surfactant adsorption is about equal to the CEC. The negative charge of the soil is gradually compensated with the adsorbed surfactant charge; therefore, the electrostatic repulsion between the soil particles gradually vanishes and the dispersion is completely flocculated. With a vermiculitic soil and a cationic surfactant the adsorption occurs initially by ion exchange, this implies surfactant

head groups in contact with the surface and tails contacting the solution; therefore, also the hydrophobicity of the soil particles increases and this is likely a second contribution to the decrease in dispersion stability. When the adsorption becomes larger than the soil CEC further adsorption will occur by hydrophobic attraction and the formation of an admicellar layer (second layer) on the surface. With further adsorption the soil particles become positive and less hydrophobic and the soil disperses again. The positive charge is indicated by the positive electrophoretic mobilities, For the Ca-vermiculite-soil, the behavior is different. The shape of the isotherm indicates that there is negligible swelling of the vermiculite. Moreover, the electrophoretic mobilities are rather low and this explains the poor initial degree of dispersion. Surfactant adsorption by ion exchange hardly changes the external particle charge and hence the mobility stays low as does the degree of dispersion. The Ca-soil begins to disperse after passing the IEP where the particles become positive and the second adsorption layer starts, but the stability of dispersion stays somewhat lower than for the Na-soil. The latter may be due to the effect of the released Ca ions on the ionic strength.

Allred and Brown [279] showed that the soil hydraulic conductivity significantly decreased with the infiltration of ionic and nonionic surfactant solutions at high concentration (1 mol/kg); the behavior is depicted in Fig. 35. The curves of N1, N2 and N3 in Fig. 35A represent the nonionic surfactants, the curves of A1 and A2 in Fig. 35B represent the anionic surfactants, the curves of C1 and C2 in Fig. 35B represent the cationic surfactants, and the curve of AM1 in Fig. 35B represents the amphoteric surfactant. The hydraulic conductivity reduction was larger for ionic surfactants than nonionic surfactants. When an anionic surfactant is adsorbed on a negatively charged soil, the negative charge of the soil surface becomes larger and the soil particles disperse easier, and the particles slip easier along each other; therefore, the hydraulic conductivity decreases. When a cationic surfactant is adsorbed on the negatively charged soil, the situation is somewhat similar to

that described in the previous section for the vermiculite soils. The stability of dispersion goes through a minimum, but when the positive charge due to surfactant adsorption is sufficient the soil particles become well dispersive and the hydraulic conductivity tends to decrease. When the electrolyte concentration is large, the influence of ionic surfactant adsorption on the decrease of hydraulic conductivity is restricted [281], because the soil dispersion ability is inhibited by the strong screening of the particle-particle repulsion.

As a nonionic surfactant does not change the particle charge its effect on the dispersion stability can only result from the way the surfactant is adsorbed. On most natural surfaces the hydrophilic head group will be in contact with the surface and similarly as for cationic surfactants a second layer may become adsorbed at surfactant concentrations around the CMC. For short EO chains the adsorption in the 'first layer' is moderate and the transition to the 'second layer' occurs in a narrow concentration range close to the CMC. For long EO chains the adsorption in the 'first layer' is larger, but due to the large head group it is difficult for the alkyl chains to associate and only when the alkyl chains are also fairly long a sufficient 'second layer' will form. Also with kaolinite the edge surface probably contributes, but on montmorillonite this contribution is relatively small. Therefore, the behavior with respect to hydraulic conductivity will strongly depend on the type of nonionic surfactant and the type of soil surface. Mustafa and Letey [298] indicated for a hydrophobic sandy loam, a hydrophilic sandy loam and a hydrophilic clay loam that nonionic surfactant adsorption induced soil dispersion by decreasing the aggregate size.

Water infiltration into dry soils with a hydrophobic surface is also affected by surfactant adsorption. Fig. 36 shows the upward water infiltration into a peat moss column [299]. The bottom of the air-dried peat moss column was set 20 cm below the water table. A 70-mM SDS solution infiltrated faster than pure water because the surface became wettable after the adsorption of SDS. On the other hand, infiltration of the surfactant solution into dry sand became slower compared to pure water infiltration, because the sand was already wettable

without surfactant. In this case, they explained that the surface tension of surfactant solution was smaller than that of pure water and the viscosity of surfactant solution was larger than pure water and both effects decreased the rate of capillary infiltration.

Acknowledgements

The authors thank Hokkaido University for providing a ‘Visiting Professor’ grant to LKK for a period of 2 months and the ‘Japan Society for the Promotion of Science’ for the financial support via ‘Grants-in-Aid for Scientific Research (No. 25252042)’.

References

[1] Koopal LK. Wetting of solid surfaces: Fundamentals and charge effects. Adv Colloid Interface Sci 2012;179:29-42.

[2] Myers D. Surfactant science and technology. 3rd ed: John Wiley & Sons; 2005.

[3] Tadros TF. Surfactants in agrochemicals: CRC Press; 1994.

[4] Mulligan CN, Yong RN, Gibbs BF. Surfactant-enhanced remediation of contaminated soil: A review. Eng Geol 2001;60:371-80.

[5] Mao XH, Jiang R, Xiao W, Yu JG. Use of surfactants for the remediation of contaminated soils: A review. J Hazard Mater 2015;285:419-35.

[6] Kosswig K. Surfactants. Ullmann's encyclopedia of industrial chemistry: Wiley-VCH; 2002.

[7] McAvoy DC, Eckhoff WS, Rapaport RA. Fate of linear alkylbenzene sulfonate in the environment. Environ Toxicol Chem 1993;12:977-87.

[8] Zoller U. Handbook of detergents: Environmental impact : Surfactant science series 121: CRC Press; 2004.

[9] Jahan K, Balzer S, Mosto P. Toxicity of nonionic surfactants. In: Kungolos AG, Brebbia CA, Zamorano M, (eds). Environmental Toxicology II. Vol. 110: WIT Press; 2008.

[10] Rebello S, Asok AK, Mundayoor S, Jisha MS. Surfactants: Toxicity, remediation and green surfactants. Environ Chem Lett 2014;12:275-87.

[11] McWilliams P. Bioaccumulation potential of surfactants: A review. Aberdeen: European Oilfield Speciality Chemicals Association; 2000. http://www.eosca.com/publications-documents

[12] Scott MJ, Jones MN. The biodegradation of surfactants in the environment. Biochimica et Biophysica Acta (BBA)-Biomembranes 2000;1508:235-51.

[13] Gheorghe S, Lucaciu I, Paun I, Stoica C, Stanescu E. Ecotoxicological behavior of some cationic and amphoteric surfactants (biodegradation, toxicity and risk assessment). In: Chamy R, Rosenkranz F, (eds). Biodegradation - life of science. INTECH; 2013.

[14] Tan KH. Principles of soil chemistry. 4th ed: CRC Press; 2011.

[15] Schwarzenbach RP, Gschwend PM, Imboden DM. Environmental organic chemistry. 2nd ed: Wiley-Interscience; 2003.

[16] Brackmann B, Hager C. The statistical world of raw materials, fatty alcohols and surfactants. CD Proceedings 6th World Surfactant Congress CESIO, Berlin, Germany2004.

[17] Mulligan CN. Environmental applications for biosurfactants. Environ Pollut 2005;133:183-98.

[18] Bustamante M, Duran N, Diez MC. Biosurfactants are useful tools for the bioremediation of contaminated soil: A review. J Soil Sci Plant Nutr 2012;12:667-87.

[19] Everett DH. Manual of symbols and terminology for physicochemical quantities and units, appendix II: Definitions, terminology and symbols in colloid and surface chemistry. Pure Appl Chem 1972;31:577-638.

[20] Koopal LK. Definitions, terminology and symbols in colloid and surface chemistry , internet version with annotations of dh everett, manual of symbols and terminology for physicochemical quantities and units, appendix II: Definitions, terminology. Web Edition; 1972. http://old.iupac.org/reports/2001/colloid_2001/manual_of_s_and_t/manual_of_s_and_t.html

[21] Matijević E, Pethica B. The properties of ionized monolayers. Part 1.—sodium dodecyl sulphate at the air/water interface. Trans Faraday Soc 1958;54:1382-9.

[22] Matijević E, Pethica B. The properties of ionized monolayers. Part 2.—the thermodynamics of the ionic double layer of sodium dodecyl sulphate. Trans Faraday Soc 1958;54:1390-9.

[23] Matijević E, Pethica B. The properties of ionized monolayers. Part 3.—the thermodynamics of the ionic double layer of sodium octanoate. Trans Faraday Soc 1958;54:1400-7.

[24] Rosen MJ. Surfactants and interfacial phenomena. 3rd ed. New York: Wiley & Sons; 2004.

[25] Koopal LK. Modeling association and adsorption of surfactants. In: Esumi K, Ueno M, (eds). Structure-performance relationships in surfactants. Surfactant science series Vol. New York: Marcel Dekker; 2003. p. 111-96.

[26] Mukerjee P, Mysels KJ. Critical micelle concentrations of aqueous surfactant systems. Vol. NSRDS-NBS 36: National Institute of Standards and Technology, Washington D.C. USA; 1971.

[27] van Os NM, Haak JR, Rupert LAM. Physico-chemical properties of selected anionic, cationic and nonionic surfactants: Elsevier; 1993.

[28] Nagarajan R, Ruckenstein E. Theory of surfactant self-assembly: A predictive molecular thermodynamic approach. Langmuir 1991;7:2934-69.

[29] Nagarajan R. Molecular packing parameter and surfactant self-assembly: The neglected role of the surfactant tail. Langmuir 2002;18:31-8.

[30] Israelachvili JN, Mitchell DJ, Ninham BW. Theory of self-assembly of hydrocarbon amphiphiles into micelles and bilayers. J Chem Soc Faraday Trans 2 1976;72:1525-68.

[31] Israelachvili J. The science and applications of emulsions—an overview. Colloids Surf A 1994;91:1-8.

[32] Mitchell DJ, Ninham BW. Micelles, vesicles and microemulsions. J Chem Soc Faraday Trans 2 1981;77:601-29.

[33] Swift RS. Organic matter characterization. In: Sparks D, Page A, Helmke P, Loeppert R, Soltanpour P, Tabatabai M, et al., (eds). Methods of soil analysis part 3-chemical methods. Madison: Soil Science Society of America; 1996. p. 1011-69.

[34] Leenheer JA. Progression from model structures to molecular structures of natural organic matter components. Ann Environ Sci 2007;1:15.

[35] Sutton R, Sposito G. Molecular structure in soil humic substances: The new view. Environ Sci Technol 2005;39:9009-15.

[36] Langford CH, Melton JR. When should humicsubstances be treated as dynamic combinatorial systems? . In: Ghabbour EA, Davies G, (eds). Humic substances: Molecular details and applications in land and water conservation. New York: Taylor & Francis; 2005. p. 65-78.

[37] Avena MJ, Wilkinson KJ. Disaggregation kinetics of a peat humic acid: Mechanism and pH effects. Environ Sci Technol 2002;36:5100-5.

[38] Koopal LK, Saito T, Pinheiro JP, van Riemsdijk WH. Ion binding to natural organic matter: General considerations and the NICA-donnan model. Colloids Surf A 2005;265:40-54.

[39] Schulten H-R, Schnitzer M. Chemical model structures for soil organic matter and soils. Soil Sci 1997;162:115-30.

[40] Duval JFL, Wilkinson KJ, Van Leeuwen HP, Buffle J. Humic substances are soft and permeable: Evidence from their electrophoretic mobilities. Environ Sci Technol 2005;39:6435-45.

[41] Nederlof MM, De Wit JC, Van Riemsdijk WH, Koopal LK. Determination of proton affinity distributions for humic substances. Environ Sci Technol 1993;27:846-56.

[42] Nederlof MM, van Riemsdijk WH, Koopal LK. Heterogeneity analysis for binding data using an adapted smoothing spline technique. Environ Sci Technol 1994;28:1037-47.

[43] Kinniburgh DG, van Riemsdijk WH, Koopal LK, Borkovec M, Benedetti MF, Avena MJ. Ion binding to natural organic matter: Competition, heterogeneity, stoichiometry and thermodynamic consistency. Colloids Surf A 1999;151:147-66.

[44] Avena MJ, Vermeer AWP, Koopal LK. Volume and structure of humic acids studied by viscometry pH and electrolyte concentration effects. Colloids Surf A 1999;151:213-24.

[45] Tan WF, Koopal LK, Weng LP, van Riemsdijk WH, Norde W. Hurnic acid protein complexation. Geochim Cosmochim Acta 2008;72:2090-9.

[46] Jones MN, Bryan ND. Colloidal properties of humic substances. Adv Colloid Interface Sci 1998;78:1-48.

[47] Tipping E. Cation binding by humic substances. Cambridge (UK): Cambridge University Press; 2002.

[48] Dudal Y, Gérard F. Accounting for natural organic matter in aqueous chemical equilibrium models: A review of the theories and applications. Earth-Sci Rev 2004;66:199-216.

[49] Merdy P, Huclier S, Koopal LK. Modeling metal-particle interactions with an emphasis on natural organic matter. Environ Sci Technol 2006;40:7459-66.

[50] Groenenberg JE, Lofts S. The use of assemblage models to describe trace element partitioning, speciation, and fate: A review. Environ Toxicol Chem 2014;33:2181-96.

[51] Tipping E. Humic ion-binding model VI: An improved description of the interactions of protons and metal ions with humic substances. Aquat Geochem 1998;4:3-47.

[52] Smith E, Rey‐Castro C, Longworth H, Lofts S, Lawlor A, Tipping E. Cation binding by acid‐washed peat, interpreted with humic ion‐binding model VI‐fd. Eur J Soil Sci 2004;55:433-47.

[53] Tipping E, Lofts S, Sonke J. Humic ion-binding model VII: A revised parameterisation of cation-binding by humic substances. Environ Chem 2011;8:225-35.

[54] Benedetti MF, Van Riemsdijk WH, Koopal LK. Humic substances considered as a heterogeneous donnan gel phase. Environ Sci Technol 1996;30:1805-13.

[55] Milne CJ, Kinniburgh DG, Tipping E. Generic NICA-donnan model parameters for proton binding by humic substances. Environ Sci Technol 2001;35:2049-59.

[56] Milne CJ, Kinniburgh DG, Van Riemsdijk WH, Tipping E. Generic NICA-donnan model parameters for metal-ion binding by humic substances. Environ Sci Technol 2003;37:958-71.

[57] Koopal LK, Van Riemsdijk WH, De Wit JCM, Benedetti MF. Analytical isotherm equations for multicomponent adsorption to heterogeneous surfaces. J Colloid Interface Sci 1994;166:51-60.

[58] Koopal LK, van Riemsdijk WH, Kinniburgh DG. Humic matter and contaminants. General aspects and modeling metal ion binding. Pure Appl Chem 2001;73:2005-16.

[59] Saito T, Nagasaki S, Tanaka S, Koopal LK. Electrostatic interaction models for ion binding to humic substances. Colloids Surf A 2005;265:104-13.

[60] Zhuravlev L. The surface chemistry of amorphous silica. Zhuravlev model. Colloids Surf A 2000;173:1-38.

[61] Chuang I-S, Maciel GE. Probing hydrogen bonding and the local environment of silanols on silica surfaces via nuclear spin cross polarization dynamics. J Am Chem Soc 1996;118:401-6.

[62] Yang J, Wang E. Reaction of water on silica surfaces. Curr Opin Solid State Mater Sci 2006;10:33-9.

[63] Iler RK. The chemistry of silica: Solubility, polymerization, colloid and surface properties, and biochemistry. New York: Wiley-Interscience; 1979.

[64] Boehm HP. Chapter 5. Advances in catalysis and related subjects, vol 16. Academic Press, New York; 1966. p. 179.

[65] Tamura H, Tanaka A, Mita K, Furuichi R. Surface hydroxyl site densities on metal oxides as a measure for the ion-exchange capacity. J Colloid Interface Sci 1999;209:225-31.

[66] Pauling L. The principles determining the structure of complex ionic crystals. J Am Chem Soc 1929;51:1010-26.

[67] Brown ID. The chemical bond in inorganic chemistry. London: Oxford Univ. Press; 2002.

[68] Brown ID, Altermatt D. Bond-valence parameters obtained from a systematic analysis of the inorganic crystal structure database. Acta Crystallogr Sect B: Struct Sci 1985;41:244-7.

[69] Brown ID. Recent developments in the methods and applications of the bond valence model. Chem Rev 2009;109:6858-919.

[70] Hiemstra T, Van Riemsdijk WH, Bolt GH. Multisite proton adsorption modeling at the solid/solution interface of (hydr) oxides: A new approach: I. Model description and evaluation of intrinsic reaction constants. J Colloid Interface Sci 1989;133:91-104.

[71] Hiemstra T, Venema P, Van Riemsdijk WH. Intrinsic proton affinity of reactive surface groups of metal (hydr) oxides: The bond valence principle. J Colloid Interface Sci 1996;184:680-92.

[72] Hiemstra T, Vanriemsdijk WH, Bruggenwert MGM. Proton adsorption mechanism at the gibbsite and aluminum-oxide solid-solution interface. Neth J Agric Sci 1987;35:281-93.

[73] Hiemstra T, Van Riemsdijk WH. Effect of different crystal faces on experimental interaction force and aggregation of hematite. Langmuir 1999;15:8045-51.

[74] Hiemstra T, van Riemsdijk WH. On the relationship between surface structure and ion complexation of oxide-solution interface. In: Hubbard AT, (ed). Encyclopedia of surface and colloid science. New York: ; Marcel Dekker; 2002. p. 3773-99.

[75] Machesky ML, Wesolowski DJ, Palmer DA, Ridley MK. On the temperature dependence of intrinsic surface protonation equilibrium constants: An extension of the revised MUSIC model. J Colloid Interface Sci 2001;239:314-27.

[76] Koopal LK. Mineral hydroxides: From homogeneous to heterogeneous modelling. Electrochim Acta 1996;41:2293-305.

[77] Koopal LK. Ion adsorption on mineral oxide surfaces. In: Dąbrowski A, Tertykh VA, (eds). Adsorption on new and modified inorganic sorbents. Studies in surface science and catalysis Vol. 99. Amsterdam: Elsevier; 1996. Chapter 3, 5. p. 757 -96.

[78] Hiemstra T, Van Riemsdijk WH. Physical chemical interpretation of primary charging behaviour of metal (hydr) oxides. Colloids Surf 1991;59:7-25.

[79] Hiemenz PC. Principles of colloid and surface chemistry, 2nd edition, revised and expanded. New York: Marcel Dekker; 1986.

[80] Hiemstra T, Van Riemsdijk WH. On the relationship between charge distribution, surface hydration, and the structure of the interface of metal hydroxides. J Colloid Interface Sci 2006;301:1-18.

[81] Hiemstra T, Yong H, Van Riemsdijk WH. Interfacial charging phenomena of aluminum (hydr) oxides. Langmuir 1999;15:5942-55.

[82] Abendroth R. Behavior of a pyrogenic silica in simple electrolytes. J Colloid Interface Sci 1970;34:591-6.

[83] Gibb AW, Koopal LK. Electrochemistry of a model for patchwise heterogeneous surfaces: The rutile-hematite system. J Colloid Interface Sci 1990;134:122-38.

[84] Hiemstra T, Van Riemsdijk WH. A surface structural approach to ion adsorption: The charge distribution (CD) model. J Colloid Interface Sci 1996;179:488-508.

[85] Rietra RP, Hiemstra T, van Riemsdijk WH. The relationship between molecular structure and ion adsorption on variable charge minerals. Geochim Cosmochim Acta 1999;63:3009-15.

[86] Schulze DG. An introduction to soil mineralogy. In: Dixon JB, Schulze DG, (eds). Soil mineralogy with environmental application. Sssa book series no. 7 Vol. Madison: Soil Science Society of America 2002. Chapter 1. p. 1-34.

[87] Johnston CT, Tombacz E. Surface chemistry of soil minerals. In: Dixon JB, Schuze DG, (eds). Soil mineralogy with environmental application. Sssa book series no. 7 Vol. Madison: Soil Science Society of America; 2002. Chapter 2. p. 37-67.

[88] Bourg IC, Sposito G, Bourg AC. Modeling the acid–base surface chemistry of montmorillonite. J Colloid Interface Sci 2007;312:297-310.

[89] Liu X, Lu X, Meijer EJ, Wang R, Zhou H. Atomic-scale structures of interfaces between phyllosilicate edges and water. Geochim Cosmochim Acta 2012;81:56-68.

[90] Liu X, Lu X, Sprik M, Cheng J, Meijer EJ, Wang R. Acidity of edge surface sites of montmorillonite and kaolinite. Geochim Cosmochim Acta 2013;117:180-90.

[91] Koopal LK, van Riemsdijk WH. Electrosorption on random and patchwise heterogeneous surfaces: Electrical double-layer effects. J Colloid Interface Sci 1989;128:188-200.

[92] Avena MJ, De Pauli CP. Proton adsorption and electrokinetics of an argentinean montmorillonite. J Colloid Interface Sci 1998;202:195-204.

[93] Tombacz E, Regdon I. Humic substances as various colloidal systems. In: Senesi N, Miano TM, (eds). Humic substances in the global environment and implications on human health. Amsterdam: Elsevier; 1994. p. 139-44.

[94] Tombácz E, Varga K, Szántó F. An X-ray diffraction study of alkylammonium humate complexes. Colloid Polym Sci 1988;266:734-8.

[95] Traina SJ, McAvoy DC, Versteeg DJ. Association of linear alkylbenzenesulfonates with dissolved humic substances and its effect on bioavailability. Environ Sci Technol 1996;30:1300-9.

[96] Otto WH, Britten DJ, Larive CK. NMR diffusion analysis of surfactant–humic substance interactions. J Colloid Interface Sci 2003;261:508-13.

[97] Koopal LK, Goloub TP, Davis TA. Binding of ionic surfactants to purified humic acid. J Colloid Interface Sci 2004;275:360-7.

[98] Yee MM, Miyajima T, Takisawa N. Evaluation of amphiphilic properties of fulvic acid and humic acid by alkylpyridinium binding study. Colloids Surf A 2006;272:182-8.

[99] Yee MM, Miyajima T, Takisawa N. Thermodynamic studies of dodecylpyridinium ion binding to fulvic acid. Colloids Surf A 2006;287:68-74.

[100] Yee MM, Miyajima T, Takisawa N. Study of ionic surfactants binding to humic acid and fulvic acid by potentiometric titration and dynamic light scattering. Colloids Surf A 2009;347:128-32.

[101] Yee MM, Miyajima T, Takisawa N. Thermodynamic studies of dodecylpyridinium ion binding to humic acid and effect of solution parameters on their binding. Colloids Surf A 2007;295:61-6.

[102] Matsuda M, Kaminaga A, Hayakawa K, Takisawa N, Miyajima T. Surfactant binding by humic acids in the presence of divalent metal salts. Colloids Surf A 2009;347:45-9.

[103] Ishiguro M, Tan WF, Koopal LK. Binding of cationic surfactants to humic substances. Colloids Surf A 2007;306:29-39.

[104] Thieme J, Niemeyer J. Interaction of colloidal soil particles, humic substances and cationic detergents studied by X-ray microscopy. In: Rehage H, Peschel G, (eds). Structure, dynamics and properties of disperse colloidal systems. Progress in colloid & polymer science Vol.: Steinkopff; Prog. Colloid Polym. Sci. 111; 1998. Chapter 33. p. 193-201.

[105] Barron W, Murray BS, Scales PJ, Healy TW, Dixon DR, Pascoe M. The streaming current detector - a comparison with conventional electrokinetic techniques. Colloids Surf A 1994;88:129-39.

[106] Walker CA, Kirby JT, Dentel SK. The streaming current detector: A quantitative model. J Colloid Interface Sci 1996;182:71-81.

[107] Kam S-K, Gregory J. The interaction of humic substances with cationic polyelectrolytes. Water Res 2001;35:3557-66.

[108] Tan W-F, Norde W, Koopal LK. Humic substance charge determination by titration with a flexible cationic polyelectrolyte. Geochim Cosmochim Acta 2011;75:5749-61.

[109] Dobias B. Surfactant adsorption and dispersion stability in mineral flotation. In: Dobias B, (ed). Coagulation and flocculation: Theory and applications Surfactant science series Vol. 126. 2nd ed. New York: Taylor and Francis (CRC Press) Boca Raton (USA); 2005. Chapter 10. p. 663-765.

[110] Shang C, Rice JA. Investigation of humate-cetyltrimethylammonium complexes by small-angle X-ray scattering. J Colloid Interface Sci 2007;305:57-61.

[111] Subbiah D, Mishra AK. Humic acid–cetyltrimethylammonium bromide interaction: A fluorimetric study. Luminescence 2009;24:84-9.

[112] Ishiguro M, Koopal LK. Binding of alkylpyridinium chloride surfactants to sodium polystyrene sulfonate. Colloids Surf A 2009;347:69-75.

[113] Chen Y, Droge ST, Hermens JL. Analyzing freely dissolved concentrations of cationic surfactant utilizing ion-exchange capability of polyacrylate coated solid-phase microextraction fibers. J Chromatogr A 2012;1252:15-22.

[114] Chen Y, Hermens JL, Droge ST. Influence of organic matter type and medium composition on the sorption affinity of c12-benzalkonium cation. Environ Pollut 2013;179:153-9.

[115] Ishiguro M, Koopal LK. Predictive model of cationic surfactant binding to humic substances. Colloids Surf A 2011;379:70-8.

[116] Droge S, Goss K-U. Effect of sodium and calcium cations on the ion-exchange affinity of organic cations for soil organic matter. Environ Sci Technol 2012;46:5894-901.

[117] Somasundaran P, Fuerstenau D. Mechanisms of alkyl sulfonate adsorption at the alumina-water interface1. J Phys Chem 1966;70:90-6.

[118] Koopal LK, Lee EM, Böhmer MR. Adsorption of cationic and anionic surfactants on charged metal-oxide surfaces. J Colloid Interface Sci 1995;170:85-97.

[119] Manne S, Cleveland J, Gaub H, Stucky G, Hansma P. Direct visualization of surfactant hemimicelles by force microscopy of the electrical double layer. Langmuir 1994;10:4409-13.

[120] Hough DB, Rendall HM. Adsorption of ionic surfactants. In: Parfitt CD, Rochester CH, (eds). Adsorption from solution at the solid/liquid interface. London: Academic Press; 1983. p. 247-319.

[121] Clunie JS, Ingram BT. Adsorption non-ionic surfactants. In: Parfitt CD, Rochester CH, (eds). London: Academic Press; 1983. p. 105-52.

[122] Manne S, Gaub HE. Molecular-organization of surfactants at solid-liquid interfaces. Science 1995;270:1480-2.

[123] Manne S, Gaub HE. Force microscopy: Measurement of local interfacial forces and surface stresses. Current Opinion in Colloid & Interface Science 1997;2:145-52.

[124] Johnson R, Nagarajan R. Modeling self-assembly of surfactants at solid–liquid interfaces. II. Hydrophilic surfaces. Colloids Surf A 2000;167:21-30.

[125] Johnson RA, Nagarajan R. Modeling self-assembly of surfactants at solid/liquid interfaces. I. Hydrophobic surfaces. Colloids Surf A 2000;167:31-46.

[126] Nagarajan R. Theory of micelle formation. In: Esumi K, Ueno M, (eds). Structure-performance relationships in surfactants Surfactant science series Vol. 112. 2nd ed. New York: Marcel Dekker (CRC Press); 1997. p. 1-109.

[127] Koopal LK, Goloub T, de Keizer A, Sidorova MP. The effect of cationic surfactants on wetting, colloid stability and flotation of silica. Colloids Surf A 1999;151:15-25.

[128] Atkin R, Craig VSJ, Wanless EJ, Biggs S. Mechanism of cationic surfactant adsorption at the solid–aqueous interface. Adv Colloid Interface Sci 2003;103:219-304.

[129] Tiberg F, Brinck J, Grant L. Adsorption and surface-induced self-assembly of surfactants at the solid–aqueous interface. Current opinion in colloid & interface science 1999;4:411-9.

[130] Zhmud B, Tiberg F. Interfacial dynamics and structure of surfactant layers. Adv Colloid Interface Sci 2005;113:21-42.

[131] Schrödle S, Richmond GL. In situ non-linear spectroscopic approaches to understanding adsorption at mineral–water interfaces. J Phys D: Appl Phys 2008;41:033001 (14pp).

[132] Paria S, Khilar KC. A review on experimental studies of surfactant adsorption at the hydrophilic solid–water interface. Adv Colloid Interface Sci 2004;110:75-95.

[133] Zhang R, Somasundaran P. Advances in adsorption of surfactants and their mixtures at solid/solution interfaces. Adv Colloid Interface Sci 2006;123:213-29.

[134] Böhmer MR, Koopal LK. Adsorption of ionic surfactants on variable-charge surfaces. 1. Charge effects and structure of the adsorbed layer. Langmuir 1992;8:2649-59.

[135] Böhmer MR, Koopal LK. Adsorption of ionic surfactants on variable-charge surfaces. 2. Molecular architecture and structure of the adsorbed layer. Langmuir 1992;8:2660-5.

[136] Lee EM, Koopal LK. Adsorption of cationic and anionic surfactants on metal oxide surfaces: Surface charge adjustment and competition effects. J Colloid Interface Sci 1996;177:478-89.

[137] Goloub TP, Koopal LK. Adsorption of cationic surfactants on silica. Comparison of experiment and theory. Langmuir 1997;13:673-81.

[138] Goloub TP, Koopal LK, Bijsterbosch BH, Sidorova MP. Adsorption of cationic surfactants on silica. Surface charge effects. Langmuir 1996;12:3188-94.

[139] Somasundaran P, Kunjappu JT. Insitu investigation of adsorbed surfactants and polymers on solids in solution. Colloids Surf 1989;37:245-68.

[140] Gebhardt JE, Fuerstenau DW. The effect of trace surfactant impurities on the adsorption of sodium dodecyl sulfonate on hematite. J Colloid Interface Sci 1984;101:278-9.

[141] Bhagat RP. Kinetics of sodium dodecyl benzene sulfonate adsorption on hematite and its interaction with polyacrylamide. Colloid Polym Sci 2001;279:33-8.

[142] Wangchareansak T, Craig VS, Notley SM. Adsorption isotherms and structure of cationic surfactants adsorbed on mineral oxide surfaces prepared by atomic layer deposition. Langmuir 2013;29:14748-55.

[143] De Keizer A, Böhmer MR, Mehrian T, Koopal LK. Adsorption of organic ions at the solid—electrolyte interface. Interpretation of common intersection points. Colloids Surf 1990;51:339-57.

[144] Nevskaia DM, Guerrero-Ruiz A, Lopez-Gonzalez JD. Adsorption of polyoxyethylenic nonionic and anionic surfactants from aqueous solution: Effects induced by the addition of nacl and CaCl2. J Colloid Interface Sci 1998;205:97-105.

[145] Rupprecht HH. Influence of solvents on adsorption of ionic surfactants on highly dispersed silicas. J Pharm Sci 1972;61:700-2.

[146] Gao YY, Du JH, Gu TR. Hemimicelle formation of cationic surfactants at the silica-gel water interface. J Chem Soc Faraday Trans 1 1987;83:2671-9.

[147] Gu T, Huang Z. Thermodynamics of hemimicellization of cetyltrimethylammonium bromide at the silica-gel water interface. Colloids Surf 1989;40:71-6.

[148] Bijsterbosch BH. Characterization of silica surfaces by adsorption from solution - investigations into mechanism of adsorption of cationic surfactants. J Colloid Interface Sci 1974;47:186-98.

[149] Koopal LK, Goloub TP. Self-assembly of ionic surfactants adsorbed on mineral oxides: Surface charge and salt effects. In: Sharma R, (ed). Surfactant adsorption and surface solubilization acs symposium series 615. 78. Washington: American Chemical Society; 1995. Chapter 6. p. 78-103.

[150] Zhu BY, Gu TR. General isotherm equation for adsorption of surfactants at solid liquid interfaces. J Chem Soc Faraday Trans 1 1989;85:3813-7.

[151] Zhu BY, Gu TR, Zhao XL. General isotherm equation for adsorption of surfactants at solid liquid interfaces .2. Applications. J Chem Soc Faraday Trans 1 1989;85:3819-24.

[152] Böhmer MR, Koopal LK. Association and adsorption of nonionic flexible chain surfactants. Langmuir 1990;6:1478-84.

[153] Böhmer MR, Koopal LK, Janssen R, Lee EM, Thomas RK, Rennie AR. Adsorption of nonionic surfactants on hydrophilic surfaces - an experimental and theoretical-study on association in the adsorbed layer. Langmuir 1992;8:2228-39.

[154] Moudgil BM, Soto H, Somasondaran P. In: Nagaraj DR, Somasundaran P, Moudgil BM, (eds). Reagents in mineral technology. Surfactant science series Vol. New York: M. Dekker (CRC Press); 1988. Chapter 3. p. 79.

[155] Pashley RM, Israelachvili JN. A comparison of surface forces and interfacial properties of mica in purified surfactant solutions. Colloids Surf 1981;2:169-87.

[156] Herder PC. Interactions between mica surfaces in dodecyl-and octylammonium chloride solutions. J Colloid Interface Sci 1990;134:346-56.

[157] Menezes JL, Yan J, Sharma MM. The mechanism of alteration of macroscopic contact angles by the adsorption of surfactants. Colloids Surf 1989;38:365-90.

[158] Mishra SK. In: Nagaraj DR, Somasundaran P, Moudgil BM, (eds). Reagents in mineral technology. Surfactant science series Vol. New York: M. Dekker(CRC Press); 1987. Chapter 7. p. 195.

[159] Novich BE. Flotation response prediction from interfacial properties. Colloids Surf 1990;46:255-69.

[160] Levitz P. Adsorption of non ionic surfactants at the solid/water interface. Colloids Surf A 2002;205:31-8.

[161] Denoyel R, Rouquerol J. Thermodynamic (including microcalorimetry) study of the adsorption of nonionic and anionic surfactants onto silica, kaolin, and alumina. J Colloid Interface Sci 1991;143:555-72.

[162] Gonzalez G, Travalloni-Louvisse AM. The effect of Triton X-100 and ethanol on the wettability of quartz. Langmuir 1989;5:26-9.

[163] Levitz P, Van Damme H, Keravis D. Fluorescence decay study of the adsorption of nonionic surfactants at the solid-liquid interface. 1. Structure of the adsorption layer on a hydrophilic solid. J Phys Chem 1984;88:2228-35.

[164] Levitz P, Van Damme H. Fluorescence decay study of the adsorption of nonionic surfactants at the solid-liquid interface. 2. Influence of polar chain length. J Phys Chem 1986;90:1302-10.

[165] Postmus BR, Leermakers FAM, Cohen Stuart MA. Self-consistent field modeling of non-ionic surfactants at the silica-water interface: Incorporating molecular detail. Langmuir 2008;24:3960-9.

[166] Del Hoyo C, Dorado C, Rodríguez-Cruz M, Sánchez-Martín M. Physico-chemical study of selected surfactant-clay mineral systems. J Therm Anal Calorim 2008;94:227-34.

[167] Poirier JE, Cases JM. Anionic surfactant adsorption onto silicate minerals the role of the cations. Colloids Surf 1991;55:333-44.

[168] Siracusa PA, Somasundaran P. Adsorption desorption and hysteresis of sulfonates on kaolinite - pH effects. J Colloid Interface Sci 1986;114:184-93.

[169] Siracusa PA, Somasundaran P. Mechanism of hysteresis in sulfonate kaolinite adsorption desorption systems - chromatographic-separation of isomers. J Colloid Interface Sci 1987;120:100-9.

[170] Ananthapadmanabhan KP, Somasundaran P. Mechanism for adsorption maximum and hysteresis in a sodium dodecylbenzenesulfonate/kaolinite system. Colloids Surf 1983;7:105-14.

[171] Lagaly G, Dékany I. Adsorption on hydrophobized surfaces: Clusters and self-organization. Adv Colloid Interface Sci 2005;114:189-204.

[172] Bergaya F, Theng BKG, Lagaly G. Modified clays and clay minerals. In: Bergaya F, Lagaly G, (eds). Handbook of clay science. 2nd ed: Elsevier; 2013. p. 261-3.

[173] Lagaly G, Ogawa M, Dekany I. Clay mineral organic interactions. In: Bergaya F, Lagaly G, (eds). Handbook of clay science. 2nd ed: Elsevier; 2013. Chapter 7.3. p. 309-78.

[174] de Paiva LB, Morales AR, Díaz FRV. Organoclays: Properties, preparation and applications. Appl Clay Sci 2008;42:8-24.

[175] Lagaly G. Interaction of alkylamines with different types of layered compounds. Solid State Ionics 1986;22:43-51.

[176] Osman MA, Ploetze M, Skrabal P. Structure and properties of alkylammonium monolayers self-assembled on montmorillonite platelets. J Phys Chem B 2004;108:2580-8.

[177] Heinz H, Vaia RA, Krishnamoorti R, Farmer BL. Self-assembly of alkylammonium chains on montmorillonite: Effect of chain length, head group structure, and cation exchange capacity. Chem Mater 2007;19:59-68.

[178] Liu X, Lu X, Wang R, Zhou H, Xu S. Interlayer structure and dynamics of alkylammonium-intercalated smectites with and without water: A molecular dynamics study. Clays Clay Miner 2007;55:554-64.

[179] Mehrian T, De Keizer A, Lyklema J. Effect of temperature on the adsorption of organic cations on charged surfaces. Langmuir 1991;7:3094-8.

[180] Mehrian T, De Keizer A, Korteweg A, Lyklema J. Thermodynamics of adsorption of dodecylpyridinium chloride on Na-kaolinite. Colloids Surf A 1993;73:133-43.

[181] Mehrian T, Dekeizer A, Korteweg AJ, Lyklema J. Thermodynamics of micellization of n-alkylpyridinium chlorides. Colloids Surf A 1993;71:255-67.

[182] Patterson D, Barbe M. Enthalpy-entropy compensation and order in alkane and aqueous systems. J Phys Chem 1976;80:2435-6.

[183] Shinoda K. Iceberg formation and solubility. J Phys Chem 1977;81:1300-2.

[184] Xu S, Boyd SA. Cationic surfactant adsorption by swelling and nonswelling layer silicates. Langmuir 1995;11:2508-14.

[185] Wang J, Han B, Dai M, Yan H, Li Z, Thomas R. Effects of chain length and structure of cationic surfactants on the adsorption onto Na–kaolinite. J Colloid Interface Sci 1999;213:596-601.

[186] Qi L, Liao W, Bi Z. Adsorption of conventional and gemini cationic surfactants in nonswelling and swelling layer silicate. Colloids Surf A 2007;302:568-72.

[187] Li Z, Bowman RS. Counterion effects on the sorption of cationic surfactant and chromate on natural clinoptilolite. Environ Sci Technol 1997;31:2407-12.

[188] Li Z, Gallus L. Surface configuration of sorbed hexadecyltrimethylammonium on kaolinite as indicated by surfactant and counterion sorption, cation desorption, and ftir. Colloids Surf A 2005;264:61-7.

[189] Li Z, Gallus L. Adsorption of dodecyl trimethylammonium and hexadecyl trimethylammonium onto kaolinite—competitive adsorption and chain length effect. Appl Clay Sci 2007;35:250-7.

[190] Borden D, Giese RF. Baseline studies of the clay minerals society source clays: Cation exchange capacity measurements by the ammonia-electrode method. Clays Clay Miner 2001;49:444-5.

[191] Ammann L. Cation exchange and adsorption on clays and clay minerals. Dissertation: Christian-Albrechts-Universität, Kiel; 2003.

[192] Malek NANN, Ramli NI. Characterization and antibacterial activity of cetylpyridinium bromide (cpb) immobilized on kaolinite with different cpb loadings. Appl Clay Sci 2015;109:8-14.

[193] Tertre E, Castet S, Berger G, Loubet M, Giffaut E. Surface chemistry of kaolinite and Na-montmorillonite in aqueous electrolyte solutions at 25 and 60 c: Experimental and modeling study. Geochim Cosmochim Acta 2006;70:4579-99.

[194] Hanna HS, Somasundaran P. Equilibration of kaolinite in aqueous inorganic and surfactant solutions. J Colloid Interface Sci 1979;70:181-91.

[195] Siracusa PA, Somasundaran P. The role of mineral dissolution in the adsorption of dodecylbenzenesulfonate on kaolinite and alumina. Colloids Surf 1987;26:55-77.

[196] Torn LH, De Keizer A, Koopal LK, Lyklema J. Mixed adsorption of poly (vinylpyrrolidone) and sodium dodecylbenzenesulfonate on kaolinite. J Colloid Interface Sci 2003;260:1-8.

[197] Torn LH, de Keizer A, Koopal LK, Lyklema J, Blokzijl W. Polymer adsorption on a patchwise heterogeneous surface. In: Lagaly G, (ed). Horizons 2000 – aspects of colloid and interface science at the turn of the millenium. Progress in colloid & polymer science Vol. 109: Steinkopff; 1998. Chapter 18. p. 153-60.

[198] Deng Y, Dixon JB, White GN. Bonding mechanisms and conformation of poly (ethylene oxide)-based surfactants in interlayer of smectite. Colloid Polym Sci 2006;284:347-56.

[199] Nevskaia D, Guerrero-Ruız A, López-González JdD. Adsorption of polyoxyethylenic surfactants on quartz, kaolin, and dolomite: A correlation between surfactant structure and solid surface nature. J Colloid Interface Sci 1996;181:571-80.

[200] Tahani A, Van Damme H, Noik C, Levitz P. Adsorption of nonionic surfactants on kaolins. J Colloid Interface Sci 1996;184:469-76.

[201] Yang K, Zhu LZ, Xing BS. Sorption of sodium dodecylbenzene sulfonate by montmorillonite. Environ Pollut 2007;145:571-6.

[202] Pan J, Yang G, Han B, Yan H. Studies on interaction of dodecyltrimethylammonium bromide with Na-and Al-montmorillonite. J Colloid Interface Sci 1997;194:276-80.

[203] Xu SH, Boyd SA. Alternative model for cationic surfactant adsorption by layer silicates. Environ Sci Technol 1995;29:3022-8.

[204] Delgado ÁV, González-Caballero F, Hunter RJ, Koopal LK, Lyklema J. Measurement and interpretation of electrokinetic phenomena. J Colloid Interface Sci 2007;309:194-224.

[205] Yariv S, Cross H. Formation of aqueous solutions and suspensions of hydrophobic colloids. Geochemistry of colloid systems. Springer; 1979. p. 157-206.

[206] Tahani A, Karroua M, Van Damme H, Levitz P, Bergaya F. Adsorption of a cationic surfactant on Na–montmorillonite: Inspection of adsorption layer by X-ray and fluorescence spectroscopies. J Colloid Interface Sci 1999;216:242-9.

[207] Zhu J, Zhu L, Zhu R, Chen B. Microstructure of organo-bentonites in water and the effect of steric hindrance on the uptake of organic compounds. Clays Clay Miner 2008;56:144-54.

[208] Cygan RT. Molecular modeling in mineralogy and geochemistry. Reviews in Mineralogy and Geochemistry 2001;42:1-35.

[209] He HP, Galy J, Gerard J-F. Molecular simulation of the interlayer structure and the mobility of alkyl chains in HDTMA+/montmorillonite hybrids. J Phys Chem B 2005;109:13301-6.

[210] Tambach TJ, Boek ES, Smit B. Molecular order and disorder of surfactants in clay nanocomposites. PCCP 2006;8:2700-2.

[211] Cygan RT, Liang J-J, Kalinichev AG. Molecular models of hydroxide, oxyhydroxide, and clay phases and the development of a general force field. J Phys Chem B 2004;108:1255-66.

[212] Kumar PP, Kalinichev AG, Kirkpatrick RJ. Hydration, swelling, interlayer structure, and hydrogen bonding in organolayered double hydroxides: Insights from molecular dynamics simulation of citrate-intercalated hydrotalcite. J Phys Chem B 2006;110:3841-4.

[213] Zhou Q, Shen W, Zhu JX, Zhu RL, He HP, Zhou JH, Yuan P. Structure and dynamic properties of water saturated CTMA-montmorillonite: Molecular dynamics simulations. Appl Clay Sci 2014;97-98:62-71.

[214] Lokar WJ, Koopal LK, Leermakers FAM, Ducker WA. Self-consistent field analysis of ionic surfactant adsorption regulation in the aqueous film between two neutral solids. J Phys Chem B 2004;108:3633-43.

[215] Lokar WJ, Koopal LK, Leermakers FAM, Ducker WA. Confinement-induced phase behavior and adsorption regulation of ionic surfactants in the aqueous film between charged solids. J Phys Chem B 2004;108:15033-42.

[216] Koopal LK, Leermakers FAM, Lokar WJ, Ducker WA. Confinement-induced phase transition and hysteresis in colloidal forces for surfactant layers on hydrophobic surfaces. Langmuir 2005;21:10089-95.

[217] Leermakers FAM, Koopal LK, Lokar WJ, Ducker WA. Modeling of confinement-induced phase transitions for surfactant layers on amphiphilic surfaces. Langmuir 2005;21:11534-45.

[218] Rheinländer T, Klumpp E, Schwuger MJ. On the adsorption of hydrophobic pollutants on surfactant/clay complexes: Comparison of the influence of a cationic and a nonionic surfactant. J Dispersion Sci Technol 1998;19:379-98.

[219] Sonon LS, Thompson ML. Sorption of a nonionic polyoxyethylene lauryl ether surfactant by 2 : 1 layer silicates. Clays Clay Miner 2005;53:45-54.

[220] Backhaus WK, Klumpp E, Narres H-D, Schwuger MJ. Adsorption of 2, 4-dichlorophenol on montmorillonite and silica: Influence of nonionic surfactants. J Colloid Interface Sci 2001;242:6-13.

[221] Giles CH, Smith D, Huitson A. A general treatment and classification of the solute adsorption isotherm. I. Theoretical. J Colloid Interface Sci 1974;47:755-65.

[222] Lee J-F, Liao P-M, Kuo C-C, Yang H-T, Chiou CT. Influence of a nonionic surfactant (Triton X-100) on contaminant distribution between water and several soil solids. J Colloid Interface Sci 2000;229:445-52.

[223] Yang K, Zhu L, Zhao B. Minimizing losses of nonionic and anionic surfactants to a montmorillonite saturated with calcium using their mixtures. J Colloid Interface Sci 2005;291:59-66.

[224] Koopal LK. The effect of polymer polydispersity on the adsorption isotherm. J Colloid Interface Sci 1981;83:116-29.

[225] Shen Y-H. Preparations of organobentonite using nonionic surfactants. Chemosphere 2001;44:989-95.

[226] Deng Y, Dixon JB, White GN. Intercalation and surface modification of smectite by two non-ionic surfactants. Clays Clay Miner 2003;51:150-61.

[227] Guégan R, Gautier M, Bény J-M, Muller F. Adsorption of a C10E3 non-ionic surfactant on a Ca-smectite. Clays Clay Miner 2009;57:502-9.

[228] Guégan R. Intercalation of a nonionic surfactant (C10E3) bilayer into a Na-montmorillonite clay. Langmuir 2010;26:19175-80.

[229] Sips R. On the structure of a catalyst surface. J Chem Phys 1948;16:490-5.

[230] Sips R. On the structure of a catalyst surface. II. J Chem Phys 1950;18:1024-6.

[231] Bolt GH, Bruggenwert MGM. Soil chemistry, A. Basic elements. Amsterdam: Elsevier; 1978.

[232] Koopal LK, Ralston J. Chain-length effects in the adsorption of surfactants at aqueous interfaces - comparison of existing adsorption models with a new model. J Colloid Interface Sci 1986;112:362-79.

[233] Koopal LK, Keltjens L. Adsorption of ionic surfactants on charged solids. Adsorption models. Colloids Surf 1986;17:371-88.

[234] Scamehorn JF, Schechter RS, Wade WH. Adsorption of surfactants on mineral oxide surfaces from aqueous-solutions .1. Isomerically pure anionic surfactants. J Colloid Interface Sci 1982;85:463-78.

[235] Drach M, Rudziński W, Narkiewicz-Michalek J. Theoretical modeling of ionic surfactant adsorption on mineral oxide surfaces. J Dispersion Sci Technol 2000;21:683-710.

[236] Lajtar L, Narkiewicz-Michalek J, Rudzinski W, Partyka S. A new theoretical approach to adsorption of ionic surfactants at water/oxide interfaces: Studies of the mechanism of cationic surfactant adsorption. Langmuir 1994;10:3754-64.

[237] Li B, Ruckenstein E. Adsorption of ionic surfactants on charged solid surfaces from aqueous solutions. Langmuir 1996;12:5052-63.

[238] Leermakers FAM, Scheutjens JMHM. Statistical thermodynamics of association colloids. I. Lipid bilayer membranes. J Chem Phys 1988;89:3264-74.

[239] Böhmer MR, Koopal LK, Lyklema J. Micellization of ionic surfactants: Calculations based on a self-consistent field lattice model. J Phys Chem 1991;95:9569-78.

[240] Leermakers FAM. Physical chemistry and soft matter (pcc); to research; to self-consistent field theory and its applications (prof.Dr.Ir. Frans leermakers). http://www.wageningenur.nl/en/Expertise-Services/Chair-groups.htm

[241] Keizer M, Van Riemsdijk WH. ECOSAT. Department of Environmental Science, Subdepartment Soil Science and Plant Nutrition: Wageningen Agricultural University Wageningen; 1998. http://www.wageningenur.nl/en/Expertise-Services/Chair-groups.htm.

[242] Gustafsson JP. Visual MINTEQ ver. 3.0 / 3.1. KTH Royal Institute of Technology, Sweden, email: gustafjp@kth.se.

[243] Kinniburgh DG, Tang CK. FIT; Technical Report WD/93/23. British Geological Survey, Natural Environment Research Council.: Keyworth, Great Britain; 1993.

[244] Zhu LZ, Yang K, Lou BF, Yuan BH. A multi-component statistic analysis for the influence of sediment/soil composition on the sorption of a nonionic surfactant (Triton X-100) onto natural sediments/soils. Water Res 2003;37:4792-800.

[245] Davis JA. Adsorption of natural dissolved organic matter at the oxide/water interface. Geochim Cosmochim Acta 1982;46:2381-93.

[246] Varadachari C, Chattopadhyay T, Ghosh K. Complexation of humic substances with oxides of iron and aluminum. Soil Sci 1997;162:28-34.

[247] Gu B, Schmitt J, Chen Z, Liang L, McCarthy JF. Adsorption and desorption of natural organic matter on iron oxide: Mechanisms and models. Environ Sci Technol 1994;28:38-46.

[248] Vermeer AWP, Van Riemsdijk WH, Koopal LK. Adsorption of humic acid to mineral particles. 1. Specific and electrostatic interactions. Langmuir 1998;14:2810-9.

[249] Saito T, Koopal LK, van Riemsdijk WH, Nagasaki S, Tanaka S. Adsorption of humic acid on goethite: Isotherms, charge adjustments, and potential profiles. Langmuir 2004;20:689-700.

[250] Murti GSR, Volk VV, Jackson ML. Soil adsorption of linear alkylate sulfonate. Soil Sci Soc Am Proc 1966;30:685-&.

[251] Urano K, Saito M, Murata C. Adsorption of surfactants on sediments. Chemosphere 1984;13:293-300.

[252] Hand VC, Williams GK. Structure-activity-relationships for sorption of linear alkylbenzenesulfonates. Environ Sci Technol 1987;21:370-3.

[253] McAvoy DC, White CE, Moore BL, Rapaport RA. Chemical fate and transport in a domestic septic system - sorption and transport of anionic and cationic surfactants. Environ Toxicol Chem 1994;13:213-21.

[254] Fytianos K, Voudrias E, Papamichali A. Behavior and fate of linear alkylbenzene sulfonate in different soils. Chemosphere 1998;36:2741-6.

[255] Westall JC, Chen H, Zhang WJ, Brownawell BJ. Sorption of linear alkylbenzenesulfonates on sediment materials. Environ Sci Technol 1999;33:3110-8.

[256] Rodriguez-Cruz MS, Sanchez-Martin MJ, Sanchez-Camazano M. A comparative study of adsorption of an anionic and a non-ionic surfactant by soils based on physicochemical and mineralogical properties of soils. Chemosphere 2005;61:56-64.

[257] Somasundaran P, Snell ED, Xu Q. Adsorption behavior of alkylarylethoxylated alcohols on silica. J Colloid Interface Sci 1991;144:165-73.

[258] Ahmed F, Ishiguro M. Effect of adsorption site potential on adsorption of sodium dodecylbenzenesulfonate in highly humic volcanic ash soil. Soil Sci Plant Nutr 2015;61:432-9.

[259] Ahmed F, Ishiguro M, Moriguchi K. Adsorption of sodium dodecylbenzene sulfonate on highly humic non-allophanic andisol at high-electrolyte concentration. J Jpn Soc Soil Phys 2012:45-54.

[260] Inoue K, Kaneko K, Yoshida M. Adsorption of dodecylbenzenesulfonates by soil colloids and influence of soil colloids on their degradation. Soil Sci Plant Nutr 1978;24:91-102.

[261] Dick SG, Fuersten.D.W., Healy TW. Adsorption of alkylbenzene sulfonate (abs) surfactants at alumina-water interface. J Colloid Interface Sci 1971;37:595-&.

[262] Ishiguro M, Song KC, Yuita K. Ion-transport in an allophanic andisol under the influence of variable charge. Soil Sci Soc Am J 1992;56:1789-93.

[263] Iwata S, Tabuchi T, Warkentin BP. Soil-water interactions: Mechanisms and applications. New York: Marcel Dekker; 1995.

[264] Ying GG. Fate, behavior and effects of surfactants and their degradation products in the environment. Environ Int 2006;32:417-31.

[265] Atay NZ, Yenigun O, Asutay M. Sorption of anionic surfactants SDS, AOT and cationic surfactant hyamine 1622 on natural soils. Water Air Soil Pollut 2002;136:55-67.

[266] Bera A, Kumar T, Ojha K, Mandal A. Adsorption of surfactants on sand surface in enhanced oil recovery: Isotherms, kinetics and thermodynamic studies. Appl Surf Sci 2013;284:87-99.

[267] Sanchez-Martin MJ, Rodriguez-Cruz MS, Sanchez-Camazano M. Study of the desorption of linuron from soils to water enhanced by the addition of an anionic surfactant to soil-water system. Water Res 2003;37:3110-7.

[268] Deshpande S, Shiau BJ, Wade D, Sabatini DA, Harwell JH. Surfactant selection for enhancing ex situ soil washing. Water Res 1999;33:351-60.

[269] Paria S. Surfactant-enhanced remediation of organic contaminated soil and water. Adv Colloid Interface Sci 2008;138:24-58.

[270] Lee JF, Hsu MH, Lee CK, Chao HP, Chen BH. Effects of soil properties on surfactant adsorption. J Chin Inst Eng 2005;28:375-9.

[271] Li XX, Yang GP, Cao XY. Sorption behaviors of sodium dodecylbenzene sulfonate (sdbs) on marine sediments. Water Air Soil Pollut 2008;194:23-30.

[272] Xu SH, Boyd SA. Cationic surfactant sorption to a vermiculitic subsoil via hydrophobic bonding. Environ Sci Technol 1995;29:312-20.

[273] Paria S, Yuet PK. Effects of chain length and electrolyte on the adsorption of n-alkylpyridinium bromide surfactants at sand-water interfaces. Ind Eng Chem Res 2006;45:712-8.

[274] Ishiguro M, Torigoe T, Kameoka Y, Akae T. Linear anionic surfactant (SDS) transport in high humic volcanic ash soil and its permeability. Irrig Drain Rural Eng J 2008;76:485-91.

[275] Kang S, Jeong HY. Sorption of a nonionic surfactant Tween 80 by minerals and soils. J Hazard Mater 2015;284:143-50.

[276] Koopal LK, Avena MJ. A simple model for adsorption kinetics at charged solid–liquid interfaces. Colloids Surf A 2001;192:93-107.

[277] West CC. Surfactant-enhanced solubilization of tetrachloroethylene and degradation products in pump and treat remediation. ACS Symp Ser 1992;491:149-58.

[278] Rouse JD, Sabatini DA, Harwell JH. Minimizing surfactant losses using twin-head anionic surfactants in subsurface remediation. Environ Sci Technol 1993;27:2072-8.

[279] Allred B, Brown GO. Surfactant-induced reductions in soil hydraulic conductivity. Ground Water Monit Rem 1994;14:174-84.

[280] Liu MW, Roy D. Surfactant-induced interactions and hydraulic conductivity changes in soil. Waste Manage (Oxford) 1995;15:463-70.

[281] Gabr MA, Chen J, Thomas R. Soil clogging during surfactant-enhanced flushing of naphthalene-contaminated sand-kaolinite. Can Geotech J 1998;35:976-85.

[282] Gardner KH, Arias MS. Clay swelling and formation permeability reductions induced by a nonionic surfactant. Environ Sci Technol 2000;34:160-6.

[283] Tumeo MA. A survey of the causes of surfactant-induced changes in hydraulic conductivity. Ground Water Monit Rem 1997;17:138-44.

[284] Warkentin BP. Soil structure: A history from tilth to habitat. Adv Agron 2008;97:239-72.

[285] Quirk JP. Interparticle forces - a basis for the interpretation of soil physical behavior. Adv Agron 1994;53:121-83.

[286] Low PF. Physical chemistry of clay-water interaction. Adv Agron 1961;13:269-327.

[287] Lagaly G, Ziesmer S. Colloid chemistry of clay minerals: The coagulation of montmorillonite dispersions. Adv Colloid Interface Sci 2003;100:105-28.

[288] Evangelou V. Environmental soil and water chemistry. New York: Wiley Interscience; 1998.

[289] Hillel D. Environmental soil physics: Fundamentals, applications, and environmental considerations: Academic press; 1998.

[290] Ishiguro M. Ion transport and permeability in an allophanic andisol at low pH. Soil Sci Plant Nutr 2005;51:637-40.

[291] Ishiguro M, Nakaishi K, Nakajima T. Saturated hydraulic conductivity of a volcanic ash soil affected by repulsive potential energy in a multivalent anionic system. Colloids Surf A 2003;230:81-8.

[292] Ishiguro M, Nakajima T. Hydraulic conductivity of an allophanic andisol leached with dilute acid solutions. Soil Sci Soc Am J 2000;64:813-8.

[293] Suarez D, Rhoades J, Lavado R, Grieve C. Effect of pH on saturated hydraulic conductivity and soil dispersion. Soil Sci Soc Am J 1984;48:50-5.

[294] Callaghan MV, Cey EE, Bentley LR. Hydraulic conductivity dynamics during salt leaching of a sodic, structured subsoil. Soil Sci Soc Am J 2014;78:1563-74.

[295] McNeal BL, Coleman NT. Effect of solution composition on soil hydraulic conductivity. Soil Sci Soc Am Proc 1966;30:308-12.

[296] McNeal BL, Layfield DA, Norvell WA, Rhoades JD. Factors influencing hydraulic conductivity of soils in presence of mixed-salt solutions. Soil Sci Soc Am Proc 1968;32:187-90.

[297] Shainberg I, Rhoades J, Prather R. Effect of low electrolyte concentration on clay dispersion and hydraulic conductivity of a sodic soil. Soil Sci Soc Am J 1981;45:273-7.

[298] Mustafa M, Letey J. The effect of two nonionic surfactants on aggregate stability of soils. Soil Sci 1969;107:343-7.

[299] Ishiguro M, Fujii T. Upward infiltration into porous media as affected by wettability and anionic surfactants. Soil Sci Soc Am J 2008;72:741-9.

Figure captions

Fig. 1. Some examples of synthetic and natural surfactants.

Fig. 2. Schematic illustration of the effect of surfactants on the surface tension of dilute aqueous solutions (a, c, d) and the adsorption isotherm (b) that can be obtained from figure (a) through application of the Gibbs equation. The kink in the surface tension plots (a, c, d) is the CMC.

Fig. 3. Set of surface tension vs. $\ln c$ curves for aqueous solutions of sodium dodecyl pyridinium chloride (*DPC*) in the presence of different concentrations of NaCl (● 0 mmol/L; □ 5 mmol/L; ○ 20 mmol/L; Δ 100 mmol/L).

Fig. 4. Example of proton binding to a humic acid at four KCl concentrations. Data from ref. [45].

Fig. 5. Comparison of the charge density curves vs. pH and ionic strength of gibbsite, silica and hematite. The ionic strength values of the curves of hematite are (Δ) 0.002 M, (X) 0.01 M, and (O) 0.1 M. Data from ref. [81-83].

Fig. 6. Proton charge density of the montmorillonite for three values of the 1-1 electrolyte concentration (symbols) and model predictions (curves). Data from ref. [92].

Fig. 7. Binding of C12PC and C16PC to PAHA (mmol surfactant/g PAHA) at I = 0.025 M and (a) pH 5, (b) pH 7, and (c) pH 10. The reduced monomer concentration, c/CMC◦, normalizes the concentration differences betwe en C12PC and C16PC. The arrows indicate the amount of negative charge (mmol/g) of PAHA in 0.02 M KNO_3 at the given pH values. Data from ref. [97].

Fig. 8. Binding isotherms for $C12P^+$–AFA system as a function of pH at: (a) I = 0.03 mol dm^{-3} and (b) I = 0.10 mol dm^{-3}, (*) pH 3.97, (○) pH 7.41, (□) pH 9.18, (△) pH 10.01. Data from ref. [99].

Fig. 9. Binding isotherms for (a) AHA system and (b) AFA system. Data from ref. [98].

Fig. 10. Binding isotherms of $C16P^+$ to humic acid (PAHA) at two ionic strengths, (a)

log-normal plot with H^+ release, (b) double logarithmic plot, and binding isotherms of $C12P^+$ to anionic polyelectrolyte (SPSS) at three ionic strengths, (c) log-normal plot, (d) double logarithmic plot. Data from ref.[103, 112].

Fig. 11. Influence of cationic surfactant carbon-chain length on binding to purified Aldrich humic acid (PAHA). $C16P^+$ = cetylpyridinium; $C12P^+$ = dodecylpyridinium; 0.005 M NaCl. (a) log-normal plot, (b) double logarithmic plot. Data from ref. [103].

Fig. 12. Binding of cationic surfactant (dodecylpyridinium chloride, C12PC) to various humic and fulvic acids at 0.005 M NaCl and pH 5. PAHA, Aldrich humic acid; IHA, Inogashira humic acid; DHA, Dando humic acid; SFA, Strichen fulvic acid; LFA, Laurentian fulvic acid. (a) log-normal plot, (b) double logarithmic plot. Data from ref.[103].

Fig. 13. Benzyldimethyldodecyl-ammonium chloride (C12-BAC) sorption to purified Aldrich humic acid (AHA) determined at different background electrolytes at pH 6 (A) and at different pH in the presence of 5 mM NaCl or $CaCl_2$ (B). The isotherms were fitted with Freundlich equation with Freundlich exponent (n_F) of 0.8. Data from ref. [114].

Fig. 14. Adsorption isotherms of SNBS (sodium C9-benzene sulfonate; pH 4.1) and DPC (C12-pyridinium chloride; pH 8.0) on rutile at 0.01 M NaCl. Panel (a) is a double logarithmic representation of the isotherms and depicts the typical four-regions isotherms; panel (b) depicts the same results in a semi-logarithmic plot. Data from ref. [118].

Fig. 15. Adsorption isotherms of sodium nonyl-benzene-sulfonate (SNBS) on rutile at pH 4.1 and three salt concentrations are depicted as log-log (a) and lin-log (b) plots. Data from ref.[134].

Fig. 16. Adsorption of SNBS and the net proton adsorption, $\Gamma(0)$, on rutile as a function of the equilibrium SNBS concentration at three pH values and two NaCl concentrations; the pH_{pznpc} of rutile is 5.85. Data from ref. [134].

Fig. 17. Adsorption isotherms for C12PC on Aerosil, measured at pH 9 and two salt concentrations (a) as log-log plot and (b) as lin-log plot. Data from ref. [137].

Fig. 18. Effect of DPC adsorption on the surface charge of Aerosil, $\Gamma(0)$, at pH 9. Data from ref. [138].

Fig. 19. Adsorption of tertiair-octylbenzene polyoxyethylene glycol surfactants on Spherosil silica at 25 ^{o}C and pH 6.5. The TBE surfactants are monodisperse [TBE = C8Φ$(EO)_{Np}$], the TX surfactants are polydisperse [TX = C8Φ$(EO)_{<Np>}$] Np is indicated in the figure. Data from ref. [160].

Fig. 20. Adsorption of C12PC on sodium kaolinite as a function of the NaCl concentration at pH 5 and 20 ^{o}C; the horizontal line indicates the isoelectric situation and the axis on the right side indicates the sign of the electrophoretic mobility. Data from ref. [179].

Fig. 21. Adsorption isotherms of C16TAC (=HDTMA) on kaolinite at pH 6.5 and two NaCl concentrations. The adsorption is expressed relative to the CEC at pH 6.5, which is 40 μmol/g. Data from ref. [184]

Fig. 22. Abstraction (adsorption + precipitation) isotherms of sodium dodecylbenzene sulfonate (SDBS) - kaolinite system at different pH (indicated), 0.1M NaCl and 25 ^{o}C. Data from ref. [195].

Fig. 23. Adsorption isotherms of three nonionic surfactants on kaolinite at pH 3.8 and T=25^{o}C. The three surfactants are polydisperse alkylbenzene polyoxyethelenes form the Triton series: TX100 = $C_8H_{17}ΦEO_{9.5}$, TX165 = $C_8H_{17}ΦEO_{16}$ and TX305 = $C_8H_{17}ΦEO_{30}$. Data from ref. [161].

Fig. 24. Characteristic C16TAC (=HDTMA) adsorption isotherms on Na- and Ca-saturated montmorillonite (Wyoming montmorillonite, SWy-1; CEC = 900 μmol/g), compared with that on Na-kaolinite (Source Clays Repository, Dept. of Geology, University of Missouri, Columbia; CEC = 40 μmol/g at pH 6.5).The adsorbed amount is expressed relative to the CEC, the concentration of C16TAC (=HDTMA) is in mol/L. The clays were free of organic matter and homo-ionic (washing first with a NaCl solution and for Ca-clays subsequently with a $CaC1_2$ solution). Data from ref. [203].

Fig. 25. (a) Adsorption of C16TAC (=HDTMA) on Na-SWy-1 in 5 mmol/L NaCl solution and the concomitant Na release. (b) Electrophoretic mobility (solid symbols) and degree of dispersion stability (open symbols) of C16TAC-Na-SWy-1 as a function of the C16TAC adsorption; (c) d(001)-spacings of C16TAC-Na-SWy-1 obtained by X-ray diffraction as a function of C16TAC adsorption at three different water contents (dried at different relative humidity, the RH values are indicated). The C16TAC adsorption is expressed relative to the CEC (900 μmol/g). Data from ref. [184].

Fig. 26. Calculated density distributions for ammonium N, alkyl C, Ca^{2+}, Br^{-} and water O for montmorillonite (Mt) with a CEC of 1060 $\mu mol_e/g$ and different loading levels of $C16TA^{+}$/C16TAB relative to the CEC; the loadings are indicated in the figure. Data from ref. [213].

Fig. 27. Snapshots of the surfactant configurations in the Mt-C16TA+/C16TAB system. The panels a, b, c and d correspond with, respectively, Figs. 25a, 25b, 25c, and 25d. The stick layers represents the Mt-layers, the atoms in the interlayer are colored: Ca = green, N = blue, C = grey, Br = brown, H = white, O water = red. Data from ref. [213].

Fig. 28. Adsorption isotherms of C12(EO)8 on different layer silicates: (▼) Na-kaolinite, (■)Na-illite, (◆) Na-montmorillonite (Na-Mt) and (▲) Ca-bentonite (Ca-Mt). Data adapted from ref. [218].

Fig. 29. Effect of carbon chain length on linear alkylbenzenesulfonate (LAS) adsorption in a sediment. Data from ref. [255].

Fig. 30. Adsorption isotherms of cationic (C16TAB), nonionic (Tergitol 15-S-7 = C11-15(EO)7; secondary alcohol ethoxylate) and anionic (SDS) surfactants for sand. Data from ref. [266]

Fig. 31. Influence of pH on cationic (C16TAB), nonionic (Tergitol 15-S-7= C11-15(EO)7) and anionic (SDS) surfactant adsorption on sand. Data from ref. [266]

Fig. 32. (a) Influence of electrolyte concentration on the adsorption of the anionic surfactant, sodium dodecylbenzenesulfonate on highly humic non-allophanic andosol. The NaCl concentrations are indicated in the figure. Symbols are measured values. Solid lines are calculated with the Langmuir-Donnan model. (b) Donnan potentials obtained with the Langmuir-Donnan model. Data from ref. [258].

Fig. 33. Sodium dodecylsulfate (SDS) adsorption and degradation in a soil suspension (highly humic nonallophanic andosol) in relation to mixing time. Data from ref. [274].

Fig. 34. The adsorption of hexadecyltrimethylammonium (HDTMA=$C16TA^{+}$) on two vermiculitic soils (Na and Ca version) and the corresponding electrophoretic mobilities and optical densities of the soil suspensions. (a) Adsorption isotherms,

(b) electrophoretic mobilities of the soils and (c) optical densities of the soils. Data from [272].

Fig. 35. Soil hydraulic conductivity during percolation with a 1 mol/kg surfactant solution (A) nonionic surfactants (N1, N2, N3), (B) anionic surfactants (A1, A2), cationic surfactants (C1, C2) and amphoteric surfactant (Am). Data from ref. [279].

Fig. 36. Comparison of upward infiltration of sodium dodecylsulfate (SDS) solution at 70 mmol/L with that of pure water in a peat moss column. The water table connected with the column was set at height 0 cm. Data from ref. [299]

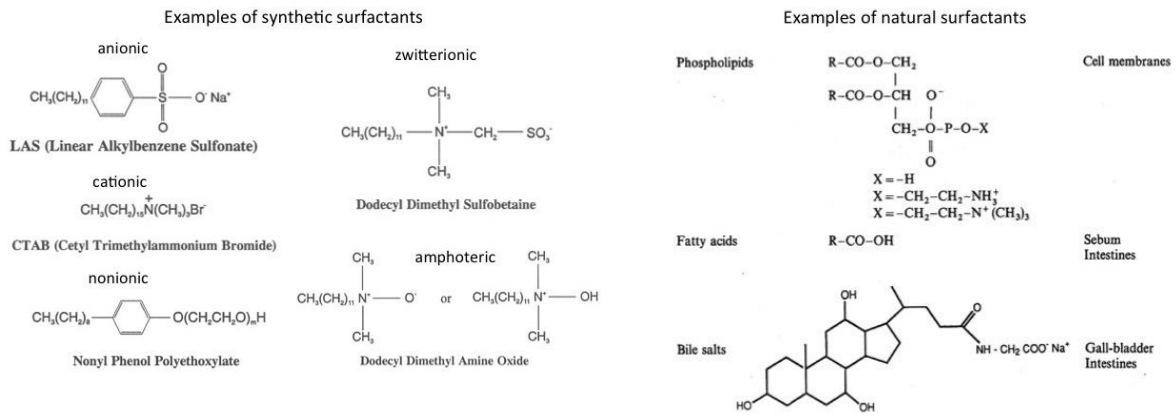
Examples of synthetic surfactants
anionic
LAS (Linear Alkylbenzene Sulfonate)
zwitterionic
Dodecyl Dimethyl Sulfobetaine
cationic
CTAB (Cetyl Trimethylammonium Bromide)
amphoteric
nonionic
Nonyl Phenol Polyethoxylate
Dodecyl Dimethyl Amine Oxide
Examples of natural surfactants
Phospholipids
Cell membranes
Fatty acids
Sebum
Intestines
Bile salts
Gall-bladder
Intestines

Fig. 1.

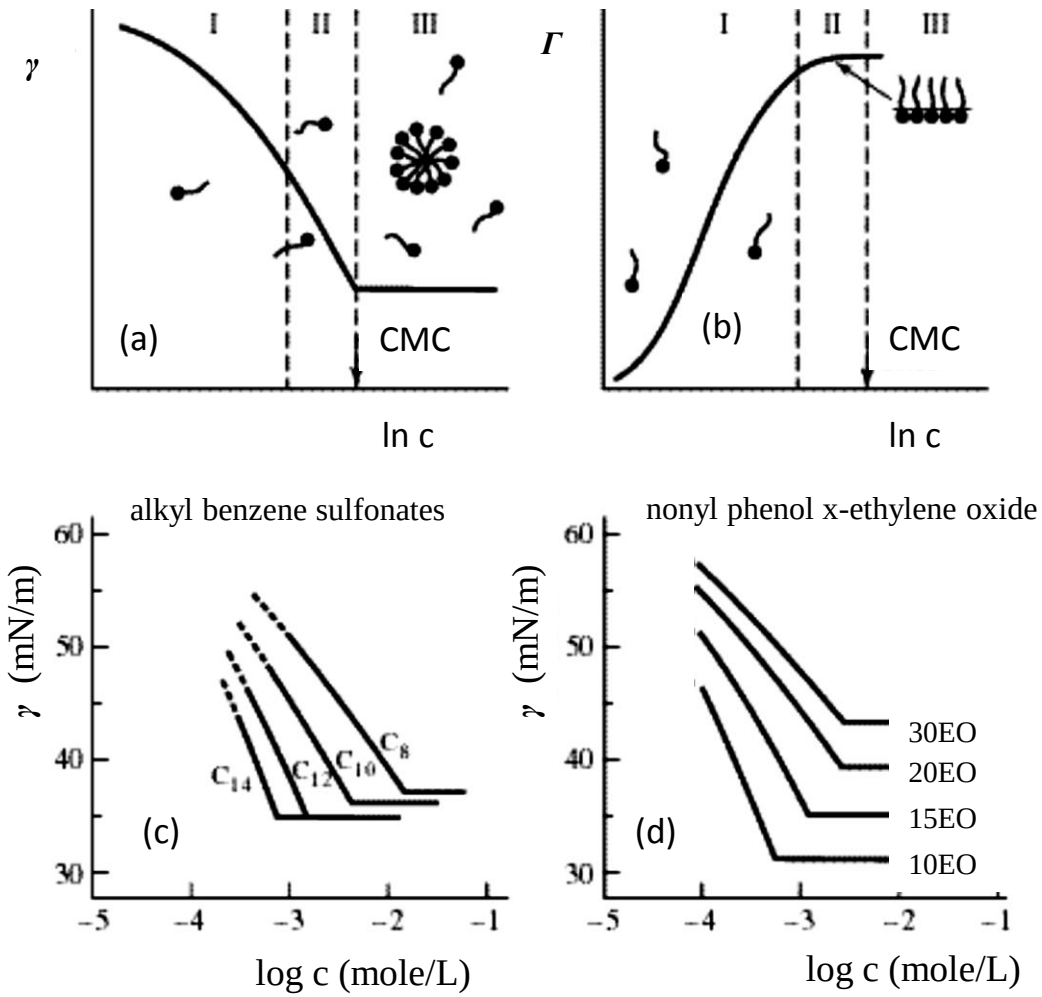
γ
I
II
III
(a)
CMC
ln c
Γ
I
II
III
(b)
CMC
ln c
alkyl benzene sulfonates
nonyl phenol x-ethylene oxide
γ (mN/m)
60
50
40
30
C8
C10
C12
C14
(c)
−5
−4
−3
−2
−1
log c (mole/L)
γ (mN/m)
60
50
40
30
30EO
20EO
15EO
10EO
(d)
−5
−4
−3
−2
−1
log c (mole/L)

Fig. 2.

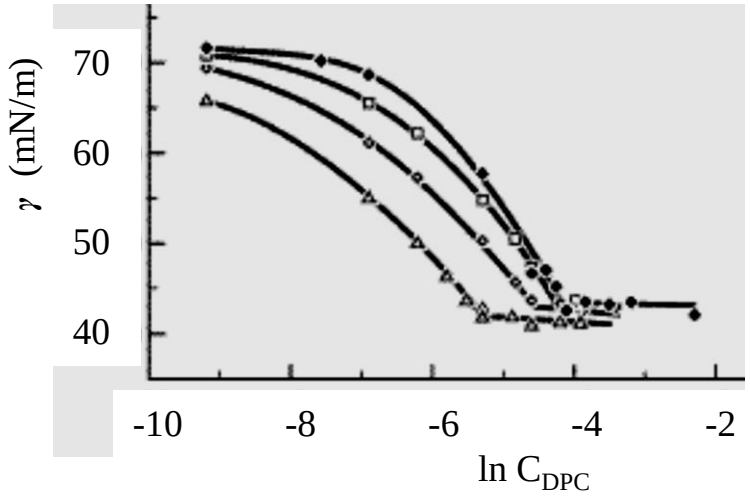

Fig. 3.

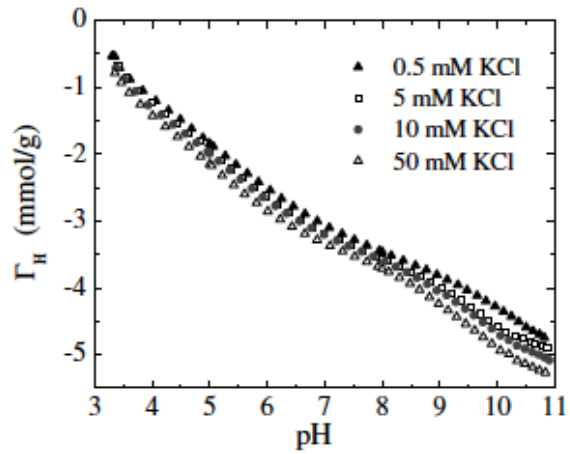
0.5 mM KCl
5 mM KCl
10 mM KCl
50 mM KCl
Γ_H (mmol/g)
pH
0
-1
-2
-3
-4
-5
3
4
5
6
7
8
9
10
11

Fig. 4.

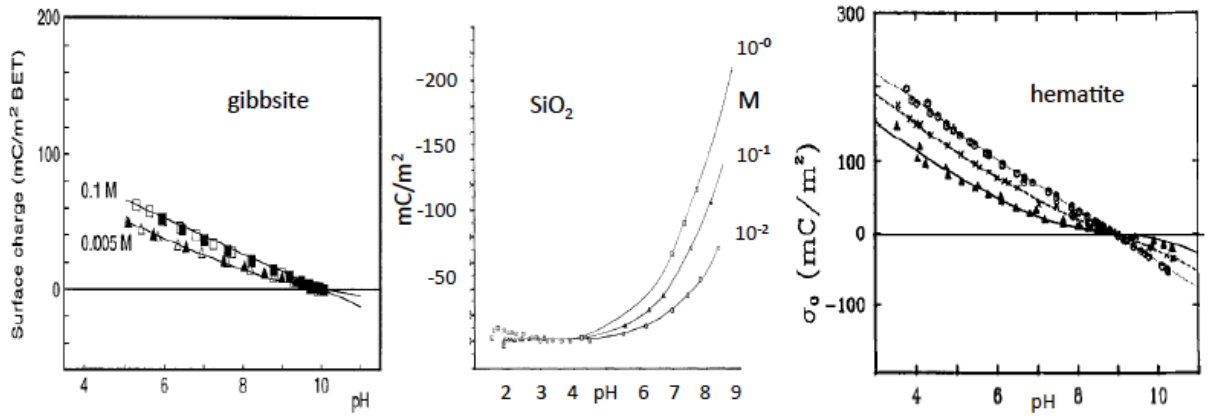
gibbsite
Surface charge (mC/m² BET)
200
100
0
0.1 M
0.005 M
4
6
8
10
pH
SiO2
mC/m²
-200
-150
-100
-50
10-0
M
10-1
10-2
2
3
4
pH
6
7
8
9
hematite
σo (mC/m²)
300
100
0
-100
4
6
pH
8
10

Fig. 5.

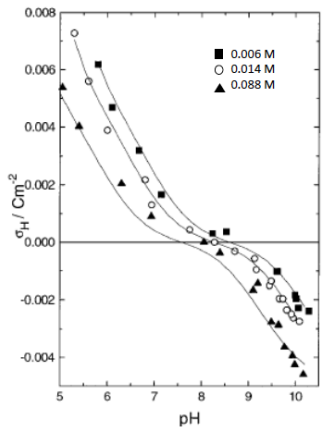
0.008
0.006
0.004
0.002
0.000
-0.002
-0.004
5
6
7
8
9
10
pH
σ_H / Cm^{-2}
0.006 M
0.014 M
0.088 M

Fig. 6.

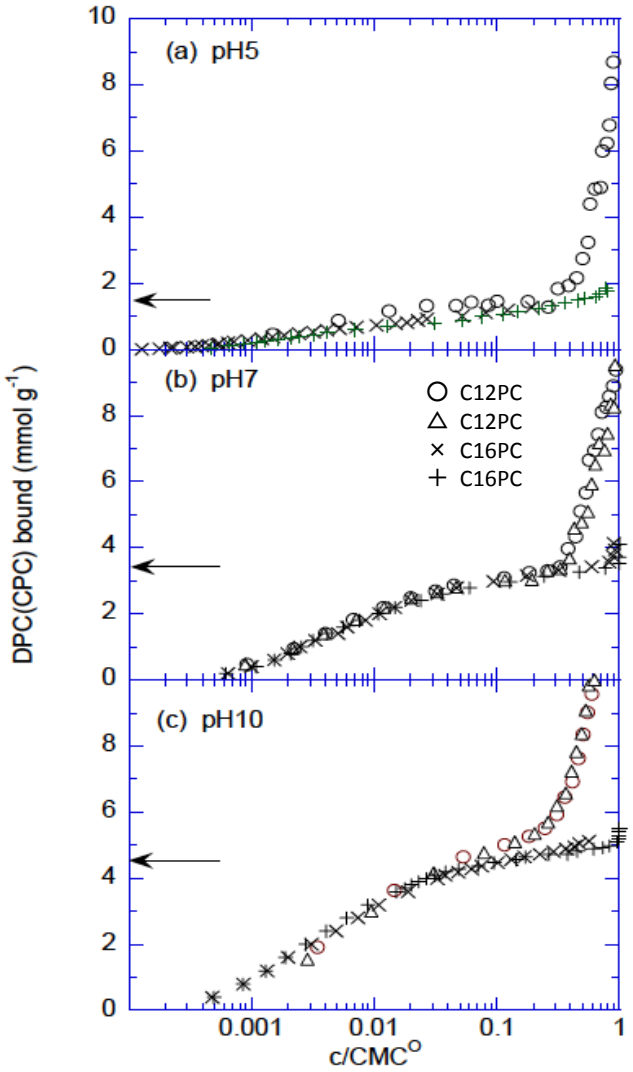
(a) pH5
(b) pH7
(c) pH10
C12PC
C12PC
C16PC
C16PC
DPC(CPC) bound (mmol g-1)
c/CMCO
0.001
0.01
0.1
1
0
2
4
6
8
10

Fig. 7.

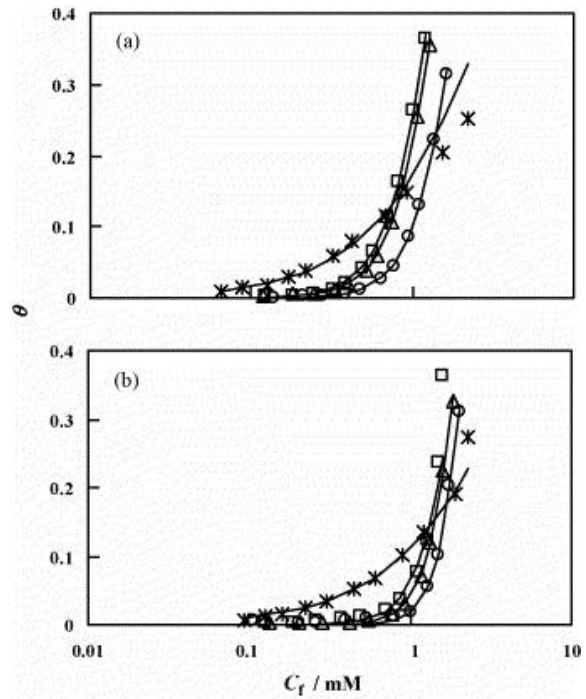

Fig. 8.

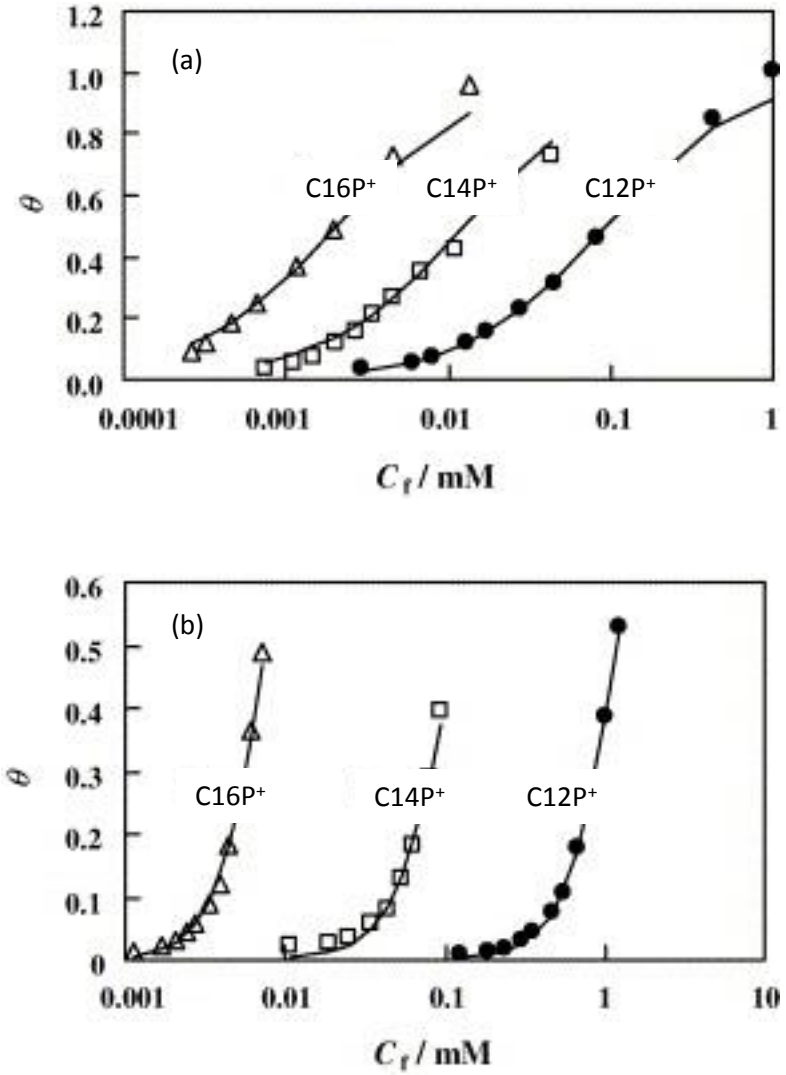
(a)
C16P+
C14P+
C12P+
θ
1.2
1.0
0.8
0.6
0.4
0.2
0.0
0.0001
0.001
0.01
0.1
1
Cf / mM
(b)
C16P+
C14P+
C12P+
θ
0.6
0.5
0.4
0.3
0.2
0.1
0
0.001
0.01
0.1
1
10
Cf / mM

Fig. 9.

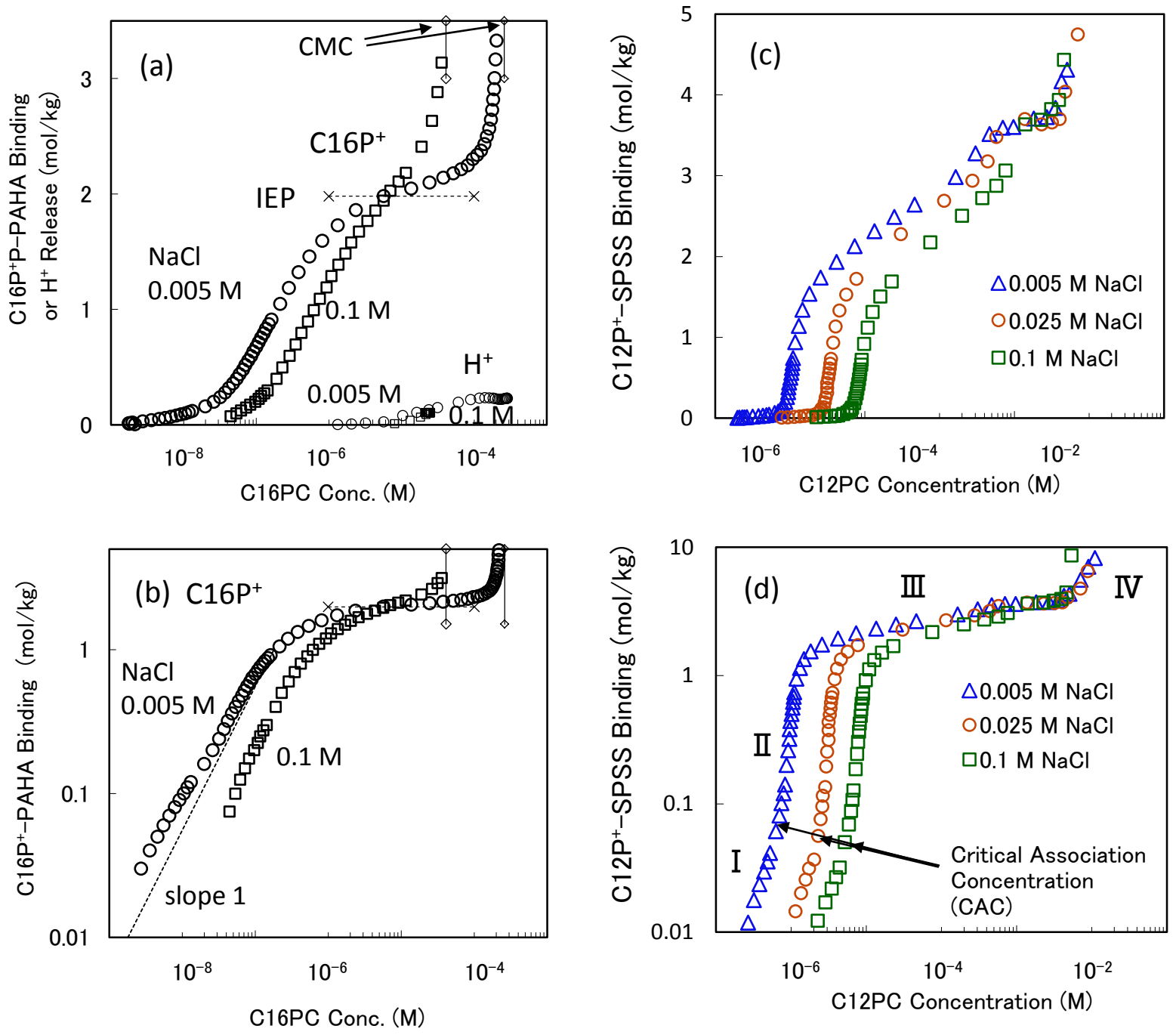
(a)
CMC
C16P+
IEP
NaCl
0.005 M
0.1 M
H+
0.005 M
0.1 M
C16P+P–PAHA Binding
or H+ Release (mol/kg)
C16PC Conc. (M)
(b) C16P+
NaCl
0.005 M
0.1 M
slope 1
C16P+–PAHA Binding (mol/kg)
C16PC Conc. (M)
(c)
C12P+–SPSS Binding (mol/kg)
0.005 M NaCl
0.025 M NaCl
0.1 M NaCl
C12PC Concentration (M)
(d)
I
II
III
IV
0.005 M NaCl
0.025 M NaCl
0.1 M NaCl
Critical Association
Concentration
(CAC)
C12P+–SPSS Binding (mol/kg)
C12PC Concentration (M)

Fig. 10.

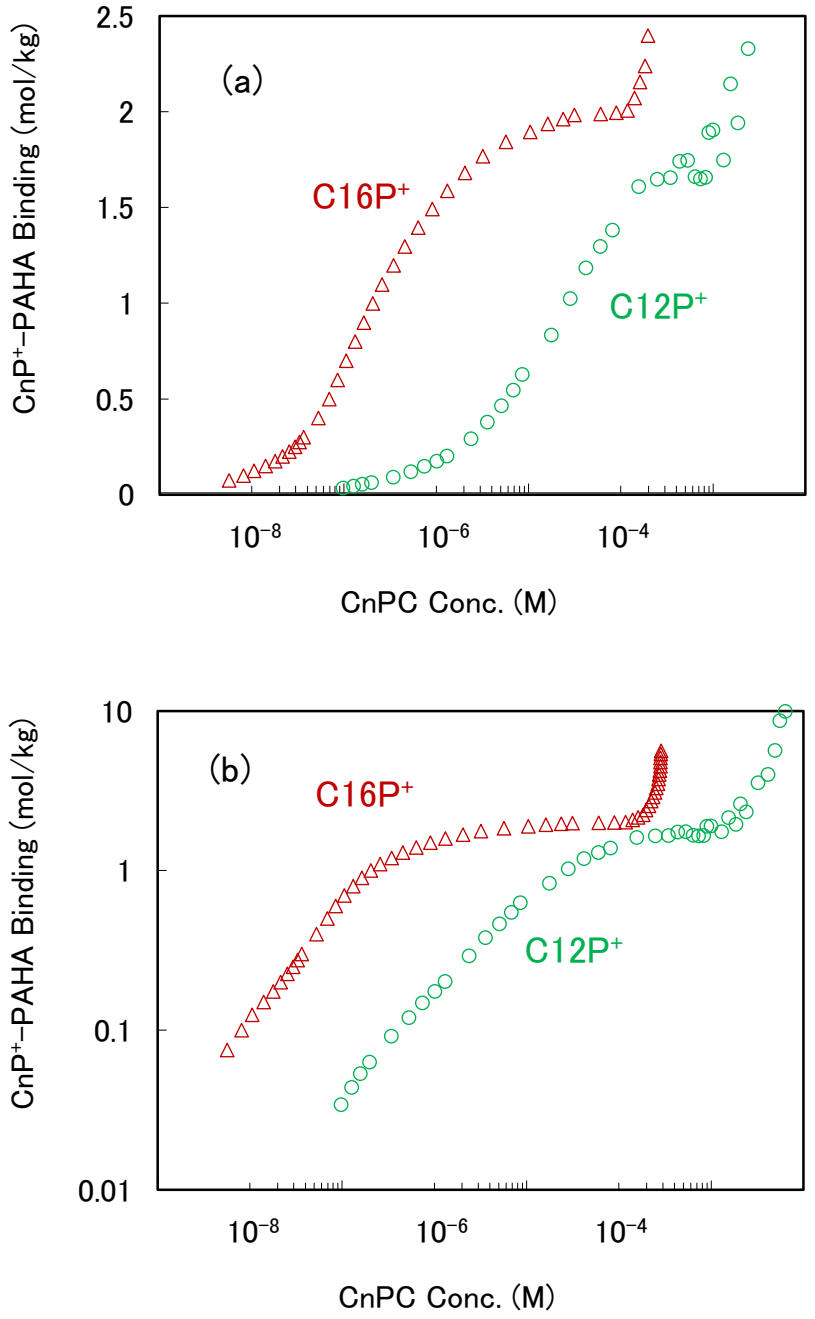
(a)
C16P+
C12P+
CnP+–PAHA Binding (mol/kg)
2.5
2
1.5
1
0.5
0
10−8
10−6
10−4
CnPC Conc. (M)
(b)
C16P+
C12P+
CnP+–PAHA Binding (mol/kg)
10
1
0.1
0.01
10−8
10−6
10−4
CnPC Conc. (M)

Fig. 11.

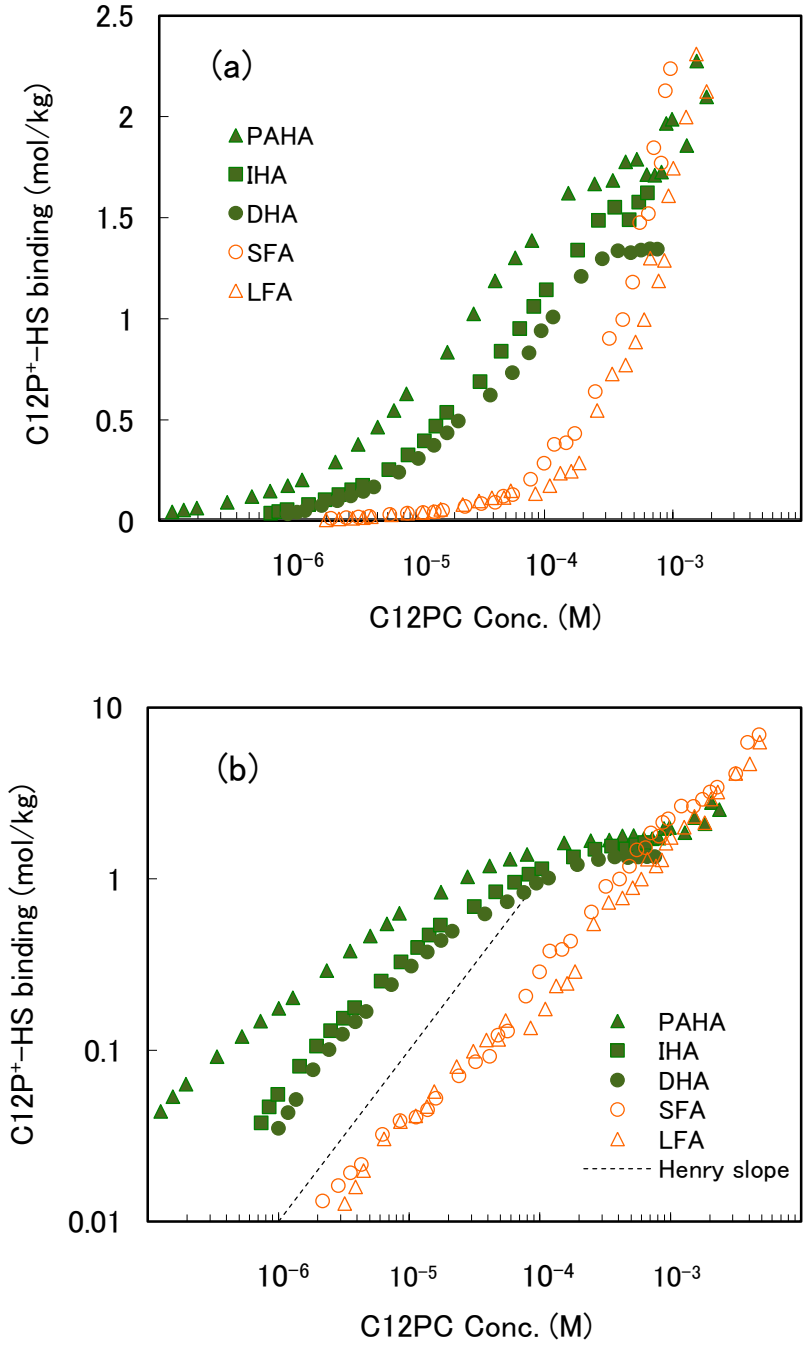
(a)
PAHA
IHA
DHA
SFA
LFA
C12P+–HS binding (mol/kg)
2.5
2
1.5
1
0.5
0
10−6
10−5
10−4
10−3
C12PC Conc. (M)
(b)
PAHA
IHA
DHA
SFA
LFA
Henry slope
C12P+–HS binding (mol/kg)
10
1
0.1
0.01
10−6
10−5
10−4
10−3
C12PC Conc. (M)

Fig. 12.

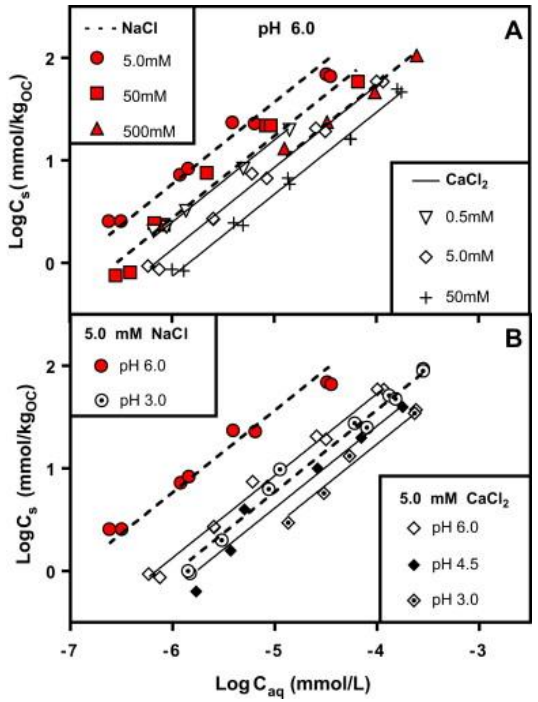
NaCl
5.0mM
50mM
500mM
pH 6.0
A
CaCl2
0.5mM
5.0mM
50mM
5.0 mM NaCl
pH 6.0
pH 3.0
B
5.0 mM CaCl2
pH 6.0
pH 4.5
pH 3.0
Log Cs (mmol/kgOC)
Log Caq (mmol/L)
2
1
0
-7
-6
-5
-4
-3

Fig. 13.

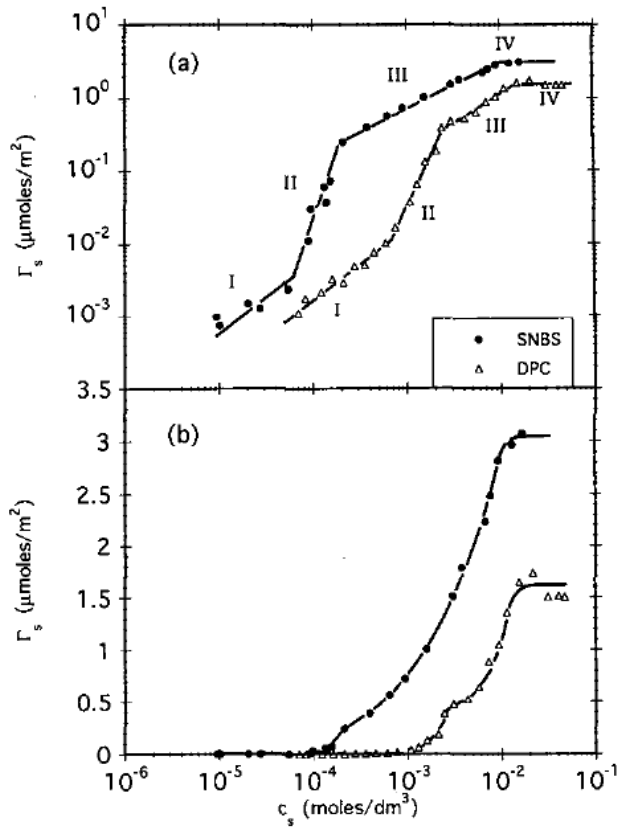

Fig. 14.

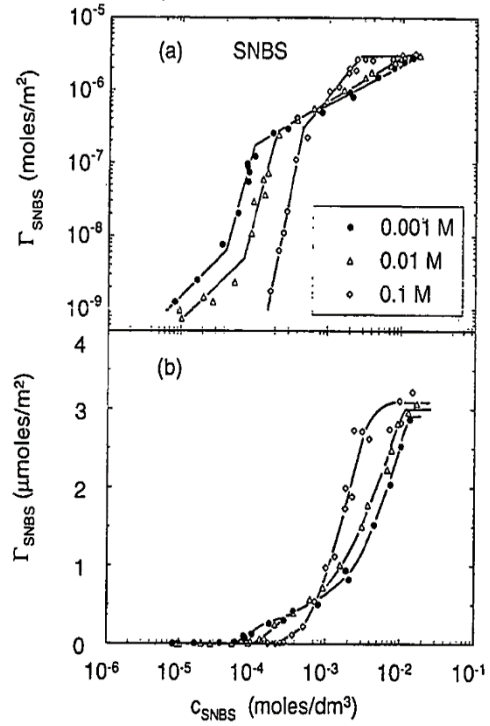
(a) SNBS
Γ_{SNBS} (moles/m^2)
10^{-5}
10^{-6}
10^{-7}
10^{-8}
10^{-9}
0.001 M
0.01 M
0.1 M
(b)
Γ_{SNBS} (μmoles/m^2)
4
3
2
1
0
10^{-6} 10^{-5} 10^{-4} 10^{-3} 10^{-2} 10^{-1}
c_{SNBS} (moles/dm^3)

Fig. 15.

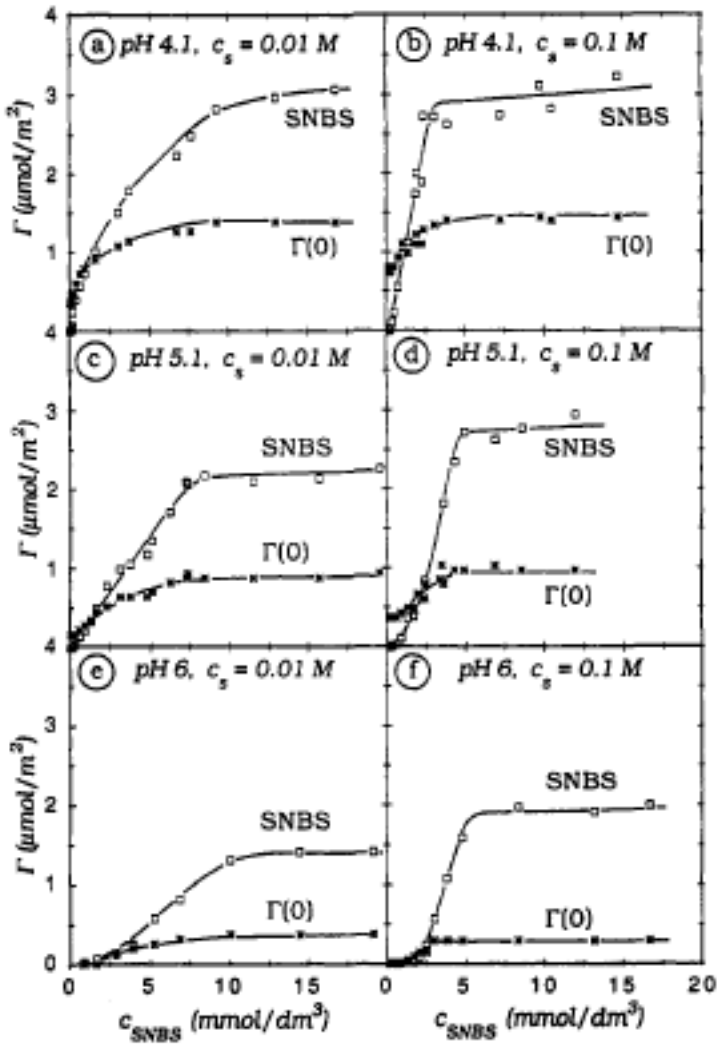
a pH 4.1, c_s = 0.01 M
b pH 4.1, c_s = 0.1 M
c pH 5.1, c_s = 0.01 M
d pH 5.1, c_s = 0.1 M
e pH 6, c_s = 0.01 M
f pH 6, c_s = 0.1 M
SNBS
Γ(0)
Γ (μmol/m²)
c_{SNBS} (mmol/dm³)

Fig. 16.

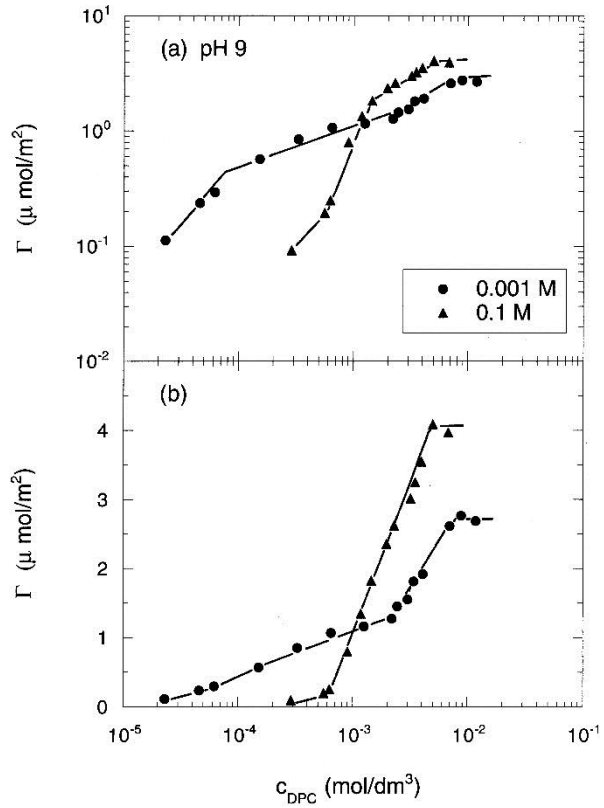

Fig. 17.

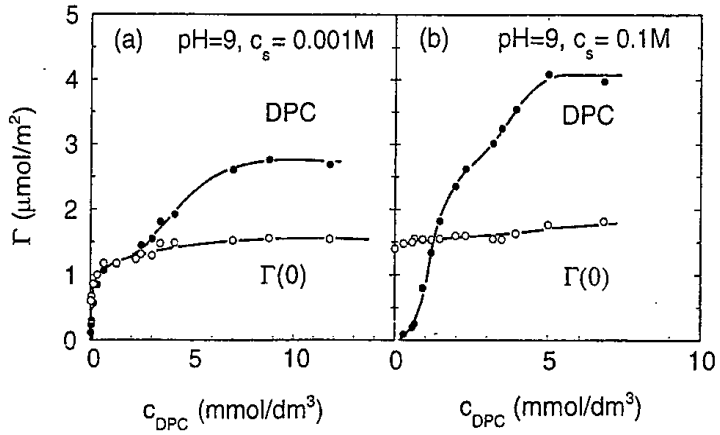
(a) pH=9, c_s = 0.001M
(b) pH=9, c_s = 0.1M
DPC
Γ(0)
Γ (μmol/m²)
c_{DPC} (mmol/dm³)
0
1
2
3
4
5
0
5
10

Fig. 18.

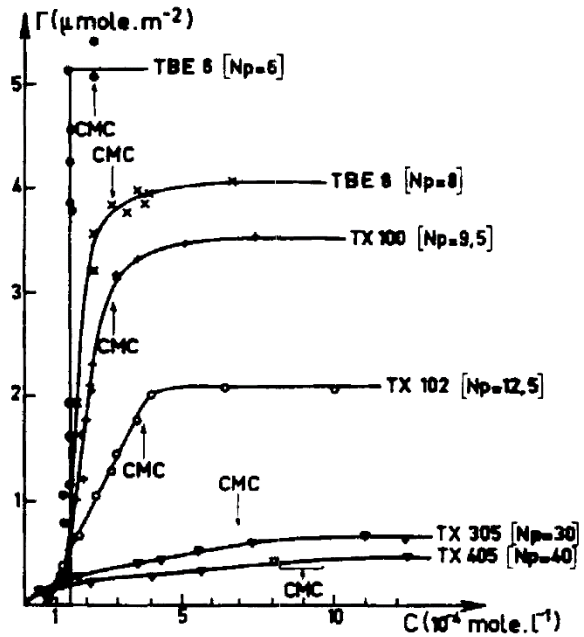
Γ(μmole.m⁻²)
TBE 6 [Np=6]
TBE 8 [Np=8]
TX 100 [Np=9,5]
TX 102 [Np=12,5]
TX 305 [Np=30]
TX 405 [Np=40]
CMC
C(10⁻⁴ mole.l⁻¹)

Fig. 19.

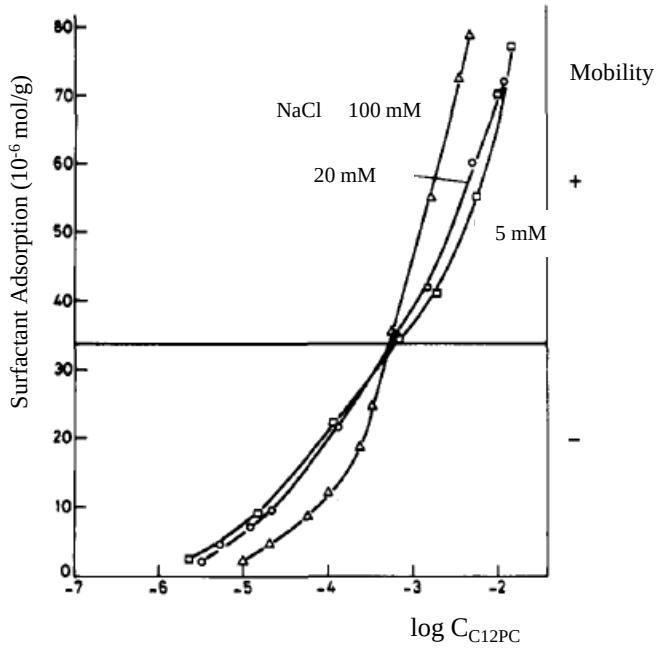
Surfactant Adsorption (10^{-6} mol/g)
80
70
60
50
40
30
20
10
0
-7
-6
-5
-4
-3
-2
log C_{C12PC}
NaCl 100 mM
20 mM
5 mM
Mobility
+
–

Fig. 20.

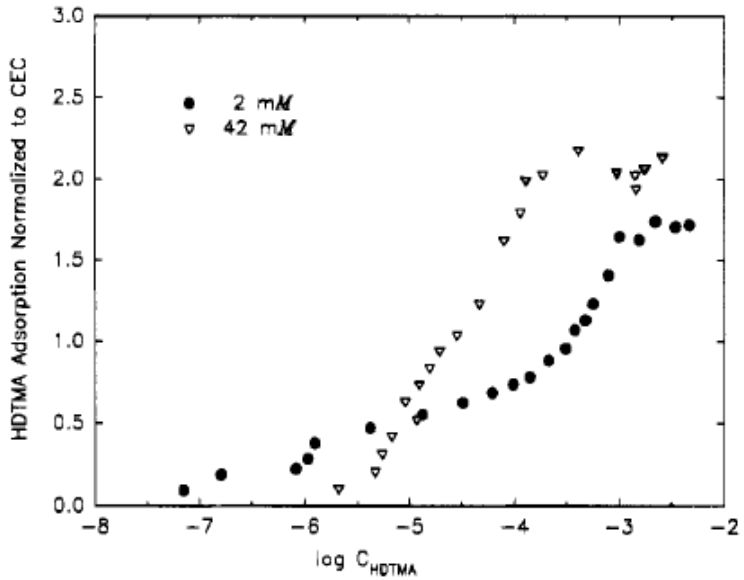
HDTMA Adsorption Normalized to CEC
3.0
2.5
2.0
1.5
1.0
0.5
0.0
2 mM
42 mM
−8
−7
−6
−5
−4
−3
−2
log C HDTMA

Fig. 21.

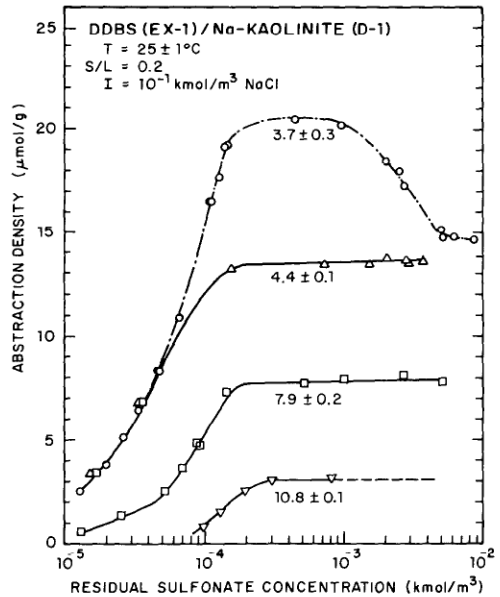
DDBS (EX-1) / Na-KAOLINITE (D-1)
T = 25 ± 1°C
S/L = 0.2
I = 10⁻¹ kmol/m³ NaCl
3.7 ± 0.3
4.4 ± 0.1
7.9 ± 0.2
10.8 ± 0.1
ABSTRACTION DENSITY (μmol/g)
RESIDUAL SULFONATE CONCENTRATION (kmol/m³)
0
5
10
15
20
25
10⁻⁵
10⁻⁴
10⁻³
10⁻²

Fig. 22.

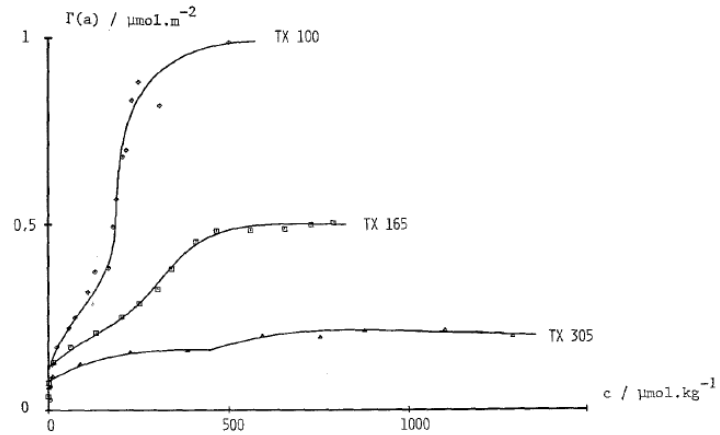

Fig. 23.

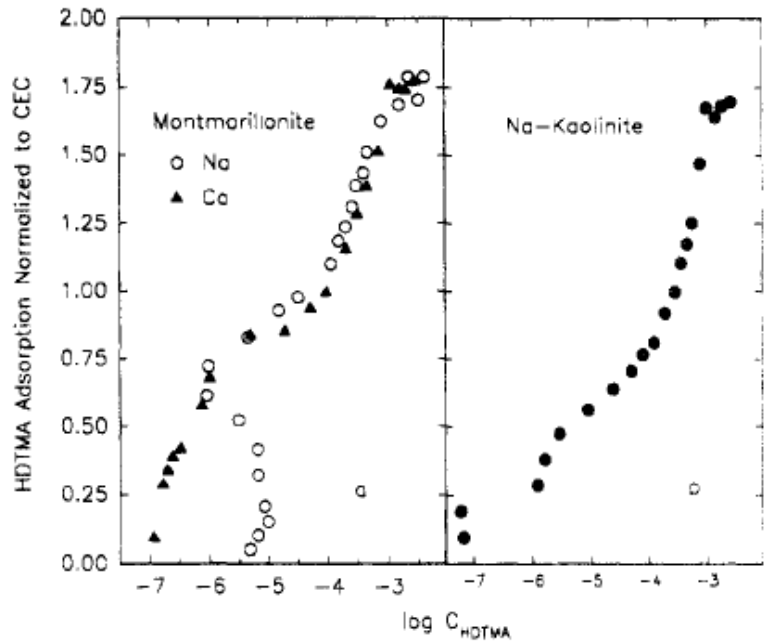
HDTMA Adsorption Normalized to CEC
2.00
1.75
1.50
1.25
1.00
0.75
0.50
0.25
0.00
Montmorillonite
Na
Ca
Na–Kaolinite
−7
−6
−5
−4
−3
log C HDTMA

Fig. 24.

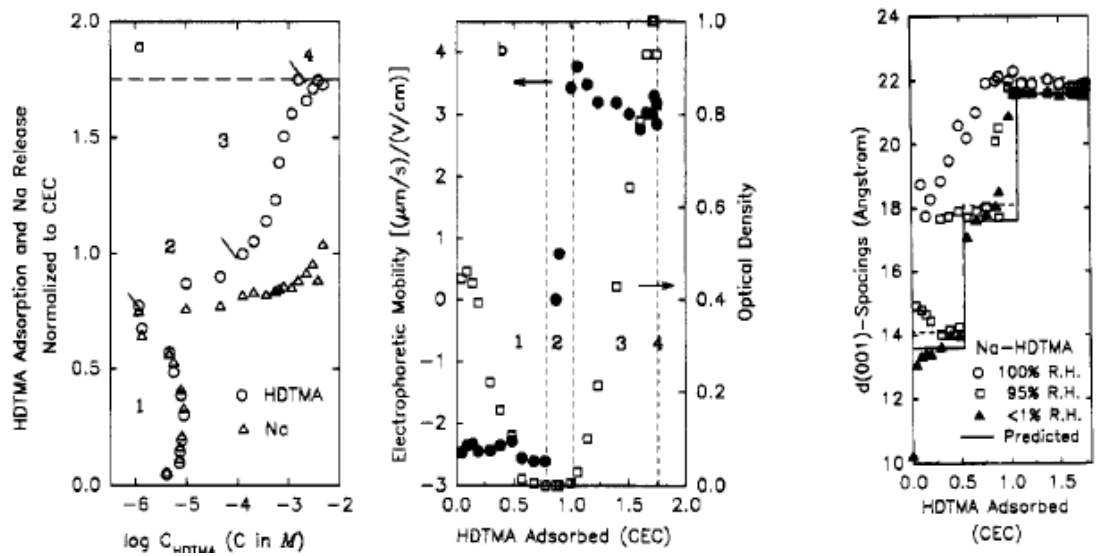
HDTMA Adsorption and Na Release
Normalized to CEC
HDTMA
Na
log C_HDTMA (C in M)
Electrophoretic Mobility [(μm/s)/(V/cm)]
Optical Density
HDTMA Adsorbed (CEC)
d(001)-Spacings (Angstrom)
Na-HDTMA
100% R.H.
95% R.H.
<1% R.H.
Predicted
HDTMA Adsorbed
(CEC)

Fig. 25.

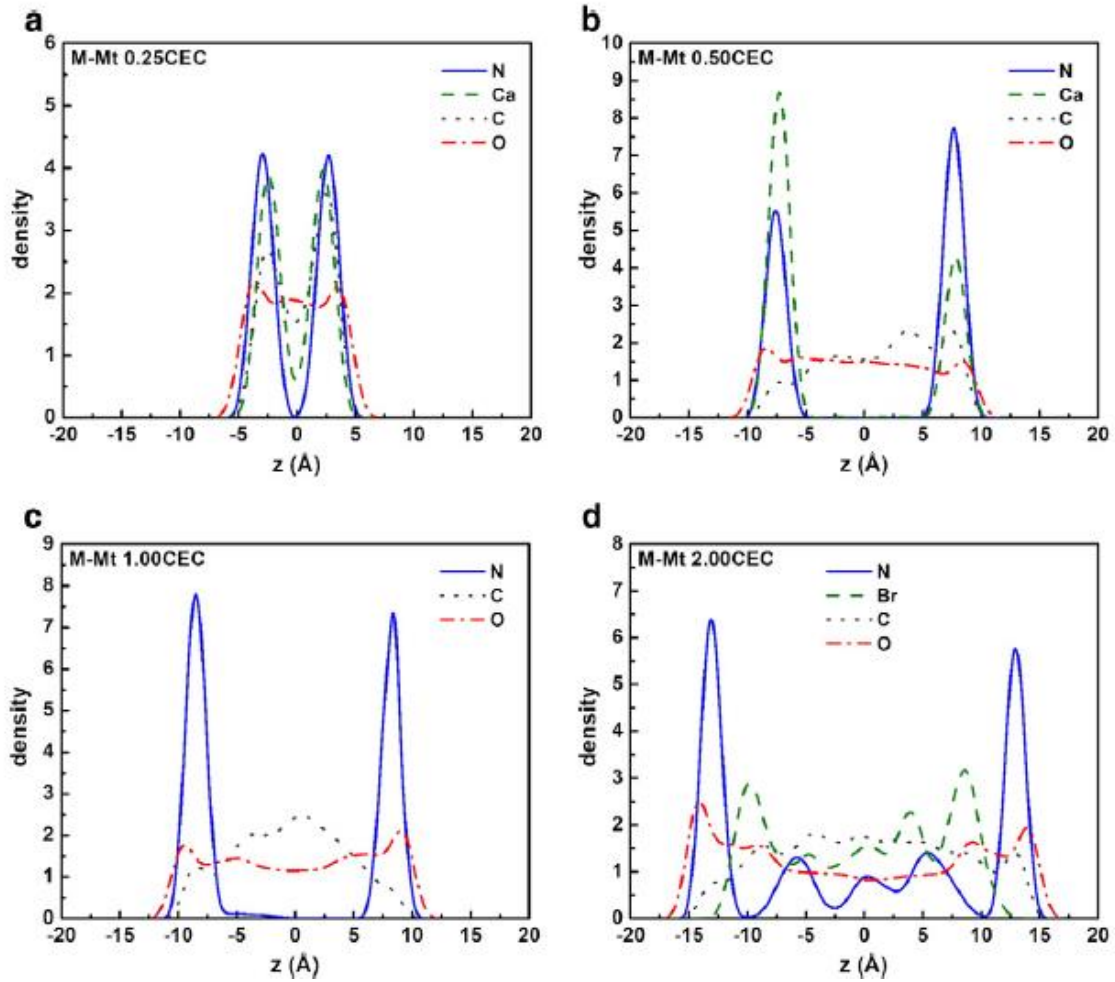
a
M-Mt 0.25CEC
N
Ca
C
O
density
z (Å)
b
M-Mt 0.50CEC
N
Ca
C
O
density
z (Å)
c
M-Mt 1.00CEC
N
C
O
density
z (Å)
d
M-Mt 2.00CEC
N
Br
C
O
density
z (Å)

Fig. 26.

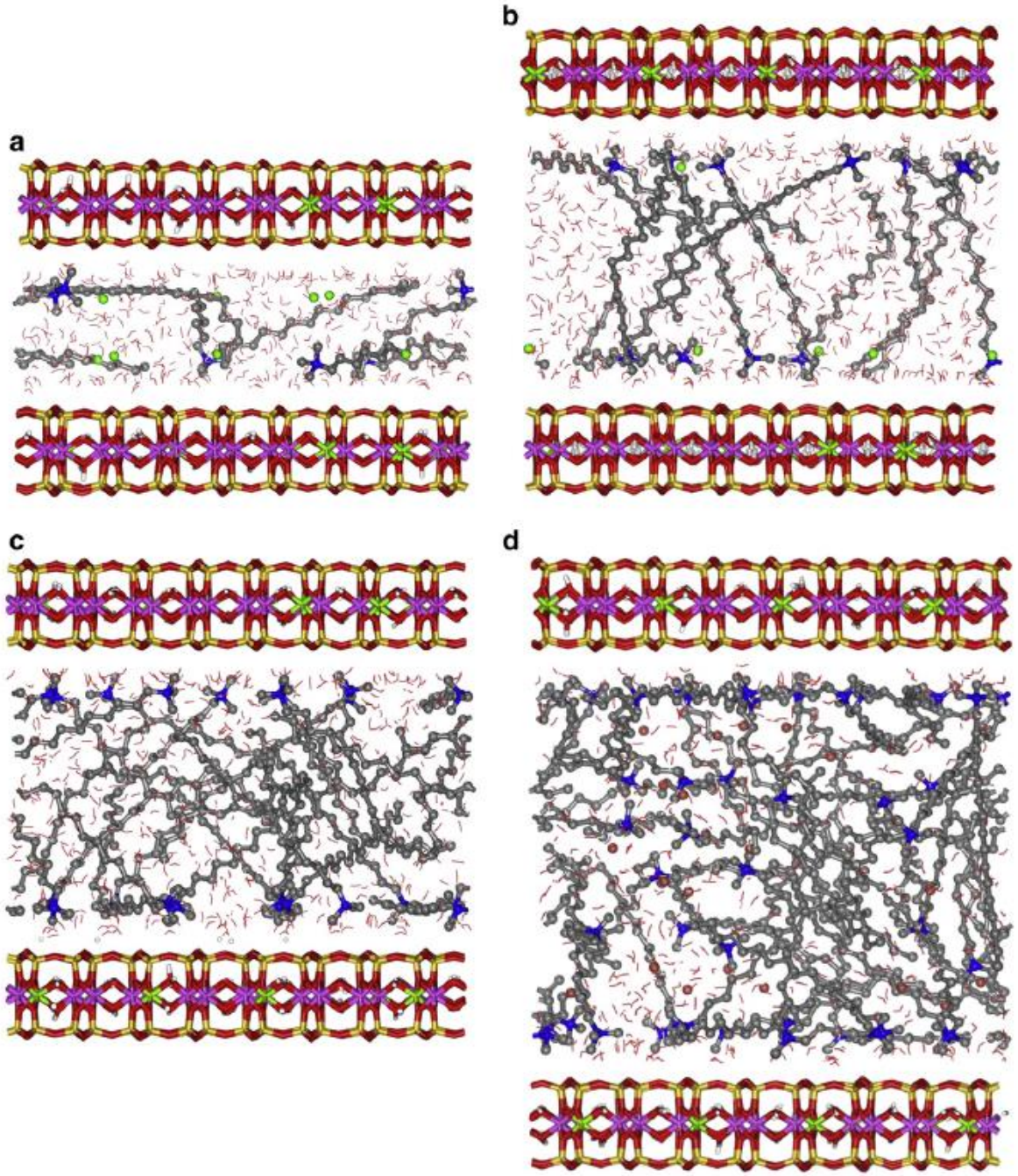

Fig. 27.

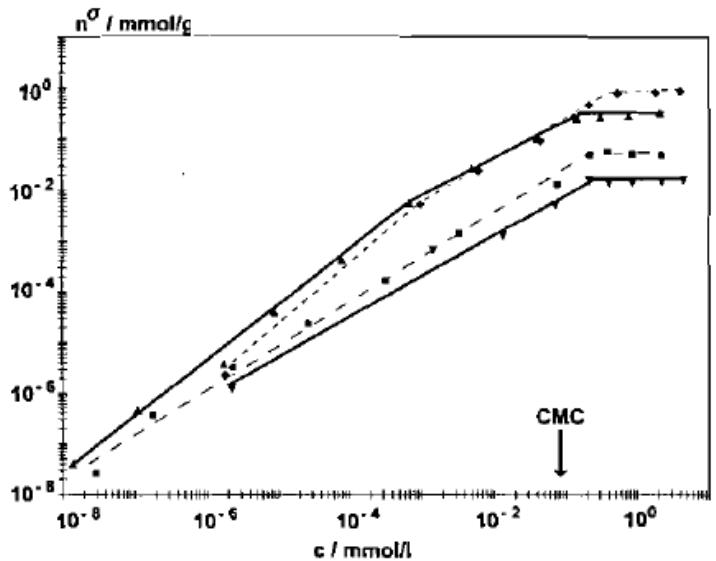
n^{σ} / mmol/g
10^{0}
10^{-2}
10^{-4}
10^{-6}
10^{-8}
CMC
10^{-8}
10^{-6}
10^{-4}
10^{-2}
10^{0}
c / mmol/l

Fig. 28.

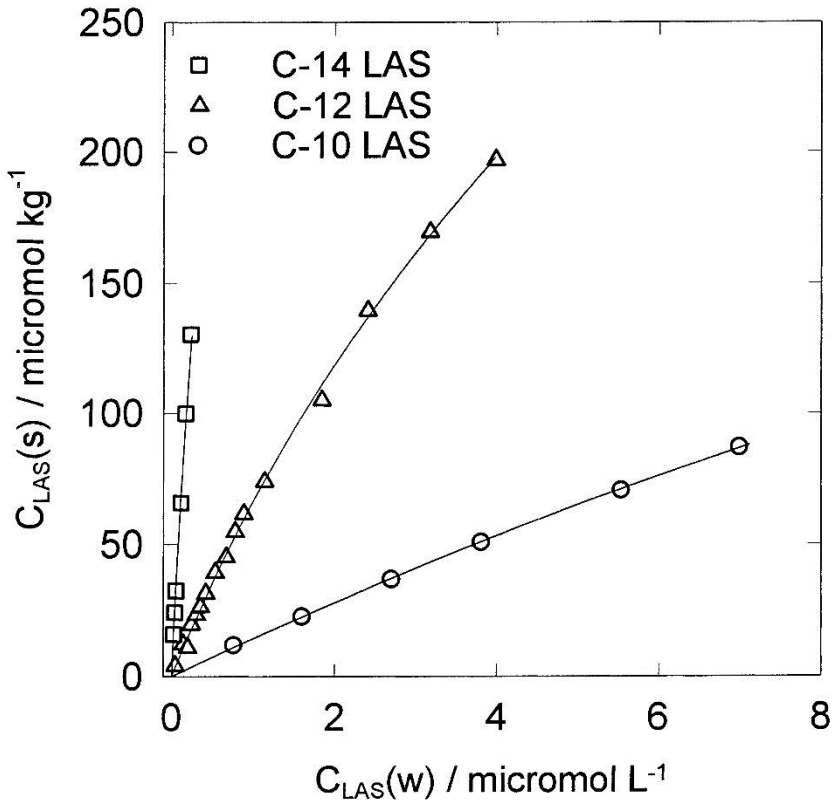
C-14 LAS
C-12 LAS
C-10 LAS
250
200
150
100
50
0
0
2
4
6
8
$C_{LAS}(s)$ / micromol kg^{-1}
$C_{LAS}(w)$ / micromol L^{-1}

Fig. 29

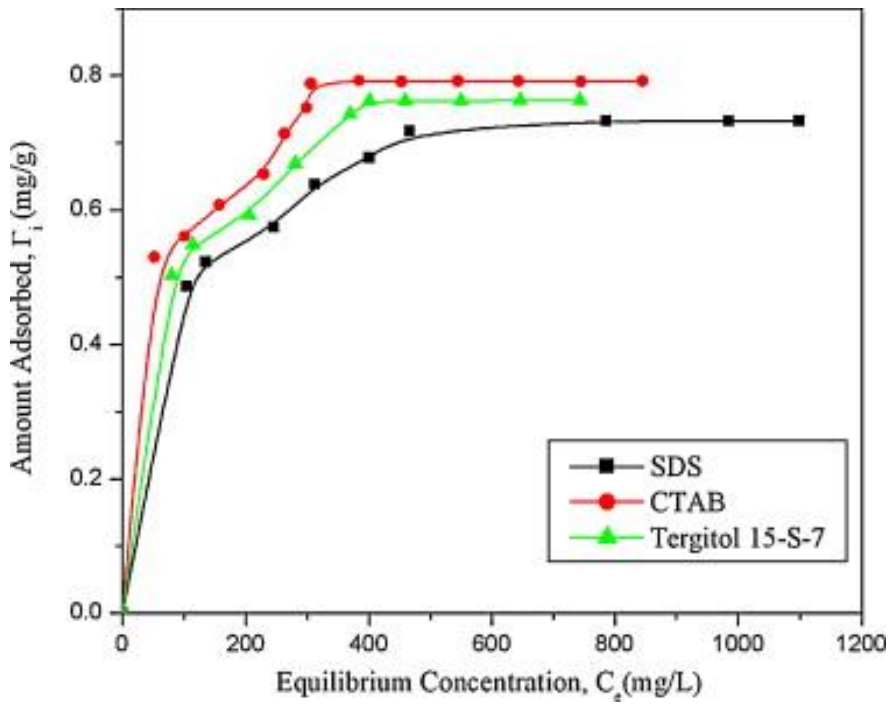
Amount Adsorbed, Γ_i (mg/g)
0.0
0.2
0.4
0.6
0.8
0
200
400
600
800
1000
1200
Equilibrium Concentration, C_e (mg/L)
SDS
CTAB
Tergitol 15-S-7

Fig. 30

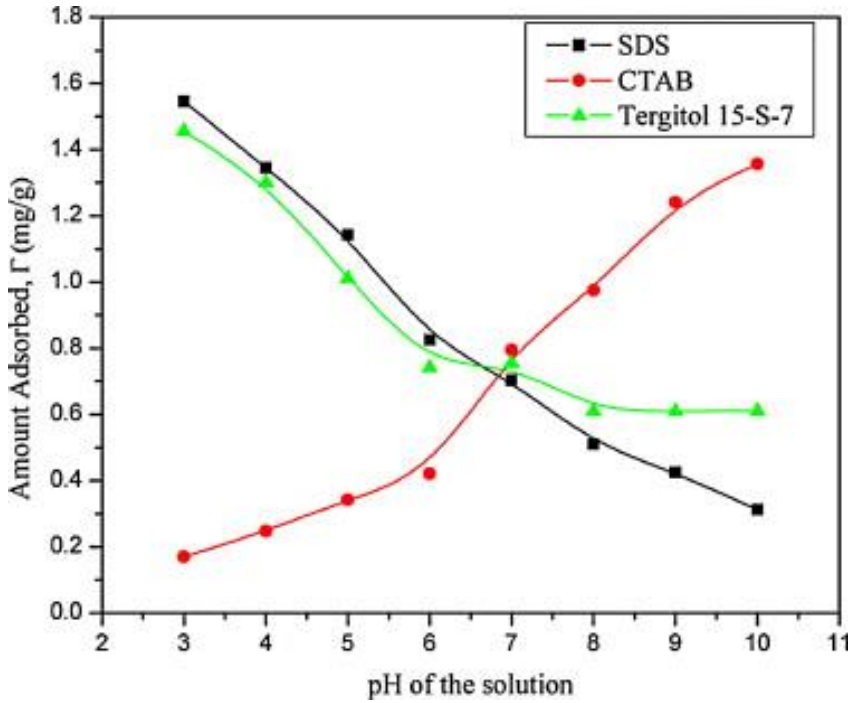
SDS
CTAB
Tergitol 15-S-7
Amount Adsorbed, Γ (mg/g)
pH of the solution
0.0
0.2
0.4
0.6
0.8
1.0
1.2
1.4
1.6
1.8
2
3
4
5
6
7
8
9
10
11

Fig. 31

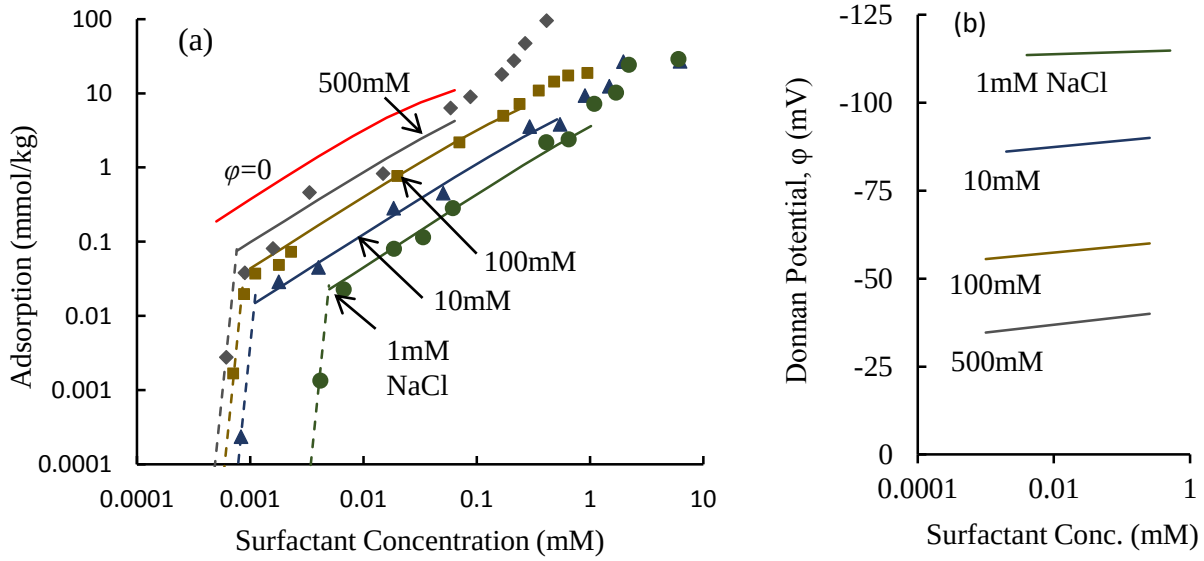
(a)
Adsorption (mmol/kg)
100
10
1
0.1
0.01
0.001
0.0001
0.0001
0.001
0.01
0.1
1
10
Surfactant Concentration (mM)
500mM
φ=0
100mM
10mM
1mM
NaCl
(b)
Donnan Potential, φ (mV)
-125
-100
-75
-50
-25
0
0.0001
0.01
1
Surfactant Conc. (mM)
1mM NaCl
10mM
100mM
500mM

Fig. 32

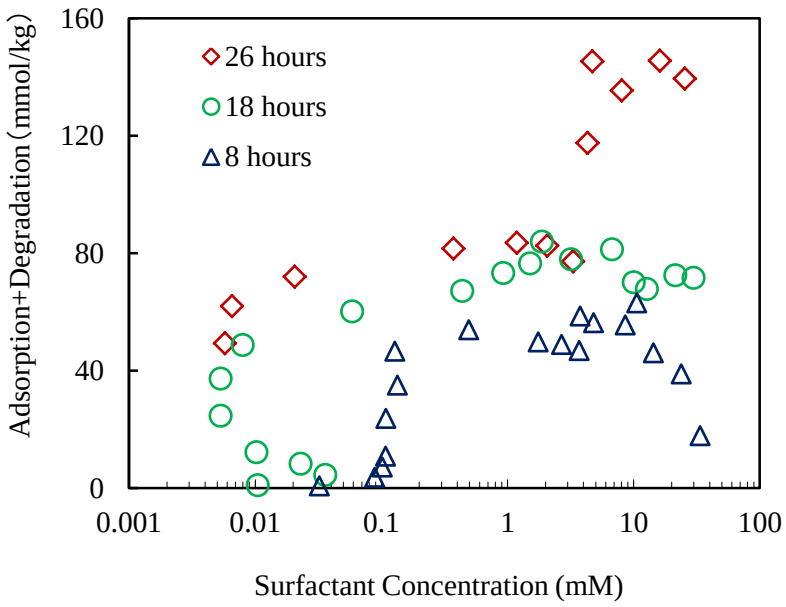
160
120
80
40
0
26 hours
18 hours
8 hours
Adsorption+Degradation (mmol/kg)
0.001
0.01
0.1
1
10
100
Surfactant Concentration (mM)

Fig. 33

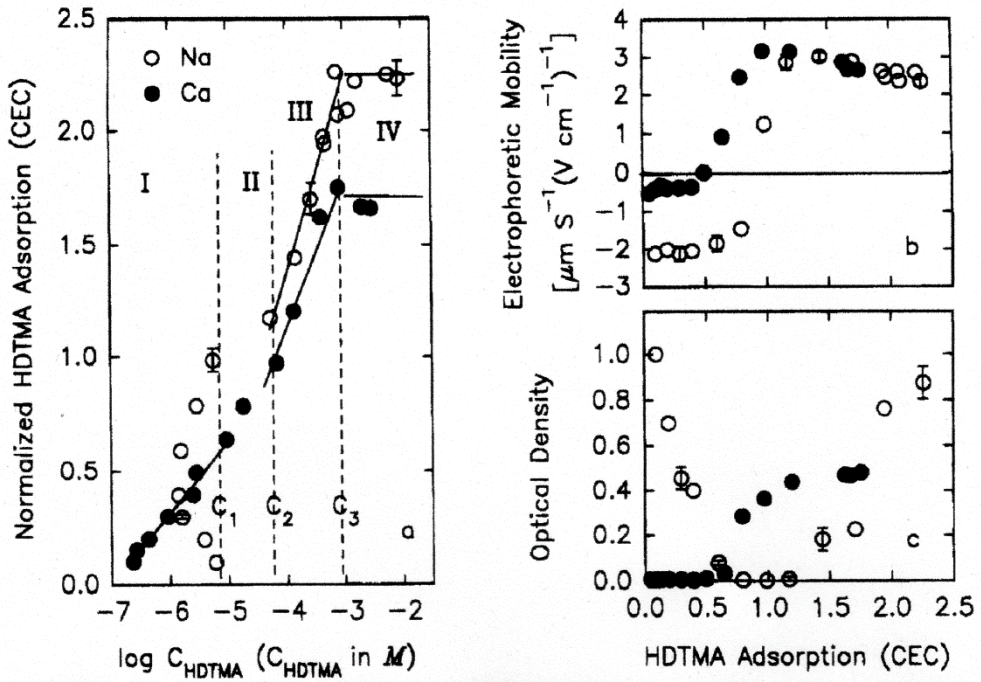
Normalized HDTMA Adsorption (CEC)
Na
Ca
I
II
III
IV
C_1
C_2
C_3
a
log C_{HDTMA} (C_{HDTMA} in M)
Electrophoretic Mobility
[$\mu m\ s^{-1}(V\ cm^{-1})^{-1}$]
b
Optical Density
c
HDTMA Adsorption (CEC)

Fig. 34

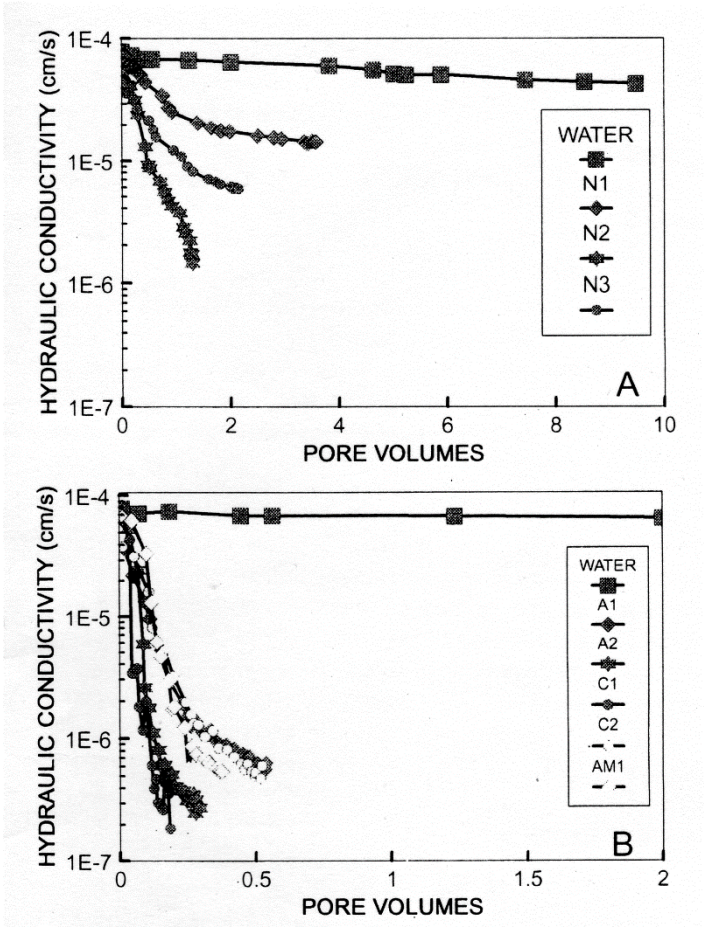
HYDRAULIC CONDUCTIVITY (cm/s)
1E-4
1E-5
1E-6
1E-7
0
2
4
6
8
10
PORE VOLUMES
WATER
N1
N2
N3
A
HYDRAULIC CONDUCTIVITY (cm/s)
1E-4
1E-5
1E-6
1E-7
0
0.5
1
1.5
2
PORE VOLUMES
WATER
A1
A2
C1
C2
AM1
B

Fig. 35

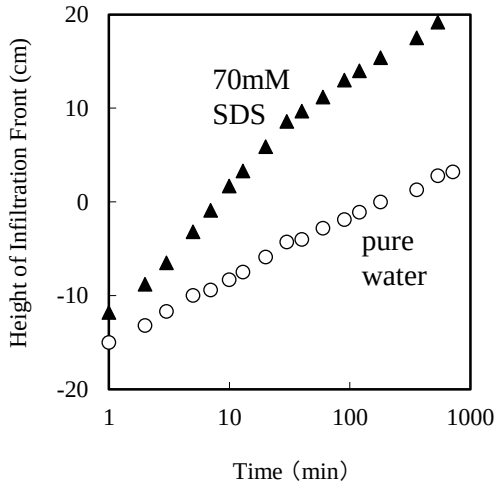
20
10
0
-10
-20
1
10
100
1000
Height of Infiltration Front (cm)
Time（min）
70mM
SDS
pure
water

Fig. 36